



Reinforcement design for antenna installations on pressurized fuselages

Pau Martinon Sort

Thesis to obtain the Master of Science Degree in
Aerospace Engineering

Examination committee

Chairperson:	Professor Fernando José Parracho Lau
Supervisors:	Professor Filipe Szolnoky Ramos Pinto Cunha
	Professor Luís Filipe Galvão dos Reis
Members of the committee:	Professor Pedro da Graça Tavares Álvares Serrão
	Engineer Carlos Manuel de Andrade Rodrigues

November 2013

Acknowledgements

The development of the thesis was possible with the support of many people to whom I need to extend my gratitude.

I would like to thank the professors Filipe Szolnoky Cunha and Luís Reis for their help, and guidance during the thesis development.

I also thank the company OGMA Industria Aeronáutica de Portugal for accepting and giving me their support through the 6 months internship. I would particularly like to thank the engineers from the company Carlos Rodrigues, João Rui Duarte, and Rui Pereira for their guidance and availability during my period in OGMA.

Eventually, I would like to express my gratitude to my friends, to my family, and to Luisa, who have always supported me during the thesis development.

Resumo

A instalação duma antena à fuselagem de um avião implica uma modificação estrutural que precisa da aplicação dum reforço. Este reforço estrutural é referido em geral como “doubler”, e tem de ser corretamente dimensionado antes de ser aplicado.

O objetivo da tese é o desenvolvimento dum grupo de ferramentas e duma metodologia para calcular e validar estruturalmente os respetivos doublers.

A análise estrutural precisa dum estudo dos aspectos relativos à estática, fadiga, e tolerância ao dano. Em termos da estática, a presente tese oferece uma metodologia e formulação necessária para o respectivo estudo. A análise á fadiga contém um estudo dos diferentes métodos possíveis para analisar um reforço doubler, inclusive métodos analíticos e de elementos finitos (FEM), e a metodologia para estimar os ciclos da vida á fadiga do componente. A análise da tolerância ao dano define uma metodologia para rapidamente analisar o crescimento de fenda da zona danificada através dum software Tolerância ao Dano (DT), e também contém um estudo dos principais conceitos DT precisos para a determinação do programa de inspeção da zona depois da modificação.

O software utilizado ao longo do desenvolvimento da tese é o MSC Patran/Nastran para todas as análises FEM; Microsoft Office Excel para o desenvolvimento das ferramentas; o AFGROW para as simulações de crescimento de fenda da analise DT.

Todos os exemplos práticos são baseados nos dados do avião Lockheed C-130.

Palavras chave: Aviões, Fuselagem, Análise Estrutural, Estática, Fadiga, Tolerância ao Dano, Doubler.

Abstract

An antenna installation to an aircraft fuselage implicates a structural modification which needs a reinforcement application. That structural reinforcement is usually called “doubler”, and must be properly designed before implementing it.

The aim of the current thesis is to develop a methodology backup with a group of tools to structurally verify and validate the application of the doublers.

The structural analysis requires a study of the statics, fatigue, and damage tolerance aspects. In the static analysis the present work provides the methodology and formulation necessary for studying it. The fatigue analysis provides of a study of the different methods for analyzing a doubler structure, including analytic and finite element methods (FEM) methods, and the methodology for estimating the component's fatigue life cycles. The damage tolerance analysis defines a methodology to rapidly assess the crack growth of a doubler structure through a Damage Tolerance (DT) software, and provides of a study of the main DT concepts necessary to reach an inspection program for the new component.

The software used during the thesis development was MSC Patran/Nastran for all the FEM analysis; Microsoft Office Excel for the developed analysis tools; AFGROW for the DT crack growth simulations.

All the practical examples are based on the Lockheed C-130 aircraft model data.

Keywords: Aircrafts, Fuselage, Structural Analysis, Statics, Fatigue, Damage Tolerance, Doubler.

List of contents

Acknowledgements	i
Resumo	iii
Abstract.....	v
List of contents	vii
List of figures	x
List of tables.....	xiii
Acronyms.....	xiv
Nomenclature	xiv
1 Introduction	1
1.1 Motivation	1
1.2 Objectives.....	1
1.3 Thesis structure	2
1.4 State of the art	3
1.4.1 Static analysis	3
1.4.2 Fatigue analysis	6
1.4.3 Damage tolerance analysis.....	9
1.5 Regulation requirements	15
2 Aerodynamic and inertial antenna structural implications	16
2.1 Analytic analysis	17
2.1.1 Aerodynamic antenna forces	17
2.1.2 Inertial forces.....	19
2.2 Finite element method analysis.....	20
2.2.1 Aerodynamic forces.....	21
2.2.2 Inertial forces.....	22
2.3 Comparison between analytic and FEM results.....	23
2.4 Summary table	24
3 Static analysis	25
3.1 Static analysis procedure flowchart.....	25
3.2 Determination of the design loads.....	25
3.2.1 Loads are known or determinable.....	25
3.2.2 Loads are unknown or undeterminable.....	26
3.2.3 Loads on the damaged area	27
3.3 Geometry definition	29
3.3.1 Adopted hypothesis.....	29
3.3.2 Design with several doublers	30
3.4 Static analysis procedure	30
3.4.1 Doubler effectiveness margin of safety	30
3.4.2 Rivet effectiveness margin of safety	31
3.4.3 Doubler and skin margin of safety.....	33

3.4.4	Screws margin of safety	34
3.4.5	Summary of contents.....	36
3.5	Developed software	37
4	Fatigue analysis	38
4.1	Fatigue analysis procedure flowchart	38
4.2	Load spectrum	38
4.2.1	Pressure load	38
4.2.2	Bending moment contribution.....	39
4.3	Stress Concentration Factor	41
4.3.1	Separate study of longitudinal and hoop stress	41
4.3.2	Determination of the load distribution	44
4.4	Fatigue life determination	60
4.4.1	Curves S-N	60
4.4.2	Scatter factor	61
4.5	Developed software	62
5	Damage tolerance analysis.....	63
5.1	Damage tolerance analysis flowchart.....	63
5.2	Crack growth analysis.....	63
5.2.1	Initial damage characterization.....	63
5.2.2	Load spectrum.....	65
5.2.3	Stress intensity factor	65
5.2.4	Crack growth rate study.....	65
5.3	Inspection requirements	66
5.3.1	Non-destructive inspection methods	66
5.3.2	Inspection determination intervals.....	67
5.4	AFGROW method.....	68
5.4.1	Inputs per growth analysis.....	68
5.4.2	Analysis methodology.....	68
5.5	Fatigue influence of modifying multiple-doublers configuration position	71
5.5.1	Configuration example case study	71
5.5.2	Analysis of the results.....	74
5.6	Developed software	75
6	Conclusions.....	77
7	Future work	79
7.1	Application of riveted doublers to a composite material fuselage	79
8	Bibliography	81
	Attachment A. Flat plate stress calculation coefficients.....	83
	Attachment B. MMPDS relevant tables	83
	Attachment B.1. Shear strength correction factor	83
	Attachment B.2. Single shear strength of solid rivets	84

Attachment B.3. Static joint strength.....	84
Attachment B.4. Ultimate single-shear strength	85
Attachment C. SCF calculus constants	86
Attachment D. Antenna example data sheet.....	87
Attachment E. FEM data resume	88
Attachment F. Fastener spring constants.....	89
Attachment G. Comparison of different methods analysis data	90
Attachment H. Comparison of multiple doublers' methods	92
Attachment I. Inter-rivet distance study data	93
Attachment J. Crack growth rate formulas summary	95
Attachment K. Non-Destructive Testing	95
Attachment L. Multiple-doublers configuration examples data.....	98

List of figures

Figure 1.1- Global project flowchart.....	2
Figure 1.2- Net tension representation	3
Figure 1.3- Net tension failure mode	3
Figure 1.4- Tearing out lengths representation	4
Figure 1.5- Tearing out failure mode	4
Figure 1.6- Minimum hole to edge distance	5
Figure 1.7- Minimum inter rivet distance	6
Figure 1.8- Fatigue main issues	6
Figure 1.9- Ground-Air-Ground loading graphic definitions for fatigue analysis [4]	7
Figure 1.10- Load spectrum scheme for applying Palmgren Miner's rule	7
Figure 1.11- Stress concentration around a hole in a flat plate	8
Figure 1.12- Damage tolerance main issues	10
Figure 1.13- Residual strength evolution against crack length.....	10
Figure 1.14- Structural strength capability during the flight life [1]	11
Figure 1.15- Crack length and crack growth rate graphics [6].....	12
Figure 1.16- Crack growth evolution with overloads applied [1].....	12
Figure 1.17- Crack size growth MSD influence [8]	13
Figure 1.18- Three failure modes scheme.....	14
Figure 1.19- Plane stresses at the crack tip for mode I	14
Figure 1.20- Idealized crack plastic zone scheme [10].....	15
Figure 2.1- General procedure for a new antenna install flowchart.....	16
Figure 2.2- Followed verification method flowchart	17
Figure 2.3- Fuselage beam simplification a), and beam section b)	18
Figure 2.4- Fuselage skin panel equivalence a), flat panel distributed load [12] b)	19
Figure 2.5- Mesh and von Mises diagram for the aerodynamic forces analysis	21
Figure 2.6- von Mises diagram for the inertial pushing forces.....	22
Figure 2.7- von Mises diagram for the inertial pushing forces.....	22
Figure 3.1- Static analysis flowchart	25
Figure 3.2- Stress against strain generic diagram	26
Figure 3.3- Load distribution evolution through doublers layers.....	28
Figure 3.4- Pressure longitudinal and hoop stresses	29
Figure 3.5- Rivet shear area	31
Figure 3.6- Rivet single versus double shear	31
Figure 3.7- Hole bearing area.....	32
Figure 3.8- Single a) and triple b) doubler with the effective rivet zones selected	33
Figure 3.9- Statics excel print screen	37
Figure 4.1- Fatigue analysis flowchart.....	38
Figure 4.2- Lockheed C-130 profile view with loading assumption	40
Figure 4.3- Tubular section with booms simplification.....	41

Figure 4.4- Load distribution around a plate with a hole	42
Figure 4.5- Quad-elements meshed perforated plate	42
Figure 4.6- von Mises diagram for cases 1 to 3, from left to right	42
Figure 4.7- Plate with a hole bi-axial stress [14].....	43
Figure 4.8- One doubler up view with a strip selected and represented	44
Figure 4.9- Fastener spring constant against plates' thicknesses	45
Figure 4.10- Doubler of n rivet row profile view.....	46
Figure 4.11- Doubler of n rivet row profile with constants schematic view	46
Figure 4.12- Print screen of the load transference calculus workbook	47
Figure 4.13- Doubler with the critical rivet strips selected	48
Figure 4.14- Two extremes fixed beam.....	48
Figure 4.15- FEM 1 strip beam element transfer forces.....	49
Figure 4.16- FEM bush element constant representation	50
Figure 4.17- FEM 1 strip shell element mesh and transfer forces	51
Figure 4.18- FEM entire doubler shell elements mesh and transfer forces	52
Figure 4.19- Splice profile schematic view	53
Figure 4.20- Experimental values for bearing load [2]	53
Figure 4.21- Bearing load results in function of the analysis method for $K_f=K$	53
Figure 4.22- Bearing load results in function of the analysis method for $K_f=0.7K$	54
Figure 4.23- Bearing load results in function of the analysis method for $K_f=0.4K$	54
Figure 4.24- Bearing load results in function of the analysis method for $K_f=0.1K$	54
Figure 4.25- Bearing load results in function of ratio K_f/K for each analysis method	55
Figure 4.26- Schematic view for the 4 different analyzed methods	57
Figure 4.27- Stress concentration factor results for the 4 different analyzed methods.....	57
Figure 4.28- Schematic view of a two row doubler strip.....	58
Figure 4.29- Non-dimensional by-pass load against inter-rivet distance	59
Figure 4.30- Non-dimensional bearing load against inter-rivet distance	59
Figure 4.31- Stress concentration factor against inter rivet distance results	59
Figure 4.32- Fatigue life cycles determination [3].....	61
Figure 4.33- Fatigue excel print screen	62
Figure 5.1- Damage tolerance analysis flowchart	63
Figure 5.2- Damage characterization's lengths.....	64
Figure 5.3- Initial crack damages for hoop and longitudinal stress states	64
Figure 5.4- Combination of different magnitude K_I [2]	65
Figure 5.5- Crack growth simulation iterative procedure.....	66
Figure 5.6- Crack growth inspection plan method.....	67
Figure 5.7- AFGROW inputs flowchart.....	68
Figure 5.8- One-doubler with the two critical sections selected	69
Figure 5.9- Representation of the analyzing method for the first row, Case1	69
Figure 5.10- Representation of the analyzing method for antenna center hole, Case2.....	70

Figure 5.11- Crack growth graphic with inputs and outputs 70

Figure 5.12- Case one versus case two 71

Figure 5.13- Two doublers with the selected zone of study 72

Figure 5.14- Case 1 one strip beam elements transfer loads result..... 72

Figure 5.15- Case 2 one strip beam elements transfer loads result..... 73

Figure 5.16- Critical zone and initial crack definition 73

Figure 5.17- Crack growth for case1 74

Figure 5.18- Damage tolerance excel print screen..... 75

List of tables

Table 1.1- Regulation requirement list	15
Table 2.1- Values for the example	19
Table 2.2- Values for the example	20
Table 2.3- Calculation parameters for the example	20
Table 2.4- Analytic results for the example	20
Table 2.5- Comparison of FEM against analytic results.....	23
Table 2.6- Extra structural load percentage calculation	23
Table 2.7- Summary of expressions and cases respectively	24
Table 3.1- Design load philosophy	27
Table 3.2- Safety margins recopilation.....	30
Table 3.3- Safety margins summary	36
Table 4.1- Required C-130 data for carrying the analysis.....	39
Table 4.2- Longitudinal and hoop forces for three cases	42
Table 4.3- von Mises analysis compilation for three cases	43
Table 4.4- Analytic analysis compilation for three cases	43
Table 4.5- Results of load distribution after FEM analysis	58
Table 5.1- Primary damage clasification	64
Table 5.2- Advantages and disadvantages of cases 1 and 2	75

Acronyms

Acronym	Meaning
AC	Advisory Circular
DOA	Design Office Approval
DT	Damage Tolerance
EASA	European Aviation Safety Agency
FAA	Federal Aviation Administration
FAR	Federal Aviation Regulations
GAG	Ground Air Ground
LEFM	Linear Elastic Fracture Mechanics
MFW	Maximum Fuel Weight
MMPDS	Metallic Materials Properties Development and Standardization
MSD	Multiple-Site Damage
MTOW	Maximum Take-off Weight
MZFW	Maximum Zero Fuel Weight
NACA	National Advisory Committee for Aeronautics
SA	Anonymous Society
SCF	Stress Concentration Factor

Nomenclature

Variable	Meaning
a	Longitudinal distance between frames
A	Tom Swift's equation constant in function of the rivets material
a_1	Longitudinal distance between antenna screws
$A_{bearing}$	Bearing effective area
A_{booms}	Boom cross-sectional area
a_c	Half of the crack length
A_{cross}	Cross section of the fastener
$A_{cut-out}$	Cut-out hole area
$A_{doubler_k}$	Transversal area of the doubler 'k'
A_{front}	Frontal area of the antenna in sq. ft.
A_{layer_x}	Area of the material layer 'x'
A_{layer_k}	Area of the material layer 'k'
A_{lost}	Lost area from the original skin
A_{net}	Net area
$A_{net_doubler}$	Net area of the doubler
A_{net_skin}	Net area of the skin
$A_{original}$	Original skin area
A_{plate}	Cross sectional area between fasteners

A_{shear}	Fastener transversal area
b	Circular distance between stringers
B	Tom Swift's equation constant in function of the rivets material
b_1	Circular distance between antenna screws
b_c	Crack length without hole
C	Fastener constant
c_c	Crack depth without hole
C_D	Drag coefficient
C_{f1}	Constant fastener row 1
C_{f2}	Constant fastener row 2
C_{fn}	Constant fastener row n
C_i	Elastic constant referent to element 'i'
C_p	Constant which depend on the material
C_{plate}	Plate characteristic constant
C_{R1}	Constant doubler plate row 1
C_{Rn}	Constant doubler plate row n
C_S	Vector of skin constants
C_{S1}	Constant skin plate row 1
C_{Sn}	Constant skin plate row n
d	Distance between fastener screws of the antenna
D	Rivet diameter
da	Crack length differential growth
da/dN	Crack growth rate
D_{cc}	Section's characteristic damage
d_{f1}	Deflection fastener row 1
d_{f2}	Deflection fastener row 2
d_{frames}	Distance between frames
d_i	Deflection referent to element 'i'
D_{model}	Equivalent diameter of the model
dN	Number of cycles differential increment
Dr	Distance between the first and the second fastener rows
d_r	Distance between the antenna screw and the frame
d_{R1}	Deflection doubler plate row 1
d_{S1}	Deflection skin plate row 1
D_{screw}	Diameter of the screw hole
E	Modulus of elasticity of the plates
e	Distance from the hole center to the edge
E_{doubler_k}	Young modulus of the layer 'k' of the doublers
E_{fast}	Modulus of elasticity of the fastener material
E_i	Modulus of elasticity of the plate 'i'

E_j	Modulus of elasticity of the plate' j '
E_{layer_x}	Young modulus of the material layer ' x '
E_{layer_k}	Young modulus of the material layer ' k '
E_{skin}	Young modulus of the skin
f_n	Reference to the fastener ' n '
FF	Fitting factor
$F_{\text{flight-max}}$	Maximum in flight force
$F_{\text{landing-max}}$	Maximum landing force
G_{fast}	Shear modulus of the fastener material
h	Vertical distance from the antenna base to the center of pressure
i	Index for number of different frequency and amplitude cycles
I	Inertia of the section
I_1	First inspection cycles number
I_{fast}	Moment of inertia of the fastener
I_{zz}	Inertia of the fuselage transversal section
K	Plate elastic constant
k	Total number of different frequency and amplitude cycles
k_{booms}	Number of mass booms
K_c	Accelerated crack growth asymptote
K_f	Fastener spring constant
K_I	Stress intensity factor
K_{Ic_crit}	Critical stress intensity factor
K_{In}	K_{Ic} for a determined loading cycle
K_{max}	Stress intensity factor corresponding to the peak applied load
K_{scatter}	Scatter factor
K_{tb}	Stress concentration factor, for bearing stress
K_{tg}	Stress concentration factor, for by-pass stress
K_x	Bush constant in the ' x ' direction
K_y	Bush constant in the ' y ' direction
K_z	Bush constant in the ' z ' direction
L	Constant which depend on the material
L_f	Aircraft length
L_{fast}	Distance between fasteners
$L_{\text{fast_length}}$	Fastener length
LF_{crit}	Critical load factor
L_m	Equivalent imposed distance between plates
M	Bending moment
m	Constant which depend on the material
Mat	Matrix of constants
M_{bend}	Bending moment the fuselage supports at the worst section

MFW	Maximum fuel weight
$MS_{\text{bearing-screws}}$	Safety margin of the antenna screws in bearing
MS_{doubler}	Safety margin of the doubler
$MS_{\text{eff-doubler}}$	Safety margin of the doublers' effectiveness
$MS_{\text{eff-rivet}}$	Safety margin of the rivet's effectiveness
$MS_{\text{shear-screws}}$	Safety margin of the antenna screws in shear
MS_{skin}	Safety margin of the skin effectiveness
MTOW	Maximum take-off weight
MZFW	Maximum zero-fuel weight
n	Constant which depend on the material
N_{det}	Minimum number of cycles from which the crack is detectable
N_f	Fatigue cycles number
n_{fact}	Load factor
N_{fail}	Number of cycles to failure
N_i	Maximum number of cycles at 'i' stress
n_i	Number of cycles at 'i' stress
N_{riv}	Effective number of rivets
P	Applied force in each particular case
p	Empirical constant
P_{aero}	Aerodynamic pressures during 1g flight
$P_{\text{app_100\%_eff}}$	Stress applied to the 100% effective doubler
P_{applied}	Applied load to the original skin portion
P_{bearing}	Ultimate design bearing load
$P_{\text{bearing_x}}$	Bearing ultimate load from the layer 'x'
$P_{\text{br-u}}$	Ultimate bearing load
$P_{\text{by-pass}}$	By-pass load
$P_{\text{crit-riv}}$	Critical rivet load
P_{diff}	Operating differential pressure
$P_{\text{doubler_x}}$	Load applied to the doubler 'x'
P_{doublers}	Load applied to the doublers
P_{drag}	Antenna drag load
P_f	Vector of fasteners' transfer loads
P_{f1}	Load transfer fastener row 1
P_{f2}	Load transfer fastener row 2
P_i	Transmission force referent to element 'i'
P_{inertial}	Inertial load
$P_{\text{layer_x}}$	Load transmitted to the layer 'x' of the doublers
P_{lost}	Lost load by the original skin portion
P_{net}	Ultimate design net tensile failure load
pp	Control in the asymptote's shape of the NASGRO equation

P_{preload}	Preload load
P_{pressure}	Pressure load
PR	Pressure at which the relief valve opens
P_{R1}	Load doubler plate row 1
P_{S2}	Load doubler plate row 2
$P_{\text{screw-shear}}$	Screw shear load
P_{skin}	Load applied to the skin
$P_{\text{su-riv}}$	Fastener shear failure load
$P_{\text{tear-out}}$	Tear-out failure load
P_{total}	Total antenna acting considered load
$P_{\text{trans_ult}}$	Load transferred by rivets at ultimate
Q	Applied load perpendicular to 'P'
q	Distributed load
qq	Control in the asymptote's shape of the NASGRO equation
r	Distance from crack tip to the center of the idealized plastic zone
R	Ratio between minimum and maximum stress
R_1	Vertical reaction force in the frontal antenna screws
R_2	Vertical reaction force in the rear antenna screws
R_{fus}	Fuselage radius
R_n	Reference to the doubler element 'n'
R_{shear}	Shear load ratio
R_{tensile}	Tensile load ratio
R_v	Vertical reaction force in the frame
S	Effective surface of the antenna
SCF	Stress concentration factor
S_{CF}	Strength correction factor
S_{eq}	Equivalent stress level
S_{max}	Maximum stress level
S_n	Reference to the skin element 'n'
T	Required torque to reach a preload level
t	Thickness of the particular case
t_{av}	Average thickness of the two plates
t_{doubler}	Doubler thickness
t_i	Plate 'i' thickness
t_j	Plate 'j' thickness
t_{skin}	Skin thickness
U	Palmgren Miner summatory
v	Free stream velocity
w	Width of the particular case
W	Antenna weight

W_f	Considered bending acting weight
$W_{\text{largest-doubler}}$	Width of the largest doubler
$W_{\text{wing-engines}}$	Conjunct wing plus engines weight
x_1	Distance from the nose to the installation place
y_{max}	Maximum distance from the gravity center of the section
α	Hole or surface factor
β	Hole filling factor
β_{IC}	Correction factor
β_m	Tabulated coefficient for the maximum stress formula
Δ	Transversal deflection of the fastener
ΔI	Recurrent inspection period
ΔK_n	Stress intensity factor equivalent
ΔK_{th}	Fatigue threshold
ΔN	Cycles iteration increment
ΔP	Transfer or bearing load
ΔP_{max}	Maximum design load
$\Delta \sigma$	Skin gross area stress
$\Delta \sigma_{\text{max}}$	Maximum design stress
$\Delta \sigma_{\text{total}}$	Extra total stress
Θ	Bearing distribution factor
ϑ	Half angle of the opening crack
μ	Lubrication coefficient
ρ	Density
σ_1	Stress in the direction 1 from the picture
σ_2	Stress in the direction 2 from the picture, perpendicular to 1
$\sigma_{\text{applied-doubler}}$	Stress applied to the doubler
$\sigma_{\text{applied-skin}}$	Stress applied to the skin
σ_{bend}	Bending stress
$\sigma_{\text{br-u}}$	Ultimate bearing stress
$\sigma_{\text{br-y}}$	Yield bearing stress
$\sigma_{\text{by-pass}}$	By-pass stimated stress
σ_{drag}	Drag force stress
σ_{hoop}	Hoop direction stress
σ_{inertial}	Inertal forces stresses
σ_{long}	Longitudinal direction stress
σ_{max}	Maximum stress
σ_{min}	Minimum stress level
σ_{press}	Pressure stress
σ_{ref}	Reference stress
σ_{res}	Residual strength requirement

σ_{s-u}	Ultimate sheat stress
σ_{s-y}	Yield shear stress
σ_{trans}	Transfer or bearing stress
σ_{t-u}	Ultimate tensile stress
σ_{t-y}	Yield tensile stress
$\sigma_{total_applied}$	Total applied stress
σ_{ult_design}	Ultimate design tensile stress
σ_{xx}	Effective 'x' direction or longitudinal stress
σ_{xy}	Effective 'xy' direction shear stress
σ_y	Yielding ultimate stress
σ_{yy}	Effective 'y' direction stress
σ_{θ}	Tension in function of the angle
$\sigma_{\pi/2}$	Tension for a θ of $\pi/2$
σ_{Ω}	Tension in function of Ω
Ω	Angle from the hole center

1 Introduction

1.1 Motivation

During the operational life of the most aircrafts, they are subjected to new updates or installation of new components. Some of these modifications require a structural reinforcement in order to ensure the security of the aircraft. Since these modifications implicate drilling holes to the fuselage skin, they always require some structural reinforcement in order to ensure the good behavior of the whole aircraft structure, avoiding a possible catastrophic failure. These structural reinforcements to metallic fuselages usually consist in metallic reinforcing layers which are riveted to the skin, and must recover that zone's structural resistance. They are called doublers, and may have different configurations.

Safety is an important issue in the aerospace industry. This thesis has been developed at the PME (Projects and Modifications Engineering) department of the company OGMA-Indústria Aeronáutica de Portugal, SA. The company is an approved DOA (Design Office Approval) by EASA. It implicates that is authorized to directly classify and approve any "minor modification". However, an antenna install implicates a structural modification to the exterior of the fuselage, so it is classified as a "major modification". Any "major modification" project must be approved by the agency EASA. That certification process requires the development of a report which must contain all the specific technical information related with the project.

Therefore the purpose of this thesis is the development of a methodology aided by a group of tools to structurally verify and validate these doublers. That output is going to be used by OGMA-Indústria Aeronáutica de Portugal, SA, with the objective of certifying some antenna installations with EASA. The main target is to optimize the structural calculus of a generic antenna installation to the fuselage of a pressurized aircraft. The direct result of the developed work is to reduce the engineering hours, therefore to accelerate the calculus and optimize the costs of any project related with.

1.2 Objectives

The main objective is to create a methodology aided by a group of tools which allow sizing and justify the reinforcement in terms of statics, fatigue and damage tolerance having as inputs the loading, geometry, and material properties. It is aimed to develop a methodology capable of obtaining the results for one configuration in less than two hours' time.

Therefore the thesis' output procedure consists in designing a doublers geometry, and then checking first the statics, then the fatigue, and eventually the damage tolerance behavior. If any of these steps is not correct, the geometry must be redefined entering in an engineering iterative process. In the Figure 1.1 the global flowchart of what is intended to be the output methodology of the thesis's can be observed.

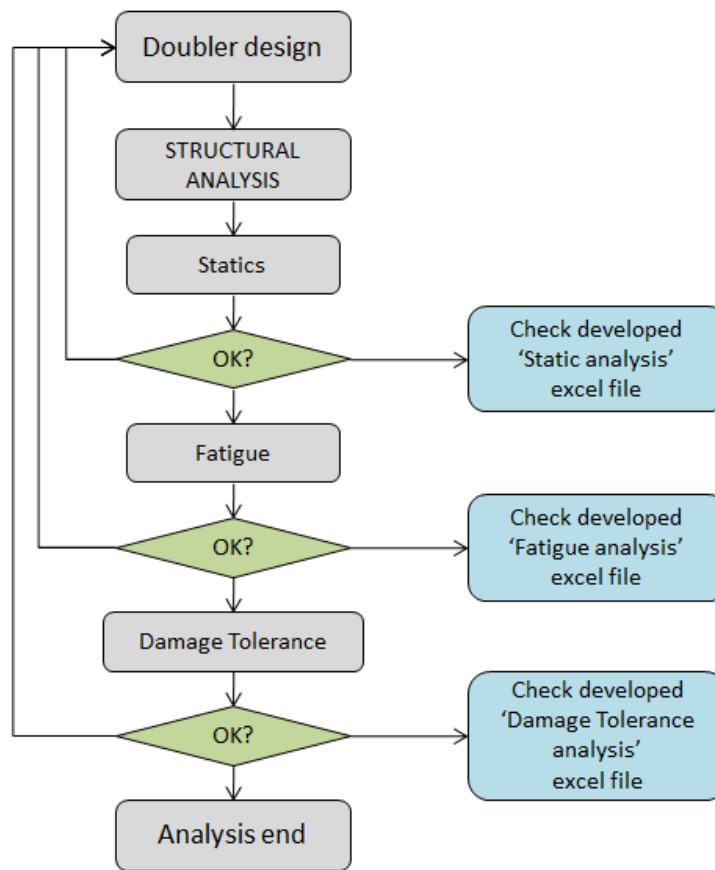


Figure 1.1- Global project flowchart

1.3 Thesis structure

The current thesis is made of 6 chapters. The first of them is the introduction, where the general scope of the thesis is presented.

The second chapter consists in a study of the aerodynamic and inertial implications of an antenna installation to the fuselage skin, where a method to determine whether the installation will simply need a doubler based reinforcement, or if it will require some extra structural modifications is defined. The current thesis just allows checking doublers reinforcements, so the second chapter defines if an antenna install is inside or outside the thesis scope.

The third chapter presents the static followed principles, and applies them with the objective of defining some safety margins which will check the static behavior of the structure.

The fourth chapter presents the fatigue followed principles, and applies them with the objective of defining a number of cycles that the aircraft modification is projected for. It will allow checking the fatigue behavior of the structure.

The fifth chapter presents the damage tolerance followed principles, and applies them with the objective of obtaining an inspection program for the structural modification. It will allow checking the damage tolerance behavior of the structure.

Eventually, the sixth chapter contains the main conclusions extracted from that project, and the seventh a future work suggestion in the same area.

1.4 State of the art

1.4.1 Static analysis

1.4.1.1 Introduction

There are many factors to have into account when analyzing the statics of a metallic fitting. The tensile, shear, bearing stresses or loads of the metallic plates, shear loads of the fasteners, etc. Some theoretical relevant concepts are shown in these sections below.

1.4.1.2 Joint failure modes

A study of all the possible failures that can occur to the material sheet is done. The most common failure modes for this kind of structures are the following ones. The references [1] and [2] have been used.

1.4.1.2.1 Net tension

Net tension failure is defined as a plate tensile failure that occurs between two fasteners along a plane normal to the applied load. When there is a hole the net area reduces and thus the tension reaches higher values if it has to carry the same load than before. In the Figure 1.2 that effect is illustrated.

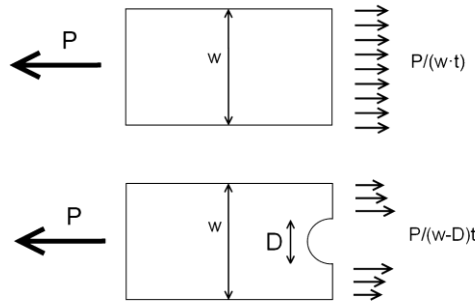


Figure 1.2- Net tension representation

The sketch of the failure mode can be seen in Figure 1.3.

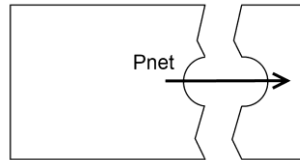


Figure 1.3- Net tension failure mode

The equation needed to estimate that (P_{net}) is the equation (1.1) [1]. The variable (σ_{t-u}) represents the ultimate tensile stress, (σ_{t-y}) is the tensile yield stress, (A_{net}) is the net area of the hole section.

$$P_{net} = \text{MIN}(\sigma_{t-u} \cdot A_{net} \text{ or } 1,5 \cdot \sigma_{t-y} \cdot A_{net}) \quad (1.1)$$

1.4.1.2.2 Tearing out

Tear out failure is a plate shear failure that occurs along two planes parallel to the applied load. Figures Figure 1.4 and Figure 1.5 show that failure mode. The equation for tearing out must only be used if test data is not available or applicable to the specific case.

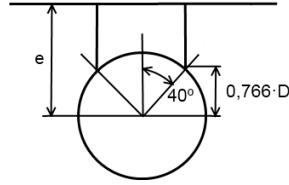


Figure 1.4- Tearing out lengths representation

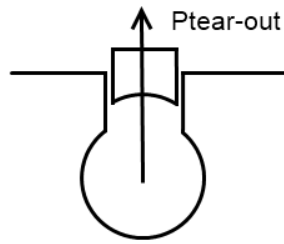


Figure 1.5- Tearing out failure mode

The expression for assessing the tear out load ($P_{\text{tear-out}}$) is the (1.2) [1]. The variable (t) is the thickness, and (D) is the hole diameter, and (e) is the distance from the hole center to the edge.

$$P_{\text{tear-out}} = \sigma_{t-u} \cdot t \cdot (2 \cdot e - 0,766 \cdot D) \quad (1.2)$$

1.4.1.2.3 Bearing failure

The bearing failure can be described as the hole's plastic deformation due to the maximum load the specimen can withstand.

From the reference [3] requirements, the bearing load (P_{bearing}) can be calculated with the equation (1.3) [1]. The variable (σ_{br-u}) is the ultimate bearing stress, and (σ_{br-y}) is the bearing yield stress.

$$P_{\text{bearing}} = \text{MIN}(\sigma_{br-u} \cdot D \cdot t \text{ or } 1,5 \cdot \sigma_{br-y} \cdot D \cdot t) \quad (1.3)$$

In the case that the hole is not a net circle (for example with the countersunk head rivets), equation (1.3) cannot be applied directly. One option is to calculate the equivalent diameter of the hole, although the best way to determine the bearing failure is through examining the available test data.

1.4.1.2.4 Fastener shear failure

Fastener shear failure consists in a shear failure of the fastener shank. The maximum load (P_{su-riv}) that meets the ultimate criteria for the fastener shear is defined by the next expression, in function of the ultimate shear stress (σ_{s-u}).

$$P_{su-riv} = \sigma_{s-u} \cdot \frac{\pi \cdot D^2}{4} \quad (1.4)$$

It is always more suitable to use the shear value from the specific data sheet from the fastener if available, or to estimate it through the reference [3] at the table shown in the Attachment B.2.

1.4.1.2.5 Transitional failure

Transitional failure involves the rest of possible failure modes. Any mechanism failure other than the shank shear, the shear out, the net tension, and the bearing is considered a transitional failure. One example of transitional failure would be the fastener pull through. This typically happens in thin sheets when fastener head is pulled through the material sheet.

1.4.1.3 Defined requirements to avoid failure

Generally it is not necessary to calculate the tear out load. There are some rules to avoid that kind of failure mode at the edge margin of a sheet. For the rivets that are placed at the edge margin, the failure can be avoided just by ensuring a distance of 2 times the diameter from the edge till the nearest hole, like can be observed in Figure 1.6.

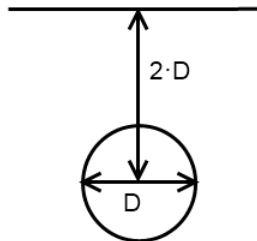


Figure 1.6- Minimum hole to edge distance

In that case, the effective bearing area is reduced by using a countersunk fastener. The countersunk does not resist the bearing load as well as the shank of the fastener. It requires the edge margin to be increased for flush head fasteners. Therefore, it is recommendable to use the average hole diameter. To avoid shearing or tearing out of material in a joint, a row spacing of $3D$, can effectively avoid the inter-fastener shear out effect. However, for the holes that are placed inside the sheet, the minimum row spacing is 4 times the diameter of the hole. That spacing which is net section critical for both tension (stress concentration factor would increase rapidly otherwise) and shear (hole-out) efficiency. In Figure 1.7 that definition is illustrated. [1] [2].

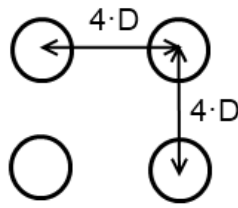


Figure 1.7- Minimum inter rivet distance

For holes that are placed inside the sheet, the minimum row spacing is around 6-8 times the diameter in order to prevent the failure due to inter-rivet compression buckling.

1.4.2 Fatigue analysis

1.4.2.1 Introduction

Safe-life:

The safe-life design philosophy was developed between the 1930's and 1940's. The main objective of it is that the important structural elements must be replaced once a determined number of life cycles has been reached. No repair was allowed on these parts. The method of analyzing a structural component in safe-life way is the fatigue analysis. The fatigue analysis gives as output a number of cycles that the concrete structural component can withstand without suffering a crack initiation. [1] This fatigue analysis also requires an accurate prediction of the stress concentration factor.

The following Figure 1.8 shows the main points of the fatigue calculations. Some theoretical relevant concepts are shown in these sections below.

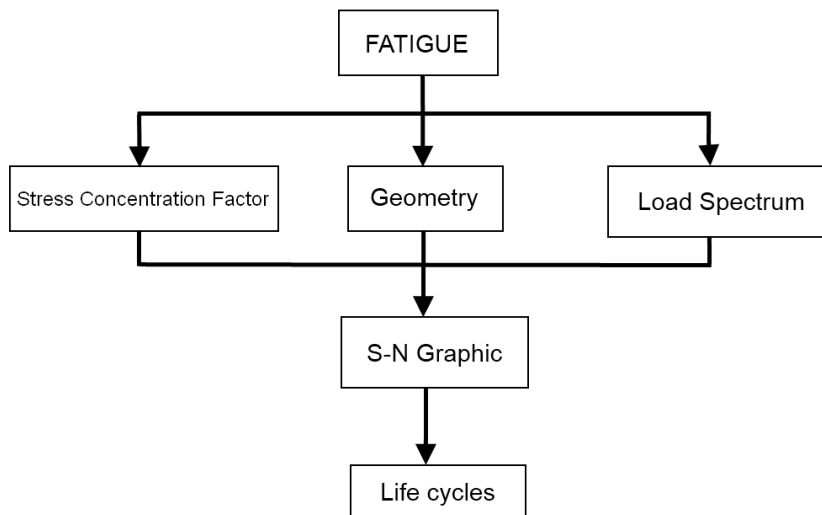


Figure 1.8- Fatigue main issues

1.4.2.2 Load spectrum

In the fatigue analysis, the considered loads cannot be the ultimate loads from the material anymore. Instead of that, the real load which the fuselage suffers must be estimated. They are usually called “running loads”.

A real fuselage load spectrum example to which an airplane fuselage is subjected is good represented in the Figure 1.9, from the reference [4]. Since the simple method adopted before is not applicable here, the Palmgren Miner's law is adopted.

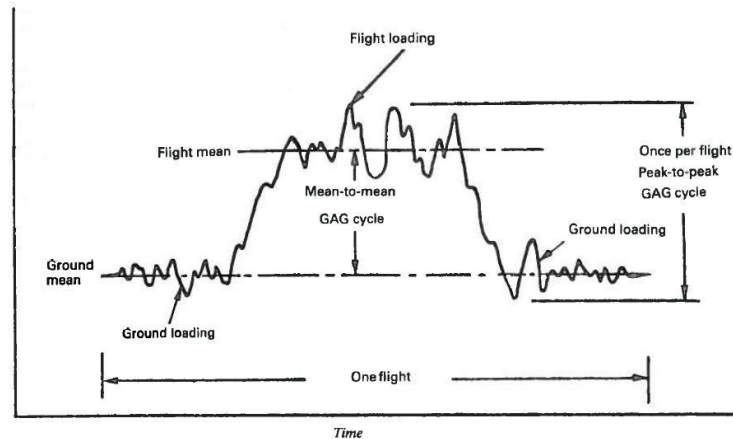


Figure 1.9- Ground-Air-Ground loading graphic definitions for fatigue analysis [4]

1.4.2.2.1 Palmgren-Miner's law

The main hypothesis of that method is that the fatigue damage that a structure absorbs at a concrete stress level is proportional to the number of cycles applied to at that level (n_i) divided by the number of cycles that cause the failure at that level (N_i). Therefore for each stress level, there is one ratio. The sub-division of the real GAG (Ground-Air-Ground) spectrum with some different spectrums is shown in the Figure 1.10. The sum of the different ratios (U) gives the ratio of damage per cycle. The total fail of the structure occurs when that ratio reaches the unity. [1][2][4]

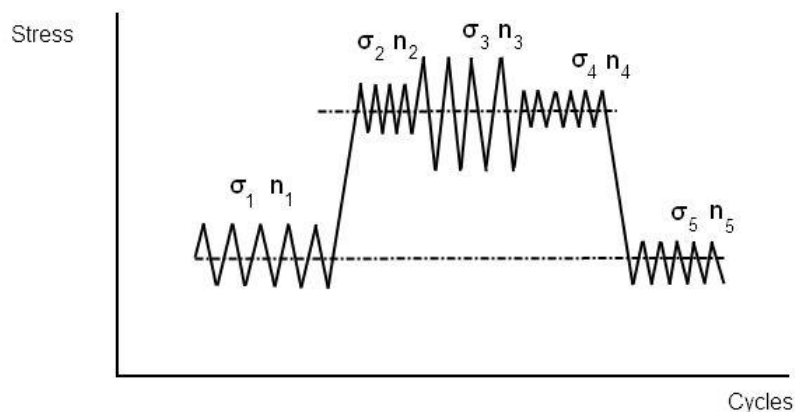


Figure 1.10- Load spectrum scheme for applying Palmgren Miner's rule

$$U = \sum_{i=1}^k \left(\frac{n_i}{N_i} \right) = 1 \quad (1.5)$$

It is important to remark that the Palmgren-Miner law is one of the most used in the aerospace industry because of its simplicity and its good results. However, it has 2 important limitations: It does not take account of both the load sequence, and the notch effect.

1.4.2.3 Stress concentration factor calculus

The stress concentration factor (SCF) is a ratio between the maximum reached stress in some location, and a reference stress which causes it. The formula (1.6) shows this ratio. The variable (σ_{\max}) is the maximum stress, and (σ_{ref}) is the reference stress.

$$\text{SCF} = \frac{\sigma_{\max}}{\sigma_{\text{ref}}} \quad (1.6)$$

Once the load spectrum has been properly defined, the next step is to define the Stress Concentration Factor, and find its worst possible location.

For either an antenna installation or a fuselage repair, a cutout, and the rivet holes must be done to the fuselage skin. When a hole is made to one panel, there will be a concentration of tension at the intersection of the hole's perimeter with the line that passes through the hole's center and is transversal to the reference stress. That effect is not taken into account when analyzing the statics of the problem, however it is critical in terms of fatigue, and must be properly analyzed. For a flat plate with a through hole, the stress concentration is represented in the Figure 1.11.

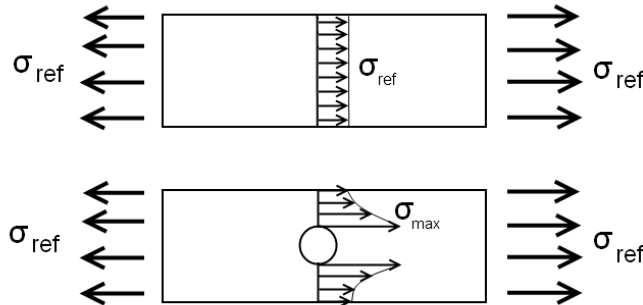


Figure 1.11- Stress concentration around a hole in a flat plate

For a simple empty hole [14],

$$\sigma_{\max} = 3\sigma_{\text{ref}} \quad (1.7)$$

However, when analyzing a fastened fitting, the load transfer is not so clear, and the applied load gets distributed between the different lines of fasteners, This will cause that in each row some part of the load gets transmitted through the fastener, and the rest of load remain in the fitting layer. That load distribution is important because will have an important effect on the stress concentration factors, and thus in the fatigue life of the specimen.

There are many different ways of estimating the stress concentration in a joint, in the bibliography or even each manufacturer may have its own one. In this thesis the analyzed formula has been the following one, which is commonly used in the aerospace industry. [4]

$$\sigma_{\max} = \sigma_{\text{trans}} + \sigma_{\text{by-pass}} = K_{\text{tb}} \frac{\Delta P}{D \cdot t} \theta + K_{\text{tg}} \frac{P_{\text{by-pass}}}{w \cdot t} \quad (1.8)$$

$$\text{SCF} = \alpha \cdot \beta \frac{\sigma_{\max}}{\sigma_{\text{ref}}} \quad (1.9)$$

The variable (ΔP) is the transfer or bearing load, ($P_{\text{by-pass}}$) is the by-pass load; (K_{tb}) and (K_{tg}) are the SCF for bearing and by-pass respectively, (θ) is the bearing distribution factor, and (α) and (β) are the hole surface and filling factors respectively, from the reference [4], and they have been introduced into the developed excel in order extrapolate the functions equations and automatize the calculus. It can be observed at the tables shown in the Attachment C.

1.4.3 Damage tolerance analysis

1.4.3.1 Introduction

Fail Safe:

The fail safe design philosophy consists in considering several possible load paths for a structural load. If one load path totally fails, the remaining load paths, which are supposed to be in perfect state, must be able to carry the additional loads without breaking. That design philosophy is used in some parts of the aircrafts nowadays, like at some wing panels, wing ribs, some stringers in both wing and fuselage, in some fittings, etc. Although the fail safe principle has optimal results and it is still used in the design of new aircraft, there is some deficiency with that design philosophy. The fractures usually do not appear in just one load path, they can appear simultaneously in several load paths at the same time. Therefore that way of analyzing a structural component is not completely trustable. To overcome that deficiency the Damage Tolerance design principle was developed.

Damage tolerance:

The damage tolerance design philosophy consists in the assumption of that any damage in the aircraft must be detected and properly repaired or replaced before their structural integrity decrease bellow the established fail safe limits. So the damage tolerance analysis has as output the inspection plan in order to ensure the detection and reparation of the damage. One way of improving the DT is through MSD, Multi-Site Damage. That philosophy assumes that the structure is damaged with different cracks that grow at the same time. When the crack growth is simulated, there are two ways the structure can fail. The analysis finishes when any of those is reached. One way is when the Stress Intensity Factor (K_{IC}) gets critical or the critical crack length is reached, which are material known properties. From the reference [3] some critical intensity factors can be obtained. The second one is the Residual Strength requirement, which must be introduced as a parameter in the AFGROW software. It is due to the fact that the residual strength requirement can be different depending on different variables, like the aircraft model, pertinent part of the aircraft, the entity which dictates the requirement, etc. So the

structure fails either when a critical crack length is reached, or when the residual strength goes under the residual strength requirement.

The three principal issues in a damage tolerance analysis are the following ones, also represented in Figure 1.12. These three issues are inter-related, therefore any change in one of them directly affects to the others. Some theoretical relevant concepts are shown in the sections below.

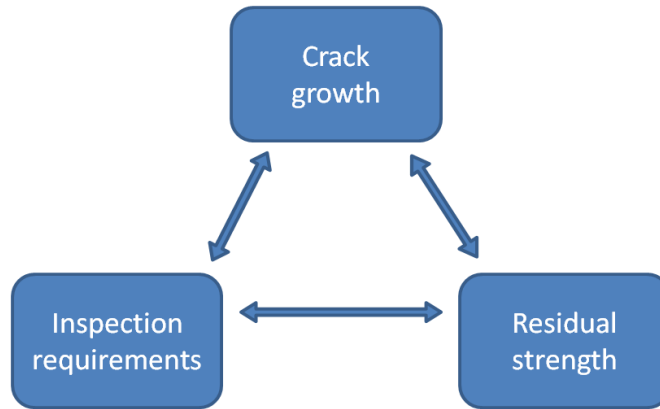


Figure 1.12- Damage tolerance main issues

1.4.3.2 Residual strength

Residual strength is the degeneration of the structural strength capability during the life of a component. The target of its assessment is to determine the amount of fatigue damage the component can withstand remaining into the fail safe requirements. In the Figure 1.13, the residual strength general behavior against the crack length can be appreciated. [1]

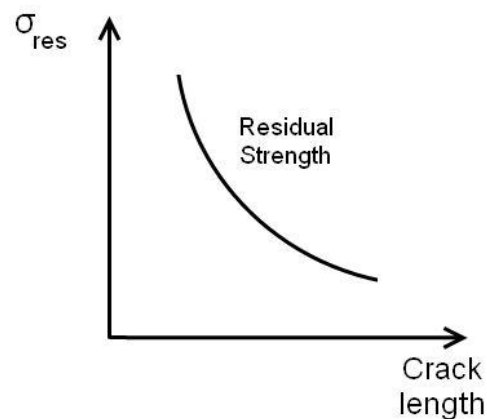


Figure 1.13- Residual strength evolution against crack length

In the Figure 1.14, from the reference [1], it can be observed how the structural strength capability of a component decreases from the ultimate load requirement during the aircraft life until the damage is detected and repaired, never reaching the residual strength limit requirement. It is important to see that the operational life loads are always below both ultimate and residual strength requirements.

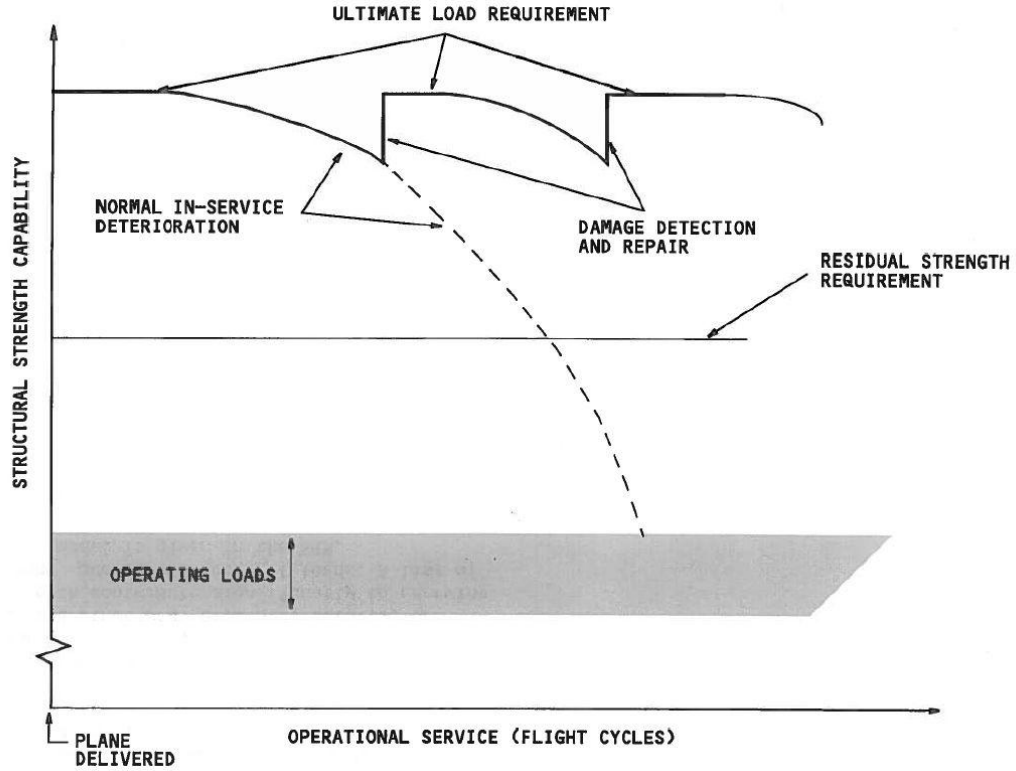


Figure 1.14- Structural strength capability during the flight life [1]

The residual strength requirement (σ_{res}) is defined at the reference [5], and the condition is shown at the following expression. It is an important parameter because defines a total failure criterion in the damage tolerance. The variable (P_{diff}) represents the operating differential pressure, and (P_{aero}) is defined as the aerodynamic pressures during 1g flight.

$$\sigma_{res} = 1.15(P_{diff} + P_{aero}) \frac{R_{fus}}{t} \quad (1.10)$$

1.4.3.3 Crack growth analysis

The main objective of the crack growth analysis is to represent the graphic of the crack length against the cycles. The slope of that graphic is called the crack growth rate. The formulas simulating this growth are studied in the section 5.2.4. The crack growth rate is defined in function of the stress intensity factor, explained in the following sections. A representation of these two graphics is shown in Figure 1.15.

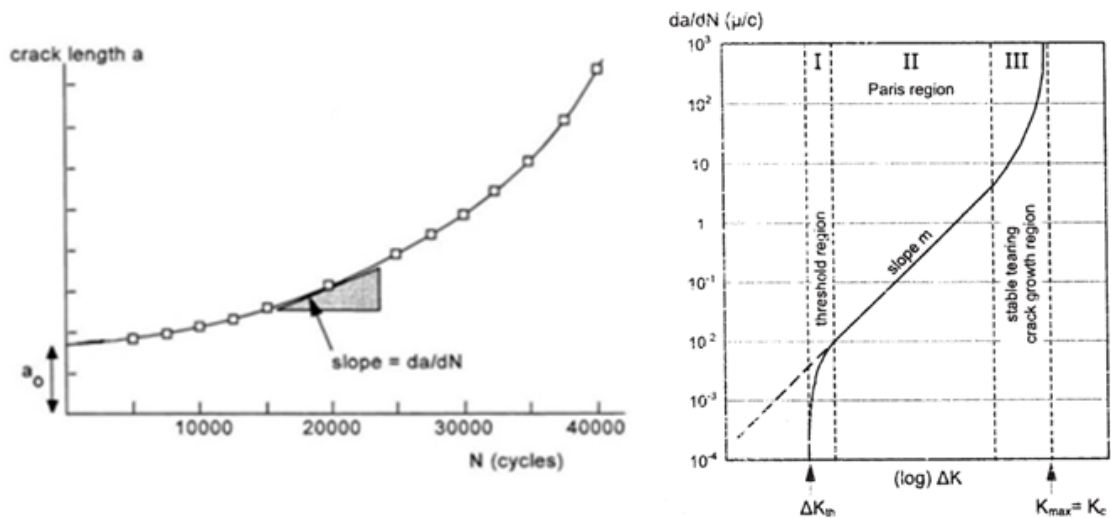


Figure 1.15- Crack length and crack growth rate graphics [6]

1.4.3.3.1 Crack retardation

Crack retardation during the service life of a component can occur due to an overloading. It consists in the application of a load higher than expected to the component. It causes an increase of the plastic zone, which makes the crack growth slope decrease, what directly implicates retardation on the crack growth. This effect is temporary and eventually rate returns to the previous level again, and is represented in the Figure 1.16. [1] [6]

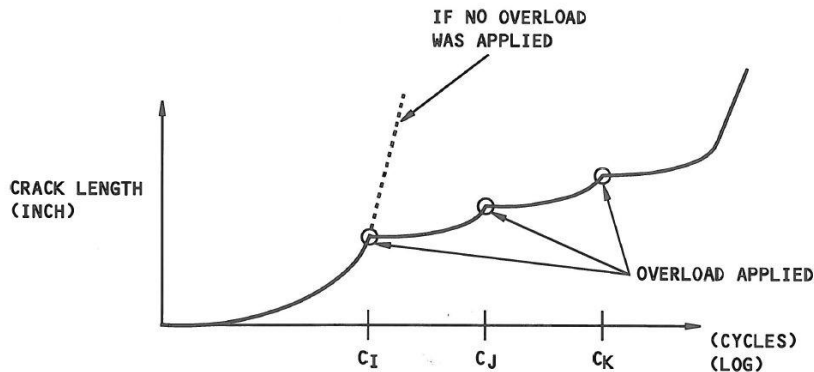


Figure 1.16- Crack growth evolution with overloads applied [1]

1.4.3.3.2 MSD Multiple-Site Damage

The damage tolerance concept design for pressurized fuselage structures was based on the crack growth prediction of single flaws in the skin. The fail-safe design of the structure predicts the cracks and includes extra load paths which intend to absorb the crack propagation. However, in 1988 Aloha Airlines accident demonstrates that the initial fail-safe design was not able to stop the crack growing, and it meant a total failure of the structure. The reason of that was that it did not take into account the possibility of several cracks propagating from different positions. The reason for that is the aging of the aircraft structure. Evaluating the airworthiness of an old aircraft which may contain multiple cracks is an important issue, because those kinds

of cracks are small, usually hidden by paint, and not easily accessible for inspection. The MSD influence in the crack growth can be observed in the Figure 1.17. [7]

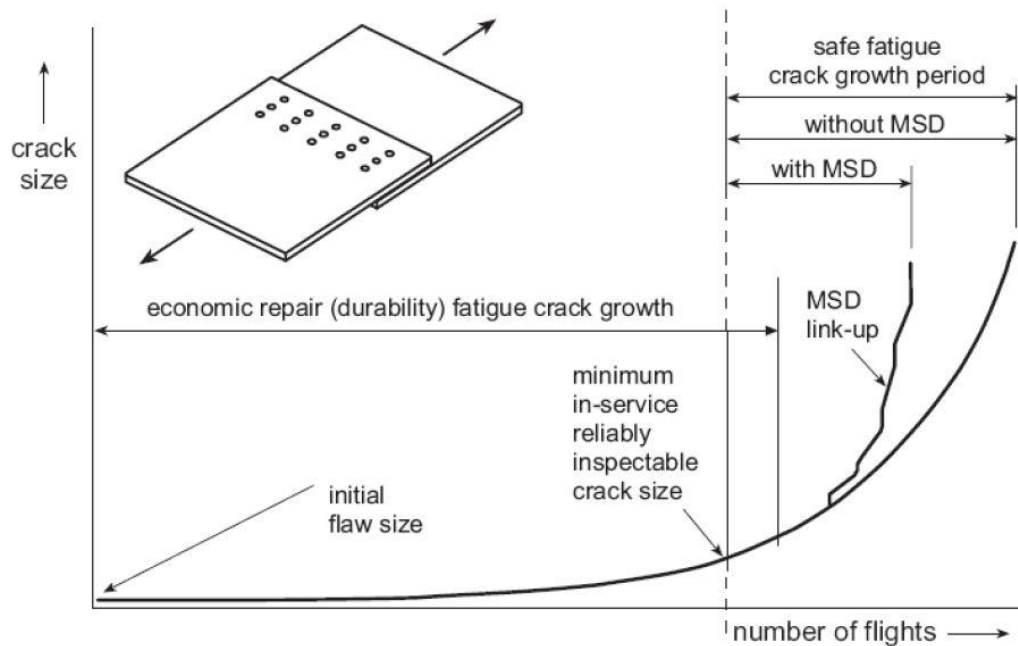


Figure 1.17- Crack size growth MSD influence [8]

1.4.3.4 Linear elastic fracture mechanics (LEFM)

LEFM is a theory or method of analyzing which allows assessing, predicting and measuring the fracture toughness and the stress intensity in the crack tip. Fracture toughness can be presented as the capability of a component of containing a crack, and suffering a load without failing, and depends on a lot of factors, like environment, temperature, applied loading range, etc. [6] [9]

1.4.3.4.1 Modes

The LEFM contemplates 3 different possible crack modes, shown in Figure 1.18:

- Mode I: Tensile stress, the crack surfaces move apart. Stress intensity factor: K_I
- Mode II: Shear stress, the surfaces slide in a direction perpendicular to the crack's edge. With stress intensity factor: K_{II}
- Mode III: Tearing or anti-plane shear stress, the surfaces move parallel to the crack's edge, one relative to the other. With stress intensity factor: K_{III}

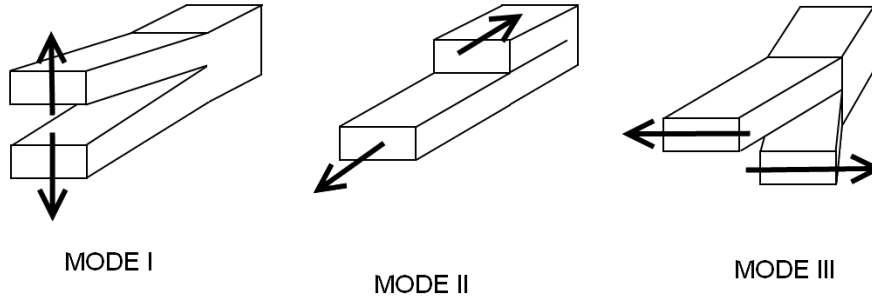


Figure 1.18- Three failure modes scheme

1.4.3.4.2 Stress intensity factor

The linear theory states that the stresses at a crack tip tend to infinite. However, in the real a plastic zone exists where these limits tend to finite values. Assessing the real stress the material is withstanding on this plastic zone is very difficult. An engineering approximation consists in carrying experimental tests and reaching the critical intensity factor (K_{Ic_crit}) for each material. It is called as materials' fracture toughness. The comparison between (K_I) and (K_{Ic_crit}) is important to determine the crack stability. The mode I stress intensity factor is the most often used in engineering design. In Figure 1.19 the stresses on the crack tip zone are represented. Below there are the correspondent expressions, which are taken from the reference [9]. The variables (σ_{xx}), (σ_{yy}) and (σ_{xy}) represent the stresses in the different directions, and (θ) is the half angle of the opening crack. The following equations (1.11), (1.12), and (1.13) have more terms, which are omitted because they do not have an important influence.

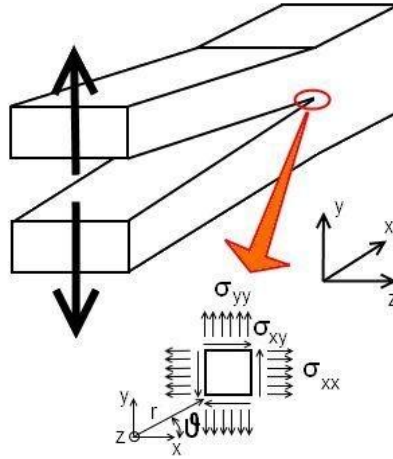


Figure 1.19- Plane stresses at the crack tip for mode I

$$\sigma_{xx} = \frac{K_{IC}}{(2\pi r)^{1/2}} \cos\left(\frac{\theta}{2}\right) \left[1 - \sin\left(\frac{\theta}{2}\right) \sin\left(\frac{3\theta}{2}\right) \right] \quad (1.11)$$

$$\sigma_{yy} = \frac{K_{IC}}{(2\pi r)^{1/2}} \cos\left(\frac{\theta}{2}\right) \left[1 + \sin\left(\frac{\theta}{2}\right) \sin\left(\frac{3\theta}{2}\right) \right] \quad (1.12)$$

$$\sigma_{xy} = \frac{K_{IC}}{(2\pi r)^{1/2}} \cos\left(\frac{\theta}{2}\right) \left[\sin\left(\frac{\theta}{2}\right) \cos\left(\frac{3\theta}{2}\right) \right] \quad (1.13)$$

1.4.3.4.3 Plastic zone crack tip

Equation (1.14) shows how the stress tends to infinite at the crack tip. However, in the reality the materials tend to reach its yielding stress (σ_y). Therefore a simple way of estimating the plastic zone size (r) is shown by the equation (1.15), and it can be observed in Figure 1.20. It is important to remark that is a case of plane stress.

$$\sigma_{yy} = \frac{K_I}{(2\pi r)^{1/2}} = \sigma_y \quad (1.14)$$

$$r = \frac{1}{2\pi} \left(\frac{K_I}{\sigma_y} \right)^2 \quad (1.15)$$

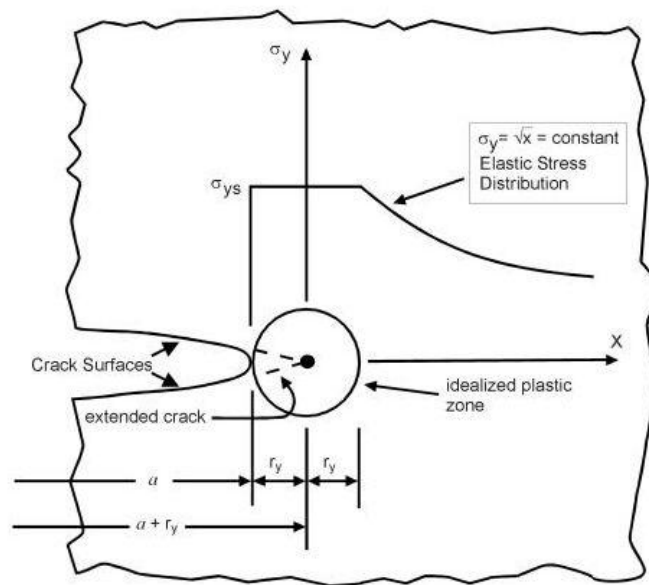


Figure 1.20- Idealized crack plastic zone scheme [10]

1.5 Regulation requirements

Table 1.1 contains the regulation requirements that have been taken into account during all the thesis technical development. They are defined by EASA, in the CS-25 report (Certifications and Specifications and Acceptable Means of Compliance for Large Aeroplanes).

Reference	Requirement	Description
CS-25	303	Factor of safety, ultimate design load
CS-25	305 (a)	Strength and deformation
CS-25	307 (a)	Proof of structure
CS-25	365 (a)(b)(c)(d)	Pressurized compartment loads, limit load
CS-25	571	Fatigue and Damage Tolerance, Residual strength
CS-25	625	Fitting factors

Table 1.1- Regulation requirement list

2 Aerodynamic and inertial antenna structural implications

The three main forces which perform at a fuselage antenna's zone are the aircraft pressurization, the inertial, and the aerodynamic loads. So the objective of that section is to evaluate the contribution of the aerodynamic and inertial forces within an antenna, and after compare them with the pressurization load. Some easy and fast methods are developed for determining whether is enough or not to provide a structure of a simple reinforcement like a doubler or group of doublers, or if otherwise it is necessary to implement more important changes (like adding extra frames or stringers) to the aircraft structure when installing an antenna on the skin of a pressurized fuselage. Figure 2.1 shows a general scheme of the process that must be followed before the antenna install.

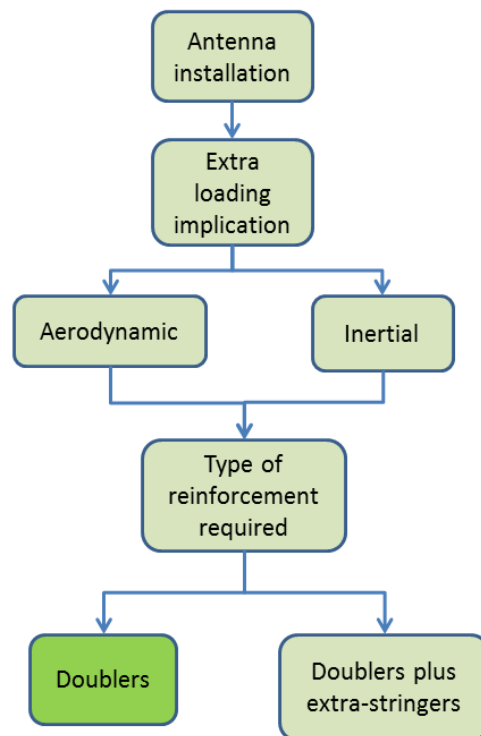


Figure 2.1- General procedure for a new antenna install flowchart

An antenna is an object with its own mass, and which is attached at the external fuselage, so the most important forces which act over it are the inertial and the aerodynamic forces. The followed procedure defines some simplifications of the structure in order to make it possible to use analytic formulas to determine if simple curved plate shape reinforcement (doubler) is enough. To validate that calculation, FEM models have been developed as well in order to verify the analytic formulas. The aerodynamic and inertial forces are studied separately. For being conservative extreme conditions are taken.

In this case the aircraft in study is the Lockheed C-130, and the antenna data chosen for the example of analysis is the L-Band S65-5366-7L from Dallas Avionics, shown in the Attachment D. Figure 2.2 shows the procedure followed in this section to validate the analytic formulas.

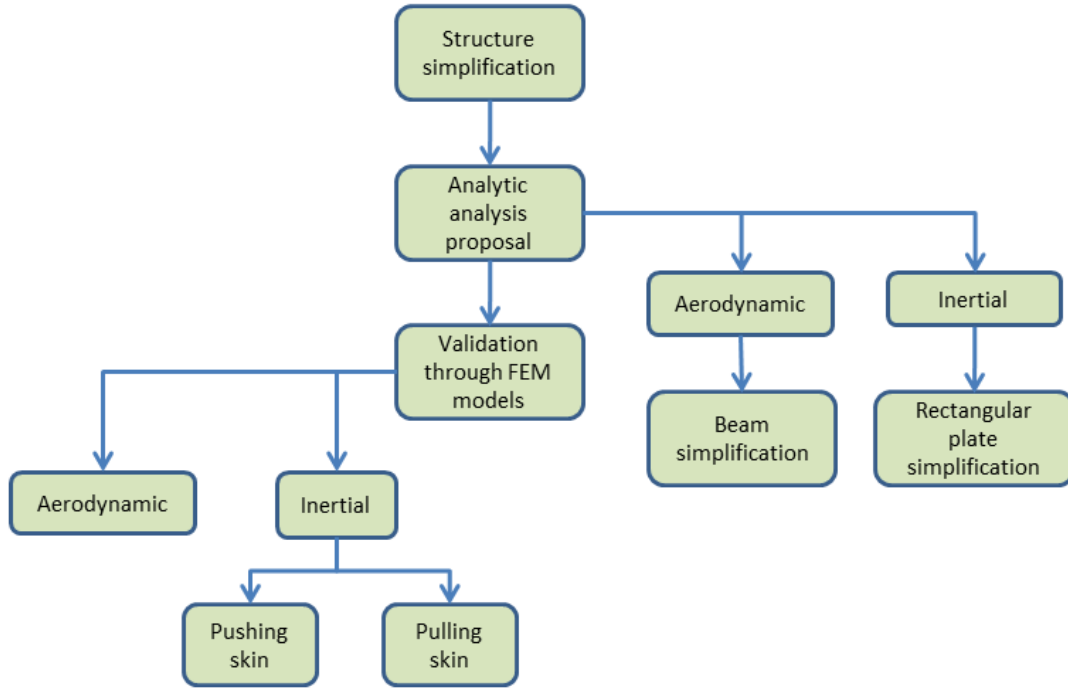


Figure 2.2- Followed verification method flowchart

2.1 Analytic analysis

2.1.1 Aerodynamic antenna forces

The antennas' shape is usually made aerodynamic in order to soft the extra load transmitted to the aircraft. However, there is always a non-ignorable drag force implication, which can be estimated in many different ways.

The first option is estimating the drag coefficient from the antenna geometry and using the basic formula for assessing the drag (2.1), where (ρ) is the air density, (v) is the free air stream speed, (S) the front effective surface of the antenna, and (C_D) the drag coefficient.

$$\text{Drag} = 0,5 \cdot \rho \cdot v^2 \cdot S \cdot C_D \quad (2.1)$$

The second option is using the next formula (2.2) given in the FAA AC 43-13-2B [11] for estimating the antenna's drag, with (A_{front}) as the frontal antenna's area in square inches.

$$\text{Drag} = 0,000327 \cdot A_{\text{front}} \cdot v^2 \quad (2.2)$$

The third and chosen option is taking the critical drag value from the pertinent antenna model data sheet, if available. In the example case the design drag value is $\text{Drag} = 1\text{oz}$ (0.28N), which corresponds to a flight condition of Mach 0.85 at 35.000ft (10668m).

The simplification adopted consists in assessing the skin stresses like if it was a beam, with the antenna placed in the worst possible position, the middle between two frames. Figure 2.3 shows it. The variable (R_v) is the vertical reaction created at the frames, (R_1) and (R_2) are the vertical reactions which transmit the Drag force to the fuselage skin through the fastening screws, (h) is the vertical distance from the skin to the estimated center of pressure of the

antenna, (d) is the distance between screws, (d_r) is the distance from screw to frame, and (t_{skin}) is the skin thickness.

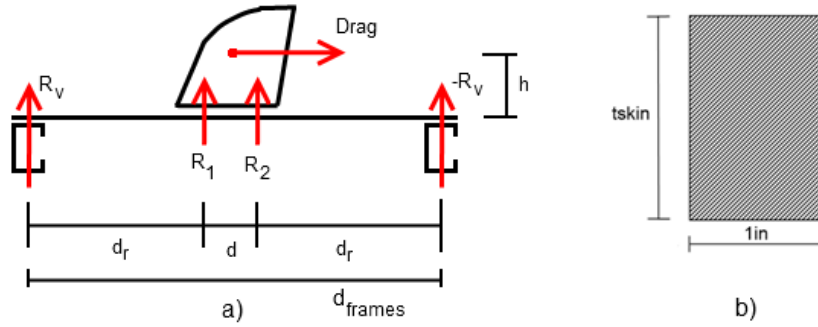


Figure 2.3- Fuselage beam simplification a), and beam section b)

Hypothesis:

- Aerodynamic and inertial loads are totally absorbed by the screw fixing points creating a moment on the skin.
- Simplification of the aircraft skin as a beam with both simply supported ends.
- The antenna installation is placed at the middle of the two frames, which is the most critical point.

The reactions created by the antenna to the fuselage skin are obtained through moment and forces equilibrium. The equation signs are taken based on Figure 2.3 scheme.

$$R_1 = -\text{Drag} \cdot \frac{h}{d} \quad (2.3)$$

$$R_2 = \text{Drag} \cdot \frac{h}{d} \quad (2.4)$$

These reactions on the antenna fasteners create a reaction at the nearest frames, which can be calculated by the equation (2.6). The variable (d_{frames}) is the inter-frames distance.

$$d_r = \frac{d_{frames} - d}{2} \quad (2.5)$$

$$R_v = \frac{R_1 \cdot d_r + R_2 \cdot (d + d_r)}{d + 2 \cdot d_r} \quad (2.6)$$

Thus the value of the bending moment (M) and the stress created on the skin at the fastener section (σ_{drag}) is:

$$M = R_v \cdot d_r \quad (2.7)$$

$$\sigma_{drag} = \frac{M}{I} \cdot y_{max} = \frac{M}{\frac{1}{12} \cdot t_{skin}^3} \cdot \frac{t_{skin}}{2} \quad (2.8)$$

The values for an example are shown in the Table 2.1.

d [in]	3,3 (84mm)
d _{frames} [in]	20 (508mm)
d _r [in]	8,35(212mm)
R _v [lbs]	-0,0068 (0.03N)
I [in ⁴]	2,08373E-05 (8.673mm ⁴)
t _{skin} [in]	0,063 (1.6mm)
M [lbs·in]	0,0574 (6.48N·mm)
σ _{drag} [psi]	86,78 (0.59MPa)

Table 2.1- Values for the example

2.1.2 Inertial forces

To estimate the most critical possible inertial forces the plane may suffer, the antenna weight and the critical design load factors of the aircraft must be determined. The simplification adopted in that case is to treat the skin portion between the frames and the stringers like a flat plate with straight boundaries and constant thickness, with a rectangular and uniform distributed load located at the center Figure 2.4. The simplification of this kind of load distribution is appropriate for the cases in which the inertial forces push against the skin. In the case that the inertial forces pull to the outside that simplification is not as accurate, although it is conservative.

The resistance of a curved plate to some load is always higher than a flat plate under the same conditions. Thus, the simplification of flat plate is conservative.

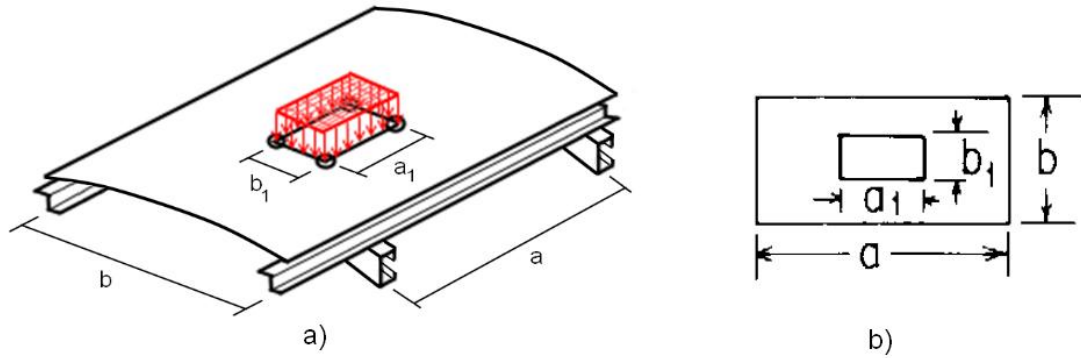


Figure 2.4- Fuselage skin panel equivalence a), flat panel distributed load [12] b)

The analytic formula (2.9) to calculate the maximum inertial stress ($\sigma_{inertial}$) has been taken from the reference [12]. The maximum stress is located at the center of the plate, with the equation (2.9). The variable (β_m) is a constant that can be found in reference's tables, (q) is the distributed load value, (W) is the antenna weight, (n_{fact}) the load factor and the rest of variables are geometrical and can be observed at the Figure 2.4.

$$\sigma_{inertial} = \frac{\beta_m \cdot q \cdot a_1 \cdot b_1}{t_{skin}^2} = \frac{\beta_m \cdot \left(\frac{W \cdot n_{fact}}{b_1 a_1} \right) \cdot a_1 \cdot b_1}{t_{skin}^2} \quad (2.9)$$

Some data from the airplane Lockheed C-130 and the antenna model must be collected, can be observed at Table 2.2. The critical up and down load factors are taken from the C-130 data at the reference [13], and they refer to the maximum load factors that an externally-mounted equipment attached to an external hard point must withstand. These load factors are designed taking into account the airspeed loads and the in-flight gust loads.

Up load factor	5,25
Down load factor	8,25
Upper frames separation [in]	20 (508mm)
Lower frames separation [in]	10 (254mm)
Upper stringers separation [in]	10 (254mm)
Lower stringers separation [in]	10 (254mm)
Antenna weight [lbs]	0,25 (1.1N)
Fastener longitudinal separation [in]	3,3 (84mm)
Fastener hoop separation [in]	1,6 (41mm)

Table 2.2- Values for the example

Then the analytic parameters Table 2.3 are calculated, in accordance with the table in the Attachment A.

	Antenna at the upper part of the fuselage	Antenna at the lower part of the fuselage
a [in]	20 (508mm)	10 (254mm)
b [in]	10 (254mm)	10 (254mm)
a ₁ [in]	3,3 (84mm)	3,3 (84mm)
b ₁ [in]	1,6 (41mm)	1,6 (41mm)
β_m	1,31	1,08

Table 2.3- Calculation parameters for the example

Finally the maximum stresses results are shown in Table 2.4.

	Antenna at the upper part of the fuselage stress [psi]	Antenna at the lower part of the fuselage stress [psi]
Down load factor	680,74 (4.69MPa)	561,22 (3.87MPa)
Up load factor	433,20 (2.99MPa)	357,14 (2.46MPa)

Table 2.4- Analytic results for the example

2.2 Finite element method analysis

In order to verify the analytic carried calculus, a FEM (Finite Element Method) model is created with the software PATRAN NASTRAN. It will give more accurate results for each case studied. The geometry is modeled like a flat plate made of Aluminum 2024 T3. The boundaries of the plate are the frames and stringers, and the imposed restrictions are zero displacements at each boundary.

2.2.1 Aerodynamic forces

The drag creates a moment to the antenna which transmits pressure to the airplane's skin through the base contact and the screws. That problem is simplified with the conservative hypothesis that the forces are just transmitted through the fasteners. Those forces are simplified as distributed loads around the adjacent to the holes mesh elements, and have contrary directions, pulling the skin at the two first screws, and pushing against the skin at the two last screws.

At Figure 2.5 it can be observed the kind of triangular mesh, the used distribution forces, and the von Mises diagram for the plate. The restrictions chosen are all external edges embedded. The FEM data can be observed at the Attachment E.

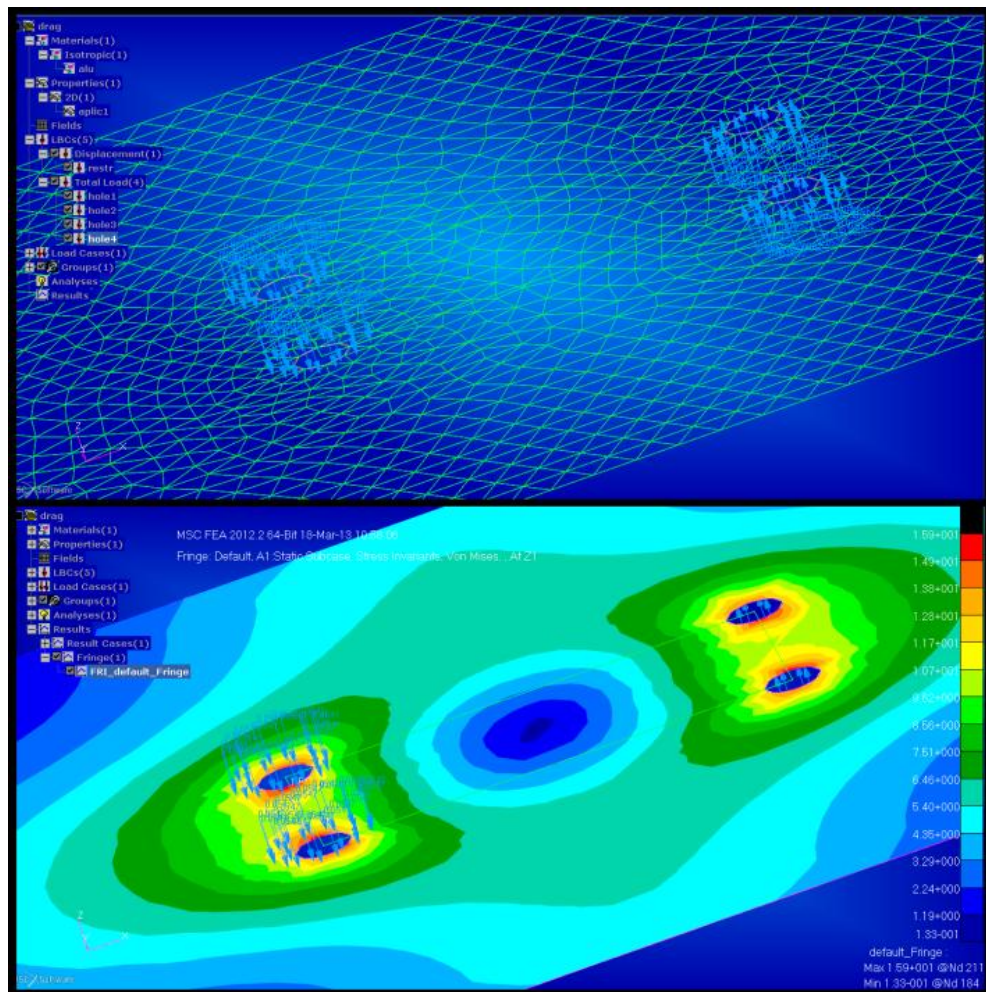


Figure 2.5- Mesh and von Mises diagram for the aerodynamic forces analysis

At the Figure 2.5 there is the result of the von Mises analysis. The maximum stress is 15,9psi (0.11MPa).

2.2.2 Inertial forces

1- Upper fuselage with down load factor

When the inertial forces push against the fuselage skin, the FEM model is represented as a distributed load within the rectangular zone between the fasteners. The restrictions chosen are all external edges embedded. The FEM data can be observed at the Attachment E. At Figure 2.6 there is the load simulated distribution and the result of the von Mises analysis. The maximum stress is 657psi (4.53MPa).

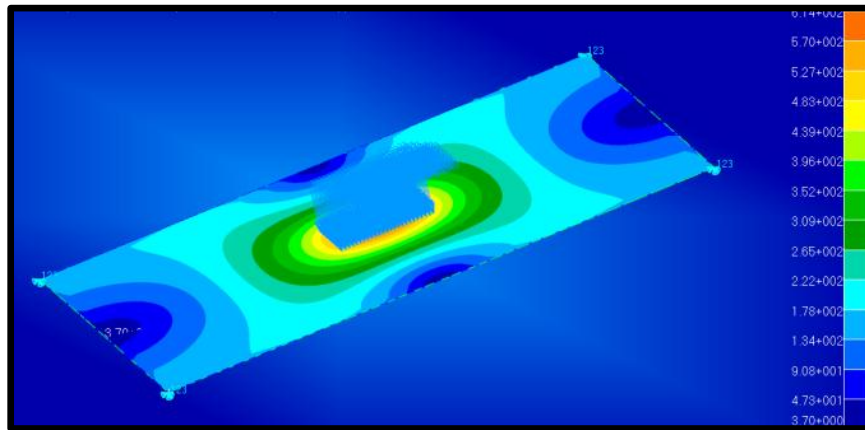


Figure 2.6- von Mises diagram for the inertial pushing forces

2- Lower fuselage with up load factor

The maximum stress resultant from the FEM analysis is 369psi (2.54MPa).

3- Upper fuselage with up load factor

In the case when the inertial antenna forces pull from the skin, the load is mainly transmitted through the fasteners. Thus, in those two next cases, the model adopted consists in the same plate but with the force distribution of the total load around the holes. To model in finite elements that case, a triangular mesh has been taken, like can be observed at the next picture. The restrictions chosen are all external edges embedded. The FEM data can be observed at the Attachment E.

At Figure 2.7 there is the result of the von Mises analysis. The maximum stress is 475psi (3.27MPa).

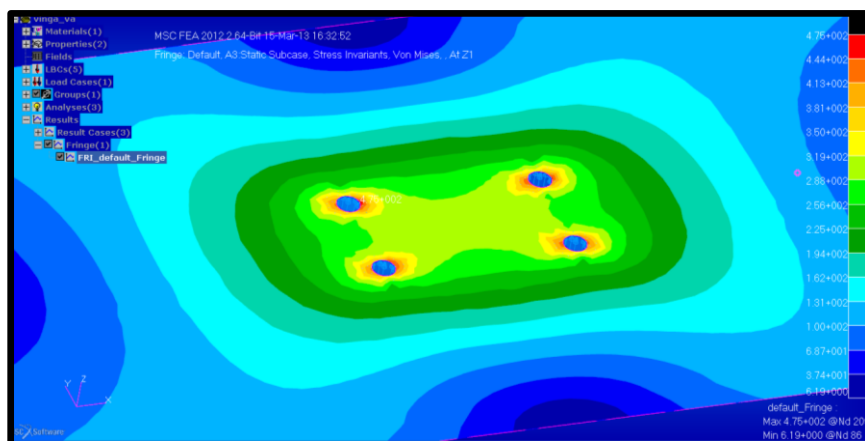


Figure 2.7- von Mises diagram for the inertial pushing forces

4- Lower fuselage with down load factor

That case is similar with the previous one, with difference in the frames separation and the applied load factor. The maximum stress is 609psi (4.20MPa).

2.3 Comparison between analytic and FEM results

In the Table 2.5 there is the comparison between the FEM and the analytic stress level calculus for the presented example.

	Analytic maximum stress [psi]	FEM maximum stress [psi]	Difference [psi]	Difference percentage
Up. fuselage, down load factor [psi]	680 (4.7MPa)	657 (4.5MPa)	-24 (0.2MPa)	3.5%
Lower fuselage, down load factor [psi]	357 (2.5MPa)	369 (2.5MPa)	+12 (0.1MPa)	3.3%
Up. fuselage, up load factor [psi]	433 (3.0MPa)	475 (3.3MPa)	+42 (0.3MPa)	8.8%
Lower fuselage, up load factor [psi]	561 (3.9MPa)	609 (4.2MPa)	+48 (0.3MPa)	7.9%
Drag [psi]	86 (0.6MPa)	16 (0.1MPa)	-71 (0.5MPa)	82%

Table 2.5- Comparison of FEM against analytic results

The drag stress difference between the analytic calculus and the finite elements analysis is the highest. That is due to the over simplifying hypothesis of taking the fuselage skin as a fixed beam, and because of the little magnitude of stress values due to the little size of the chosen antenna for the example. In spite of that, the analytic calculus is conservative and simple, giving a fast method of determining the stress level that an antenna may cause to the fuselage due to inertial and aerodynamic forces.

Due to the low difference between the rest of stress values, can be concluded that that FEM analysis verify the use of the proposed analytic formulas.

The next step is thus to compare the results with the ultimate stress level design ($\sigma_{ult-design}$) for the aircraft. The case of upper fuselage with down load factor is taken as representative since it is the highest obtained value. In the Table 2.6 there are the results from the analysis. The presented value for the ultimate design load has been calculated through the formulas (3.2) and (3.5), presented in the section 3.2.1, and corresponds to the maximum pressurization fuselage stress for the aircraft.

$\sigma_{inertial}$ [psi]	680 (4.69MPa)
σ_{drag} [psi]	86 (0.59MPa)
$\sigma_{ult-design}$ [psi]	20995 (144.76MPa)
Extra structural load percentage implication	3,7%

Table 2.6- Extra structural load percentage calculation

In this case example, the extra stresses caused by both the aerodynamic and inertial forces are about a 3.7% of the ultimate design load. So the conclusion is that the aerodynamic and inertial loads are little in comparison with the pressurization load.

The percentage limit for considering the possibility of adding extra reinforcements to the skin for the antenna installation depends on the definition of that limit, and must be properly defined by the engineer. A value higher than 5% it is considered of a considerable importance.

2.4 Summary table

Here there is a resume, Table 2.7, of the analytic formulas to use to estimate easily the percentage of extra load created by an antenna to the fuselage.

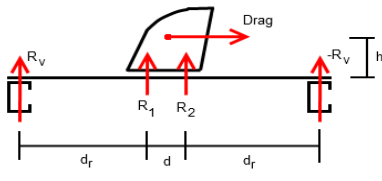
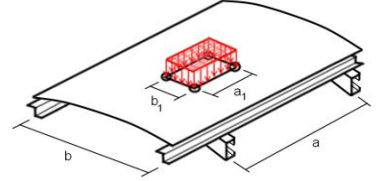
$\sigma_{\text{drag}} = \frac{\left(\frac{\left(\text{Drag} \cdot \frac{h}{d} \right) \cdot d_r - \text{Drag} \cdot \frac{h}{d} \cdot (d - d_r)}{d + 2 \cdot d_r} \right) \cdot \left(\frac{d_{\text{frames}} - d}{2} \right)}{\frac{1}{12} \cdot t_{\text{skin}}^3} \cdot \frac{t_{\text{skin}}}{2} \quad (2.10)$		 <p>The diagram shows a cross-section of a fuselage with a curved upper skin. A horizontal arrow labeled 'Drag' points to the right. Below the skin, there are two vertical reaction arrows labeled 'R_v' at the ends and two vertical reaction arrows labeled 'R₁' and 'R₂' under the skin. The horizontal distance between the end reactions is 'd_r', and the distance between the middle reactions is 'd'. The total width of the section is 'd_r + d + d_r'. The height of the section is 'h'.</p>
$\sigma_{\text{inertial}} = \frac{\beta_m \cdot \left(\frac{W \cdot n_{\text{fact}}}{b_1 a_1} \right) \cdot a_1 \cdot b_1}{t_{\text{skin}}^2} \quad (2.11)$		 <p>The diagram shows a cross-section of a fuselage with a curved upper skin. A red rectangular area is shown on the skin, representing the antenna. The width of the antenna is 'a₁' and the height is 'b₁'. The total width of the section is 'b' and the total height is 'a'.</p>

Table 2.7- Summary of expressions and cases respectively

3 Static analysis

3.1 Static analysis procedure flowchart

In the Figure 3.1 there is the static analysis specific flowchart. All the steps are better explained within the following sections.

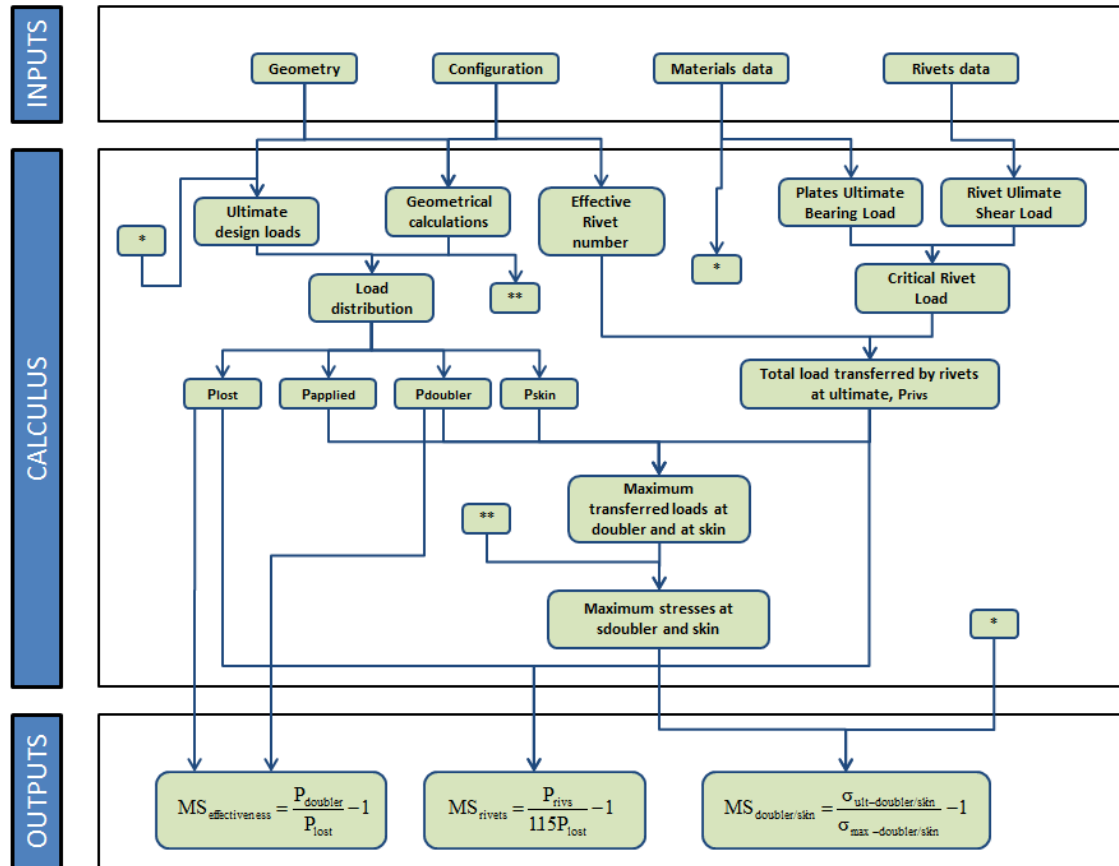


Figure 3.1- Static analysis flowchart

3.2 Determination of the design loads

There are two basic different philosophies for determining the design loads that will be used during any structural project for an aircraft:

- The aircraft loads are known or can be determined.
- The aircraft loads are not known or cannot be determined.

3.2.1 Loads are known or determinable

In this project the studied part is the skin fuselage. The main force that the fuselage skin must withstand is the pressurization [4]. There are different options to assess the stresses caused by the pressurization; here the one that simplify the fuselage as a cylindrical shell with internal pressure will be used. Thus the hoop and longitudinal stresses can be determined with the equations (4.1) and (4.2), from the reference [4].

The (PR) value used for that calculus may be the pressure at which the relief valve opens, which is a characteristic value for any aircraft model. In the case of the Lockheed C-130 that value corresponds to 7,8psi [13].

Since the hypothesis of defining the fuselage as a cylinder is valid, it is more suitable to use the value of the hoop stress as maximum design stress ($\Delta\sigma_{\max}$) for the ultimate load determination procedure, since it is more conservative.

$$\Delta\sigma_{\max} = \sigma_{\text{hoop}} \quad (3.1)$$

Once the maximum possible skin stress is determined there are 3 criteria (defined at the reference [5]) which allow to find the limit load in function of the maximum design load (ΔP_{\max}). The most restrictive of them must be applied in each case.

1. Assessing the maximum stresses that the structural component may have, and multiplying it by the 1.33 factor

$$\text{Limit load} = \Delta P_{\max} \cdot 1,33 \quad (3.2)$$

2. Assessing the maximum stresses that the structural component may have caused by the internal pressure and the maximum in flight load ($F_{\text{flight_max}}$). After that, adding the safety factor.

$$\text{Limit load} = \Delta P_{\max} + F_{\text{flight_max}} \quad (3.3)$$

3. Assessing the maximum stresses that the structural component may have caused by the internal pressure and the maximum landing load ($F_{\text{landing_max}}$). After that, adding the safety factor.

$$\text{Limit load} = \Delta P_{\max} + F_{\text{landing_max}} \quad (3.4)$$

Finally the ultimate load is calculated through the next expression, using the 1.5 safety factor from the reference CS 25.303 (1).

$$\text{Ultimate design load} = \text{Limit load} \cdot 1,5 \quad (3.5)$$

3.2.2 Loads are unknown or undeterminable

In that second possible philosophy the chosen option basically consists in using the ultimate characteristic load from directly from the material data as a design stress. It can be observed in Figure 3.2.

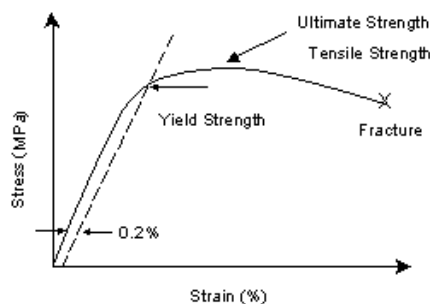


Figure 3.2- Stress against strain generic diagram

Eventually the used value will be the minimum between (σ_{t-u}) and (σ_{t-y}) multiplied by 1,5.[5]

$$\text{Ultimate load} = \text{MIN}(\sigma_{t-u} ; 1,5 \cdot \sigma_{t-y}) \quad (3.6)$$

That value is used as a design value when the flight loads are not available or it is too expensive to determine it. Using directly the data from the material properties is always more conservative, as can be observed at the following table, in the case of the aircraft Lockheed C-130, whose fuselage is made of Aluminum 2024 T3 material, with a 0,063" thickness, and a medium fuselage radius of 85". In the Table 3.1 the two possible design philosophies values for the fuselage are shown.

Design philosophy	Ultimate design load [ksi]
Known loads	21 (145MPa)
Not-known loads [3]	57 (393MPa)

Table 3.1- Design load philosophy

From here on, the ultimate loads from the materials' properties will be used for the all the following static calculus design.

3.2.3 Loads on the damaged area

Once the ultimate design loads have been calculated, the loads on the damaged area must be properly assessed. The option of internal doublers for reinforcement of a structure is always the best choice for an antenna installation. That is due to the fact that when using internal doublers two effects are avoided: physical interferences with the antenna base structure, and aerodynamic interferences. However it must be considered the possibility that the antenna installation is carried out in a zone where it is not possible to use internal doublers. In that case the use of external doublers or internal plus external (stacked) doublers should be considered.

All the following calculus were done for both hoop and longitudinal stresses in the developed software.

The considered original skin area of study is taken as the biggest doubler width multiplied by the skin thickness. The variable (A_{original}) is the original skin area, ($W_{\text{largest-doubler}}$) is the width of the largest doubler.

$$A_{\text{original}} = W_{\text{largest doubler}} \cdot t_{\text{skin}} \quad (3.7)$$

Due to the fact that holes are made for the antenna installation, there is a reduction of the net area of the original skin. The lost area (A_{lost}) is considered at the worst transversal section which corresponds to where the antenna hole is made. In that section the skin loses the net area due to the antenna hole, and due to the rivets with which share the section. The variable (D_{cc}) represents the characteristic damage of the section.

$$A_{\text{lost}} = D_{\text{cc}} \cdot t_{\text{skin}} \quad (3.8)$$

The skin with the original (without holes) area was carrying a load (P_{applied}). That load is calculated through the next formula.

$$P_{\text{applied}} = A_{\text{original}} \cdot \sigma_{t-u} \quad (3.9)$$

Due to the lost area there is a lack of load transmission capability. That lost load (P_{lost}) is calculated at the next formula.

$$P_{\text{lost}} = A_{\text{lost}} \cdot \sigma_{t-u} \quad (3.10)$$

Once the applied load has been calculated, it is necessary to assess how that load will be distributed through the skin and the different doublers once the antenna installation is done. Since the ultimate loads from the material are taken as ultimate design loads, a supposition for the doubler's effectiveness is done.

Doubler 100% effective expression is defined at the equation (3.11). The variable (P_{layer_x}) represents the load transmitted to a layer 'x' of the doubler conjunct, with transversal section areas (A_{layer_x}), and Young's modulus (E_{layer_x}). The variables (A_{layer_k}) and (E_{layer_k}) are the transversal area and the young modulus of each material layer respectively.

$$P_{\text{layer}_x} = P_{\text{applied}} \cdot \frac{A_{\text{layer}_x} \cdot E_{\text{layer}_x}}{\sum_{k=1}^{\text{layers}} [A_{\text{layer}_k} \cdot E_{\text{layer}_k}]} \quad (3.11)$$

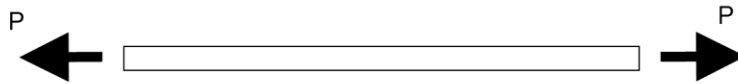
Doubler 50% effective is defined with the equations (3.12) for the skin layer, and (3.13) for each doubler layer. The variables (P_{doubler_x}) and (P_{skin}) represent the transmitted load for each respective layer, with transversal section areas (A_{doubler_k}) and (A_{skin}). The elastic modulus for the skin and doublers is respectively defined by (E_{skin}) and (E_{doubler_k}).

$$P_{\text{skin}} = P_{\text{applied}} \cdot \frac{A_{\text{skin}} \cdot E_{\text{skin}}}{A_{\text{skin}} \cdot E_{\text{skin}} + 0,5 \cdot \sum_{k=1}^{\text{doublers}} [A_{\text{doubler}_k} \cdot E_{\text{doubler}_k}]} \quad (3.12)$$

$$P_{\text{doubler}_x} = P_{\text{applied}} \cdot \frac{0,5 \cdot A_{\text{doubler}_x} \cdot E_{\text{doubler}_x}}{A_{\text{skin}} \cdot E_{\text{skin}} + 0,5 \cdot \sum_{k=1}^{\text{doublers}} [A_{\text{doubler}_k} \cdot E_{\text{doubler}_k}]} \quad (3.13)$$

It must be taken into account that the holes size is not relevant in the three previous formulas. It is due to the fact that the holes size is in the numerator and in the denominator of all the terms. Thus in the end the load distribution is just function of the material and the thickness of each layer.

Skin before installation:



Skin with the antenna hole:



Skin with antenna hole and doubler/s

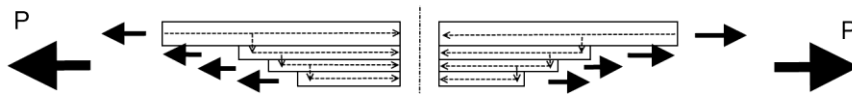


Figure 3.3- Load distribution evolution through doublers layers

Through the previous formula the distribution load values can be found. Eventually the sum of the different load values when installing the doublers will give the initial applied load. In Figure 3.3 a scheme of that distribution can be seen.

When each load value for the doubler and skin load are calculated, the value of the percentage that each layer is carrying can be obtained. It will give to the user a good estimative of how the doublers structure is working. To get that the following calculus may be done.

$$P_{\text{layer}_x} = \frac{P_{\text{layer}_x}}{P_{\text{applied}}} \cdot 100 \quad (3.14)$$

In the case of a 100% effective the doubler is supposed perfect and carries the entire possible load. Supposing the doubler is a 50% effective, the doubler would carry less load, therefore the skin would be suffering more. As from that point, the hypothesis of a 100% effective doubler is taken for the rest of the static analysis.

3.3 Geometry definition

3.3.1 Adopted hypothesis

3.3.1.1 Flat assumption

For the whole structural study, the metallic fuselage skin is supposed to be a flat shape plate instead of a curved shape plate. It will simplify all the calculus as from that point. The justifications for it are the assumption of a big radius compared with the skin thickness, and that the main force which acts on the skin is the pressure [4]. The pressurization creates two main stresses in the cylindrical shell that is the airplane's fuselage. This stresses are contained in the plane of the skin. Therefore in stresses terms the performance will be the same either a flat or a curved shell is simulated. In the Figure 3.4 the pressure stresses can be observed.

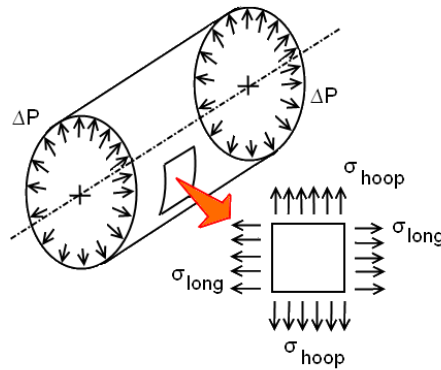


Figure 3.4- Pressure longitudinal and hoop stresses

3.3.1.2 Screws structural contribution

The screws are not considered in the structural calculus of the doubler. They are supposed just to support the antenna to the fuselage. The safety margin in terms of tensile, shear, and

bearing stress will also analyzed, but their contribution is not essential for the doubler endurance, therefore they are just considered like holes with its proper diameter in the structure. It will make the results more conservative.

3.3.1.3 Separate study of longitudinal and hoop

The study of the doubler is done separately for longitudinal and hoop direction. The reason for that is mainly related with fatigue and DT purposes, and explained in the section 4.3.1.

3.3.2 Design with several doublers

In static terms any kind of repair or reinforcement for an antenna installation can be made just with one layer of constant thickness. However, for fatigue and damage tolerance purposes, is better to have variable thickness [4]. It is due to its influence to the stress concentration.

From manufacturing and maintenance point of view, it is always cheaper to acquire constant thickness plates than to manufacture a variable thickness plate. So various layers of constant thickness are used and statically analyzed as well.

3.4 Static analysis procedure

Once the geometrical values and the load distribution values have been calculated, the static analysis can begin. The objective of that analysis is to find some safety margins which define the static behavior of the structure. The list of safety margins that are to be found is shown in the Table 3.2.

Safety Margin	Interpretation
$MS_{\text{eff-doubler}}$	Indicates the capability of the doubler to make the skin suffer at least the same or less load than before the installation hole
$MS_{\text{eff-rivet}}$	Gives an estimation of how the rivets are supporting the shear stress, which is the most probable failure mode they may have
MS_{doubler}	Indicates the performance of the doubler
MS_{skin}	Indicates the performance of the skin
$MS_{\text{shear-screws}}$	Gives a value for the screws shear performance
$MS_{\text{bearing-screws}}$	Gives a value for the screws bearing performance

Table 3.2- Safety margins recopilation

3.4.1 Doubler effectiveness margin of safety

When the antenna installation is done, an effective loss of material happens due to the holes. The removed material originates a loss of the capability of load transmission. The first step of the static analysis is to ensure that the removed material is given back to the structure, and eventually the skin must carry less or at least the same than was carrying before. That loss of transmission can be assessed through the following safety margin calculus. So there will be two safety margins for the doubler effectiveness, for both hoop and longitudinal analysis.

$$MS_{\text{eff-doubler}} = \frac{P_{\text{doubler}}}{P_{\text{lost}}} - 1 \quad (3.15)$$

3.4.2 Rivet effectiveness margin of safety

3.4.2.1 Rivet ultimate shear load

There are two main ways to calculate the bearing load:

- Analytical
- Specific data from the particular rivet datasheet
- Tables from the reference MMPDS-01 [3]

Analytical:

Fastener shear failure consists in a shear failure of the fastener shank. The maximum load that meets the ultimate criteria for the fastener shear is defined by the equation (3.16). The shear area (A_{shear}) to be considered is shown in the Figure 3.5.

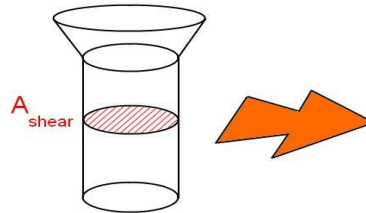


Figure 3.5- Rivet shear area

$$P_{\text{su-riv}} = \sigma_{\text{s-u}} \cdot A_{\text{shear}} \cdot S_{\text{CF}} = \sigma_{\text{s-u}} \cdot \frac{\pi \cdot D^2}{4} \cdot S_{\text{CF}} \quad (3.16)$$

The value for the Strength Correction Factor (S_{CF}) can be obtained from the reference [3] at the table 8.1.2.1(b), shown in the Attachment B.1. These values are function of the rivet diameter, and the sheet material thickness, and the kind of shear, single or double. The difference between single and double shear can be seen at the Figure 3.6.

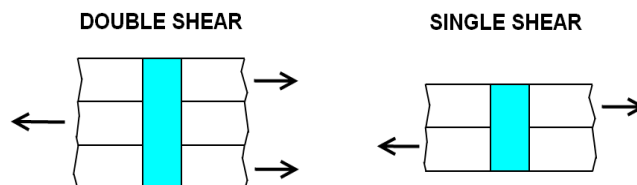


Figure 3.6- Rivet single versus double shear

Specific data from the rivet datasheet:

If the data sheet from the rivet manufacturer contains this information it is the most trustable way of getting a value of ultimate shear load the rivet can withstand. It is not always available.

Tables MMPDS:

It is always more suitable to directly use the shear load value from the specific data sheet from the fastener if available, or to estimate it through the reference [3] MMPDS-01 at the table 8.1.2(b) shown in the Attachment B.2 .

3.4.2.2 Doubler and skin bearing load

There are two main ways to calculate the bearing load:

- Analytical
- Tables MMPDS

Analytical:

The bearing load value ($P_{bearing}$), equation (3.17) for a hole can only be analytically assessed when the rivet head is not inside of the plate, what means that the plate must have a simple cylindrical hole, like is shown in the Figure 3.7.

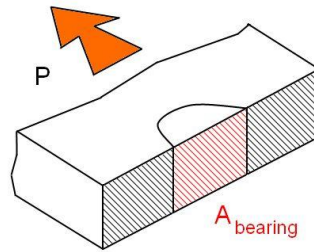


Figure 3.7- Hole bearing area

$$P_{bearing} = \text{MIN}\{\sigma_{br-u} \cdot D \cdot t ; 1,5 \cdot \sigma_{br-y} \cdot D \cdot t\} \quad (3.17)$$

Tables MMPDS:

However, the rivets used for antenna installations are countersunk-type. The skin layer contains the head of the rivet. Therefore the ultimate bearing load allowable for the layer which contains the head can't be obtained simply analytically, the value must be taken from tables. This value can be obtained from the reference [3] at the table 8.1.2.2(f) shown in the Attachment B.3.

3.4.2.3 Critical rivet load

For each zone of the doubler repair installation, it must be defined which is the most critical failure mode. Thus, in each zone the bearing ultimate load of the different sheets, and the ultimate shear load of the rivets which are at the same zone must be compared.

Let's introduce the hypothetic frame of an antenna reinforcement composed of multiple doublers with a rivet contained between the different sheet layers. In terms of the sheet bearing, the difference of material and or thickness may cause differences on the ultimate bearing load of the different sheets. Therefore one sheet has a smaller bearing ultimate load in comparison with the others. However, the sheet with smallest ultimate bearing load will not enter in bearing deformation unless the rest of more resistant sheets have already entered in bearing deformation. It will give a value of critical bearing load. However, the rivet also has a defined

ultimate shear load, which might be smaller than the assessed critical bearing load, and it would mean that the rivet would fail for shear before than the metallic layers for bearing.

Thus, the critical value of that zone is the lowest resultant of comparing the maximum bearing load of the different layers ($P_{bearing_x}$). The minimum of these two values will give the critical load value for that zone. The variable ($P_{crit-riv}$) is the critical rivet load.

$$P_{crit-riv} = \min\{P_{su-riv} ; \max(P_{bearing_x})\} \quad (3.18)$$

3.4.2.4 Rivet effectiveness

The critical rivet load value must be multiplied by the number of effective rivets (N_{riv}) in that zone, giving the critical zone load value. In the equation (3.19) it can be observed how the safety margin for the rivet effectiveness ($MS_{eff-riv}$) is calculated.

$$MS_{eff-riv} = \frac{P_{crit-riv} \cdot N_{riv}}{1,15 \cdot P_{lost}} - 1 \quad (3.19)$$

The fitting factor 1.15 is applied in accordance with the current normative, the reference [5].

The (N_{riv}) value is the number effective of rivets that are actually withstanding the load. That value must be obtained for both longitudinal and hoop direction. In Figure 3.8 is shown the way to take the value in a generic case and longitudinal direction, for 1 doubler case, and for a 3 doubler case. In hoop direction the procedure can be easily extrapolated.

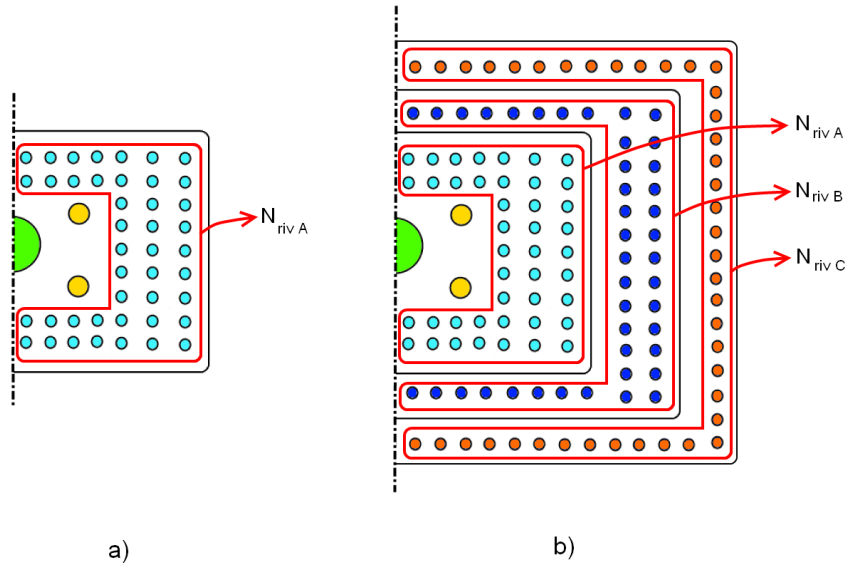


Figure 3.8- Single a) and triple b) doubler with the effective rivet zones selected

3.4.3 Doubler and skin margin of safety

For assessing the safety margin of the doubler ($MS_{doubler}$), it is necessary to determine which is the design tension applied on it. This value can be either the critical load transferred by the rivets at ultimate stress or the value for the load in doubler calculated through the hypothesis 100% effective before. Therefore the final used value will be the lowest one between them two. It can be observed in the equation (3.21). The variable (σ_{ult_design}) is the ultimate

design load value, ($\sigma_{\text{applied_doubler}}$) is the stress applied to the doubler, ($A_{\text{net_skin}}$) is the net transversal area of the skin, and ($A_{\text{net_doubler}}$) is the net transversal area of the doubler.

$$MS_{\text{doubler}} = \frac{\sigma_{\text{ult_design}}}{\sigma_{\text{applied_doubler}}} - 1 \quad (3.20)$$

$$MS_{\text{doubler}} = \frac{\min \{ \sigma_{t-u} ; 1.5\sigma_{t-y} \}}{\min \left\{ \frac{P_{\text{transf_ult}}}{A_{\text{net_doubler}}} ; \frac{P_{\text{doublers}}}{A_{\text{net_doubler}}} \right\}} - 1 \quad (3.21)$$

For a single doubler case, where the variable ($P_{\text{trans_ult}}$) is the load transferred by the rivets at the ultimate, and ($P_{\text{app_100\%_eff}}$) is the stress applied with the 100% effective hypothesis:

$$P_{\text{trans_ult}} = P_{\text{crit_riv}} \cdot N_{\text{riv}} \quad (3.22)$$

$$P_{\text{doublers}} = P_{\text{app_100\%_eff}} \quad (3.23)$$

For more than one doubler case, where de index (k) represents each doubler layer.

$$P_{\text{trans_ult}} = \sum_{k=1}^{\text{doublers}} [P_{\text{crit_riv}_k} \cdot N_{\text{riv}_k}] \quad (3.24)$$

$$P_{\text{doublers}} = \sum_{k=1}^{\text{doublers}} P_{\text{app_100\%_eff}_k} \quad (3.25)$$

For assessing the safety margin of the skin (MS_{skin}), the skin applied load must be determined. It can be done subtracting the previously calculated applied doublers tension ($\sigma_{\text{applied_doubler}}$) to the total applied stress ($\sigma_{\text{total_applied}}$). It can be observed in the following formulas.

$$MS_{\text{skin}} = \frac{\sigma_{\text{ult_design}}}{\sigma_{\text{applied_skin}}} - 1 \quad (3.26)$$

$$MS_{\text{skin}} = \frac{\min \{ \sigma_{t-u} ; 1.5\sigma_{t-y} \}}{\frac{P_{\text{applied}} - \min \{ P_{\text{transf_ult}} ; P_{\text{doublers}} \}}{A_{\text{skin}}}} - 1 \quad (3.27)$$

3.4.4 Screws margin of safety

3.4.4.1 Preload calculus

The value for the fastener preload must be previously calculated. From the reference [15], the maximum pre-axial load must be between 30 to 40% the ultimate load. The ultimate load value for both tensile and shear can be obtained two different ways:

- From the specific data sheet of the screw model.
- From the reference [3] at the tables 8.1.5(a), 8.1.5(b₁), 8.1.5(b₂) shown at the Attachment B.4.

If it is available, is always recommendable to take the values from the specific data of the fastener model. Although, if it is not available, it is always safe to use the MMPDS tables values.

If it is also necessary to calculate the necessary torque (T) to reach that preload (P_{preload}), there is a suitable formula for that. It involves a lubrication coefficient (μ) that is fitted from 0.15 to 0.25 the calculated Preload, and the screw diameter (D_{screw}). [15]

$$P_{\text{preload}} = \frac{T}{\mu \cdot D_{\text{screw}}} \quad (3.28)$$

3.4.4.2 Shear margin of safety

The screws are supporting the antenna fixed to the fuselage skin. So the the first step is to estimate the loads that the antenna is transmitting to the screws. Three kinds of loads are analyzed.

- Inertial loads
- Pressure loads
- Aerodynamic loads

The sum of them three give the total contribution estimated load that the antenna transmits. The expressions for assessing the inertial (P_{inertial}) and pressure loads (P_{pressure}) are shown below. The variable (LF_{crit}) represents the critical load factor, ($A_{\text{cut-out}}$) is the cut out hole area, and (PR) is the maximum differential pressure at which the relieve valve of the aircraft opens.

$$P_{\text{inertial}} = LF_{\text{crit}} \cdot W \quad (3.29)$$

$$P_{\text{pressure}} = PR \cdot A_{\text{cut-out}} \quad (3.30)$$

The ways of calculating drag load (P_{drag}) are already explained in the section 2.1.1.

To estimate the total transmitted load (P_{total}), the conservative assumption of that all the three critical loads are acting simultaneously is taken, like can be observed in the next expression.

$$P_{\text{total}} = P_{\text{inertial}} + P_{\text{pressure}} + P_{\text{drag}} \quad (3.31)$$

Finally the safety margin ($MS_{\text{shear-screws}}$) is calculated with the formula from the reference [15]. Two conservative hypotheses are taken: The shear acting load ($P_{\text{screw-shear}}$) is the previously obtained total load, and the tensile acting load (P_{tensile}) is the total load plus the preload. The variables (R_{shear}) and (R_{tensile}) are the shear and tensile components, from the reference [15], and according to the airworthiness requirements the fitting factor (FF) is applied, usually equivalent to 1.15 [5].

$$R_{\text{shear}} = FF \frac{P_{\text{screw-shear}}}{P_{\text{s-u}}} = 1.15 \frac{P_{\text{total}}}{P_{\text{s-u}}} \quad (3.32)$$

$$R_{\text{tensile}} = FF \frac{P_{\text{tensile}}}{P_{\text{t-u}}} = 1.15 \frac{(P_{\text{preload}} + P_{\text{total}})}{P_{\text{t-u}}} \quad (3.33)$$

$$MS_{\text{shear-screws}} = \frac{1}{(R_{\text{shear}} + R_{\text{tensile}})} - 1 \quad (3.34)$$

3.4.4.3 Bearing margin of safety

The bearing acting load must be estimated in order to get a bearing safety margin ($MS_{\text{bearing-screws}}$). It can be estimated with the value in which the cut-out hole enters in bearing. That safety margin is usually high. The variable ($P_{\text{br-u}}$) is the ultimate bearing load.

$$P_{\text{br-u}} = (t_{\text{skin}} + t_{\text{doubler}}) \cdot D \cdot \sigma_{\text{br-u}} \quad (3.35)$$

$$MS_{\text{bearing-screws}} = \frac{P_{\text{br-u}}}{P_{\text{total}}} - 1 \quad (3.36)$$

3.4.5 Summary of contents

The Table 3.3 contains a resume of the already presented safety margins.

MS	Formula	Eq. Ref.
Doubler effectiveness	$MS_{\text{eff-doubler}} = \frac{P_{\text{doubler}}}{P_{\text{lost}}} - 1$	(3.15)
Rivet effectiveness	$MS_{\text{eff-riv}} = \frac{P_{\text{crit-riv}} \cdot N_{\text{riv}}}{1,15 \cdot P_{\text{lost}}} - 1$	(3.19)
Doubler	$MS_{\text{doubler}} = \frac{\min \{ \sigma_{t-u} ; 1.5 \sigma_{t-y} \}}{\min \left\{ \frac{P_{\text{transf_ult}}}{A_{\text{net_skin}}} ; \frac{P_{\text{doubler}}}{A_{\text{net_doubler}}} \right\}} - 1$	(3.21)
Skin	$MS_{\text{skin}} = \frac{\min \{ \sigma_{t-u} ; 1.5 \sigma_{t-y} \}}{\sigma_{\text{total_applied}} - \sigma_{\text{applied_doubler}}} - 1$	(3.27)
Screws or bolts shear	$MS_{\text{shear-screws}} = \frac{1}{(R_{\text{shear}} + R_{\text{tensile}})} - 1$	(3.34)
Screws or bolts bearing	$MS_{\text{bearing-screws}} = \frac{P_{\text{br-u}}}{P_{\text{br}}} - 1 = \frac{P_{\text{br-u}}}{P_{\text{total}}} - 1$	(3.36)

Table 3.3- Safety margins summary

3.5 Developed software

In the Figure 3.9 there is an image taken from the developed excel file, which implements all the previously calculus related with the static analysis for one configuration.

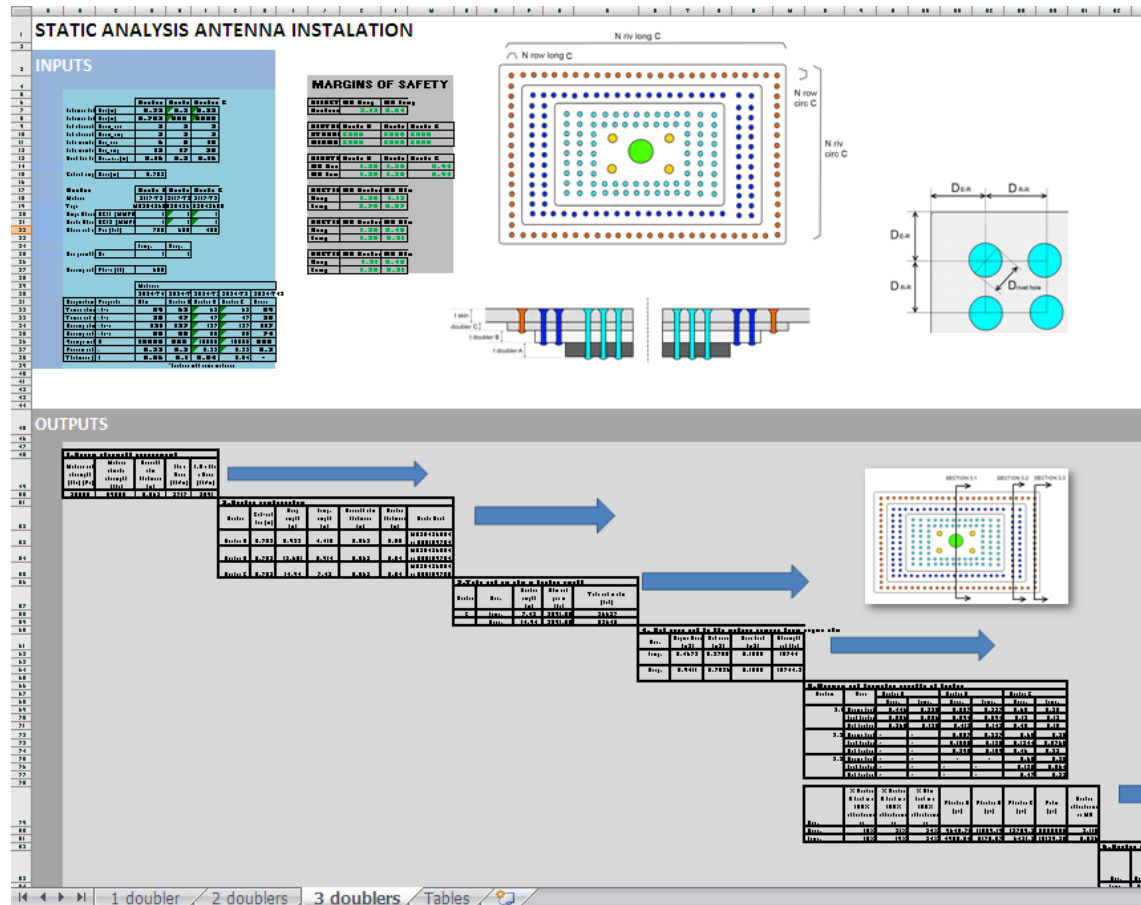


Figure 3.9- Statics excel print screen

4 Fatigue analysis

4.1 Fatigue analysis procedure flowchart

The Figure 4.1 shows the fatigue analysis flowchart summary. All the steps are better explained within the following sections.

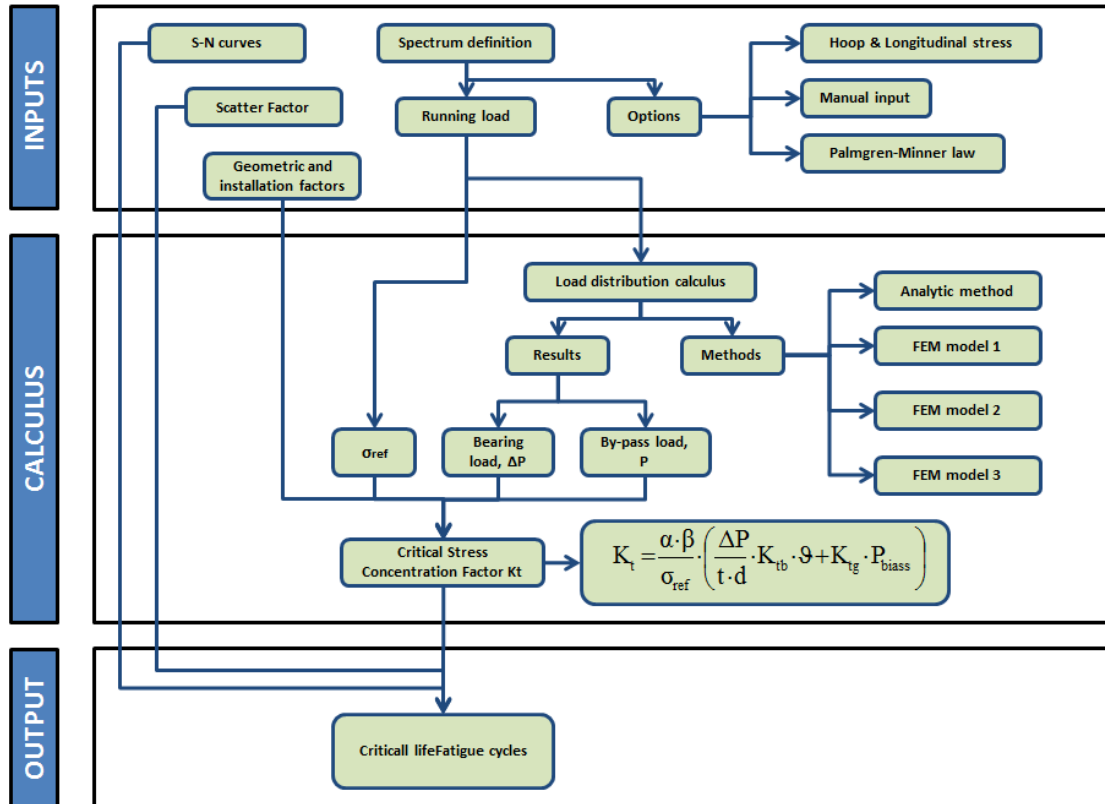


Figure 4.1- Fatigue analysis flowchart

The three main points of the fatigue analysis are: the geometry, the load spectrum, and the stress concentration factor determination. Once the static behavior of one case is checked, the next step is to verify the fatigue response of the pertinent structure. There is an important change in the adopted philosophy. In the static analysis, the loads that were considered were the ultimate loads of the material. However, in the fatigue analysis, the considered loads will be the running loads the aircraft can suffer. Therefore the running loads must be estimated in order to be able to carry this analysis.

4.2 Load spectrum

4.2.1 Pressure load

The main concerning fatigue structural load at the fuselage is the pressurization load cycles, so in many cases it is the only considered load, resulting on a stress in the circular direction (σ_{hoop}), and the other component in the longitudinal direction (σ_{long}). The formulas for calculating it are shown in the equations (4.1) and (4.2) [2]. However depending on the

geometry of the aircraft, the bending moment may have an important contribution. That contribution is assessed in the next section 4.2.2. The variable (R_{fus}) is the fuselage radius, and (PR) is the pressure value at which the relief valve opens. It can be observed that the hoop stress is 2 times the longitudinal stress.

$$\sigma_{hoop} = PR \cdot \frac{R_{fus}}{t} \quad (4.1)$$

$$\sigma_{long} = PR \cdot \frac{R_{fus}}{2 \cdot t} \quad (4.2)$$

4.2.2 Bending moment contribution

Both the pressure and bending moment loads can have different amplitudes and frequencies. So the direct assumption of only one cyclic pressure load of constant amplitude in the GAG spectrum is not valid anymore, there are some cases in which the bending moment created by the fuselage cannot be ignored and must be assessed. The equation (4.4) includes the value of the longitudinal bending moment component (M_{bend}), for calculating the bending stress (σ_{bend}), knowing the values for the section's inertia (I_{zz}), the maximum distance from the centroid is (y_{max}), and (σ_{press}) is the pressure caused stress.

$$\sigma_{long} = \sigma_{press} + \sigma_{bend} \quad (4.3)$$

$$\sigma_{long} = \frac{1}{2} \frac{PR \cdot R_{fus}}{t} + \frac{M_{bend}}{I_{zz}} \cdot y_{max} \quad (4.4)$$

For assessing the bending moment, the aircraft C-130 model is taken as an example, since it is the main object of study of that thesis. The following Table 3.3 has some relevant information of it.

MTOW [lbs]	Maximum take-off weight	155000 (70308 kg)
MZFW [lbs]	Maximum zero-fuel weight	120000 (54432 kg)
MFW [lbs]	Maximum fuel weight	17200 (7802 kg)
$W_{wing-engines}$ [lbs]	Wing plus engines weight	15500 (7031 kg)
PR [psi]	Maximum differential pressure	7.8 (0.053 MPa)
W_f [lbs]	Considered bending acting weight	60000 (27216 kg)
x_1 [in]	Critical antenna position	188 (4775 mm)
L_f [in]	Total fuselage length	1200 (30480 mm)
R_{fus} [in]	Fuselage radius	85 (2159 mm)

Table 4.1- Required C-130 data for carrying the analysis

To estimate the maximum bending stress created by the structure to the aircraft skin at the antenna location, the first step is to estimate the weight that is actually contributing to the moment. To estimate that weight two different ways have been taken. The first one consists in taking the maximum take-off weight, and after extract from it the values correspondent to the maximum fuel weight, and the wing weight. The second method basically consists in taking the

maximum zero fuel weight, and dividing it by 2. The results can be pretty similar. It is shown in the next expressions, for the C-130 aircraft. It is recommendable to take the maximum of both values to add conservatism to the analysis.

$$W_f = \frac{(MTOW - MFW - W_{\text{wing\&engines}})}{2} = 61150 \text{ lbs } (27738 \text{ kg}) \quad (4.5)$$

$$W_f = \frac{MZFW}{2} = 60000 \text{ lbs } (27216 \text{ kg}) \quad (4.6)$$

The next step is to calculate the bending moment value. The load is conservatively considered as a uniformly distributed load of the previously calculated weight, and therefore the bending moment is calculated exactly as if the airplane fuselage was a beam with annular section. The hardest solicited positions at the fuselage skin in bending moment terms are the ones placed at both edges of the central box of the fuselage, which supports the wings, represented in green color in Figure 4.2, in which there is a schematic view of the Lockheed C-130 airplane with some distances and the load distribution (q).

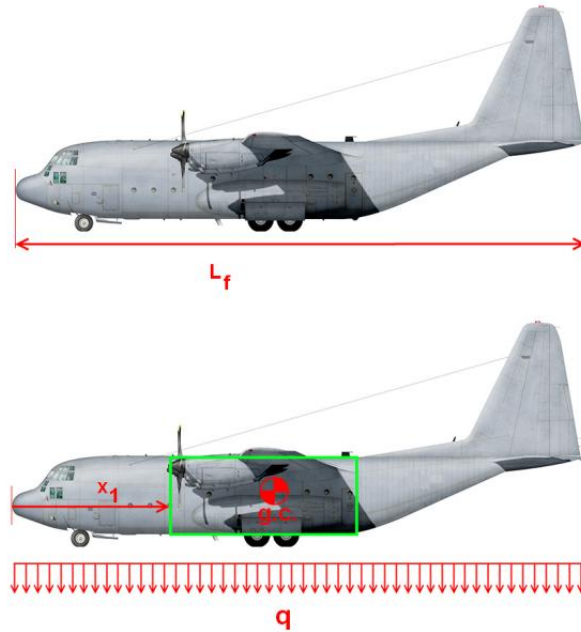


Figure 4.2- Lockheed C-130 profile view with loading assumption

$$q = \frac{W_f}{L_f} = 50 \text{ lb/in } (892 \text{ kg/m}) \quad (4.7)$$

$$M_{\text{bend}} = q \cdot \frac{x_1^2}{2} = 883600 \text{ lb}\cdot\text{in } (10167 \text{ kg}\cdot\text{m}) \quad (4.8)$$

The next step is to calculate the stress of the pertinent section. The section's inertia moment is necessary to calculate the stress. A good hypothesis is to consider the section as a skin annulus with mass booms which correspond to the stringers that are fitted to the skin. However, with conservative purpose the stringers have eventually been ignored. The simplified section is shown in Figure 4.3.

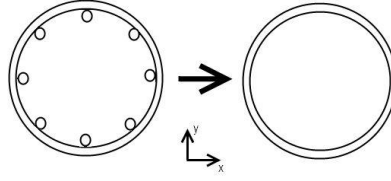


Figure 4.3- Tubular section with booms simplification

So the inertia moment and the bending stress of the section are estimated by the next expression. The variable (k_{booms}) is the mass booms number, and (A_{booms}) is its cross-section area.

$$I_{zz} = \frac{\pi}{4} \cdot ((R_{fus}^4 - (R_{fus} - t)^4) + k_{booms} \cdot A_{booms} \cdot R_{fus}^2) \approx \pi \cdot t \cdot R_{fus}^3 = 121548 \text{ in}^4 \quad (0.05059 \text{ m}^4) \quad (4.9)$$

$$\sigma_{bend} = \frac{M_{bend}}{I_{zz}} R_{fus} = 618 \text{ psi} \quad (4.26 \text{ MPa}) \quad (4.10)$$

$$\sigma_{press} = \frac{PR}{t} \cdot R_{fus} = 5261 \text{ psi} \quad (36.27 \text{ MPa}) \quad (4.11)$$

Thus the final longitudinal stress for the worst possible case of bending moment including the load factor (n_{fact}) is the next one.

$$\sigma_{long} = \sigma_{bend} \cdot n_{fact} + \sigma_{press} = 5880 \text{ psi} \quad (40.54 \text{ MPa}) \quad (4.12)$$

That value must be compared with the hoop stress value for the aircraft. Therefore the eventual conclusion is that for the C-130 aircraft the hoop stress is always bigger than the longitudinal stress in normal conditions. The difference is quite big so the bending moment is negligible for the calculus.

$$\sigma_{hoop} = 2\sigma_{press} = 10524 \text{ psi} \quad (72.56 \text{ MPa}) \quad (4.13)$$

$$\sigma_{hoop} > \sigma_{long} \quad (4.14)$$

Depending on the aircraft model, the bending moment may cause important stresses relatively to the differential pressure stress. It mainly depends on the relation between the fuselage longitudinal length, and the aircraft radius. For the Lockheed C-130 aircraft, the bending moment influence is not relevant due to the fact of its little fuselage length in comparison with the width, so the running load can be taken just as the hoop pressure cycle.

4.3 Stress Concentration Factor

4.3.1 Separate study of longitudinal and hoop stress

For studying the doubler it is much more simple to carry an analysis with just one direction of load. In order to check the conservatism of the simplification, a simple shell with a hole in the center is created.

In both cases the level of applied tension is exactly the same, but the objective is to demonstrate that an analysis with just one transversal load will have higher values of tension around the hole than in the other case.

That edge distributed load transmits through the doubler section until it reaches the center hole. The hole acts like a lack of material at the net section. However the applied load remains at the same level, so what happens is that the stream lines of tension get distributed around the hole, and the tension around it increases. In the Figure 4.4 the situation is illustrated, and the studied cases are defined in the Table 4.2. It is a simple Aluminum quadrangular flat plate of 10"x10" and a thickness of 0.063", with a 2.5" hole placed in the middle.

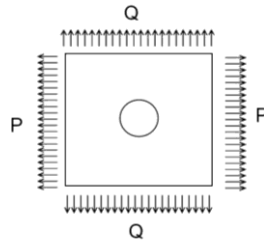


Figure 4.4- Load distribution around a plate with a hole

	P [lbs]	Q [lbs]
Case1	100 (445N)	100 (445N)
Case2	100 (445N)	50 (222N)
Case3	100 (445N)	0

Table 4.2- Longitudinal and hoop forces for three cases

A FEM model was developed to study this case by Patran/Nastran. A spider mesh with QUAD elements is created in order to have more reliable results. The mesh shape can be observed at the Figure 4.5. The restrictions chosen are all external edges fixed. The FEM data can be observed at the Attachment E. The von-Mises results for the cases 1 to 3 are illustrated at Figure 4.6.

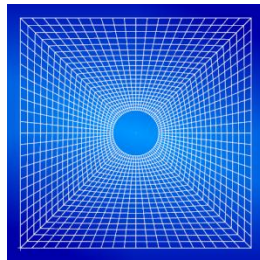


Figure 4.5- Quad-elements meshed perforated plate

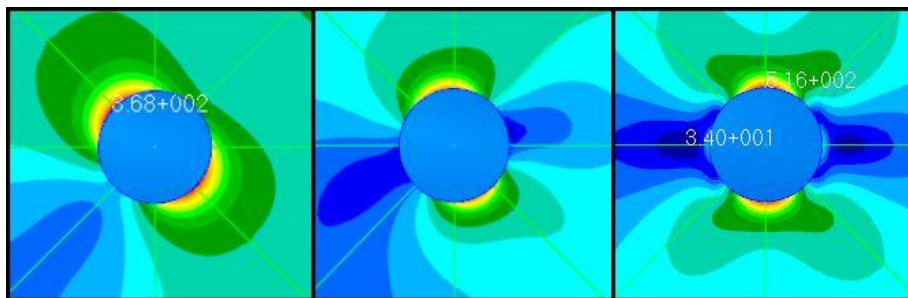


Figure 4.6- von Mises diagram for cases 1 to 3, from left to right

For analyzing the tension concentration, the stress concentration factor is assessed. To calculate it, (σ_{ref}) must be estimated. It is estimated through the expression (4.15).

$$\sigma_{ref} = \frac{P}{t \cdot w} = \frac{100}{0,063 \cdot 10} = 158.73 \text{psi (1.09N)} \quad (4.15)$$

The results of the different analysis (shown in Figure 4.6) are shown in Table 4.3.

	von Mises [psi]	SCF
Case1	368 (2.54 MPa)	2,32
Case2	388 (2.67 MPa)	2,44
Case3	516 (3.56 MPa)	3,25

Table 4.3- von Mises analysis compilation for three cases

In order to have confidence in these results, an analytic formula to calculate the stress concentration effect has been found. That formula has been taken from the reference [14] and a case of a plate hole in an in-plane bi axial stress condition has been analyzed, shown in the Figure 4.7. The formula (4.16) is used. The variable (σ_{Ω}) is the stress in function of the angle from the hole center (Ω), and (σ_1) and (σ_2) are represented in the Figure 4.7. So if a (σ_2) is taken as the reference stress, the stress concentration factor reaches the expression (4.18).

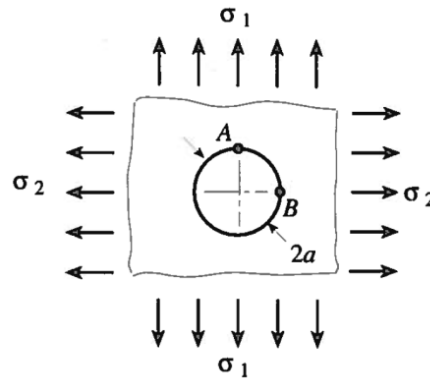


Figure 4.7- Plate with a hole bi-axial stress [14]

$$\sigma_{\Omega} = (\sigma_1 + \sigma_2) - 2(\sigma_2 - \sigma_1)\cos(2\Omega) \quad (4.16)$$

$$\frac{\sigma_{\pi}}{2} = 3\sigma_2 - \sigma_1 \quad (4.17)$$

$$SCF = 3 - \frac{\sigma_1}{\sigma_2} \quad (4.18)$$

Finally the 3 cases previously studied by FEM methods, are analytically tested, and the results for the SCF are exposed in the following Table 4.4.

	σ_1 [psi]	σ_2 [psi]	SCF
Case1	100 (0.68MPa)	100(0.68MPa)	2
Case2	50 (0.34MPa)	100 (0.68MPa)	2.5
Case3	0	100 (0.68MPa)	3

Table 4.4- Analytic analysis compilation for three cases

The analytic results confirm the validity of the FEM analysis and conclusions previously carried. The stress reaches its maximum at the boundaries of the hole, where there is the concentration of tensions. As can be observed at the table above, the maximum stress is lower when the load is applied in both directions. So that the conclusion of that analysis allows to study a structural case like a doubler repair just in one direction, due to that it is a conservative hypothesis. The obtained results will be higher than in reality, but more easy obtainable and always from the safety side.

4.3.2 Determination of the load distribution

The target of this section is to determine the load distribution through the rivet lines. In Figure 4.8 a generic doubler can be observed. The red selection is referred to the analyzed strip, whose load distribution scheme is also shown in the same figure. The (ΔP) corresponds with the transfer load, and the skin by-pass load is the ($P_{\text{by-pass}}$). These two variables must be obtained in order to assess the stress concentration factors across the fasteners.

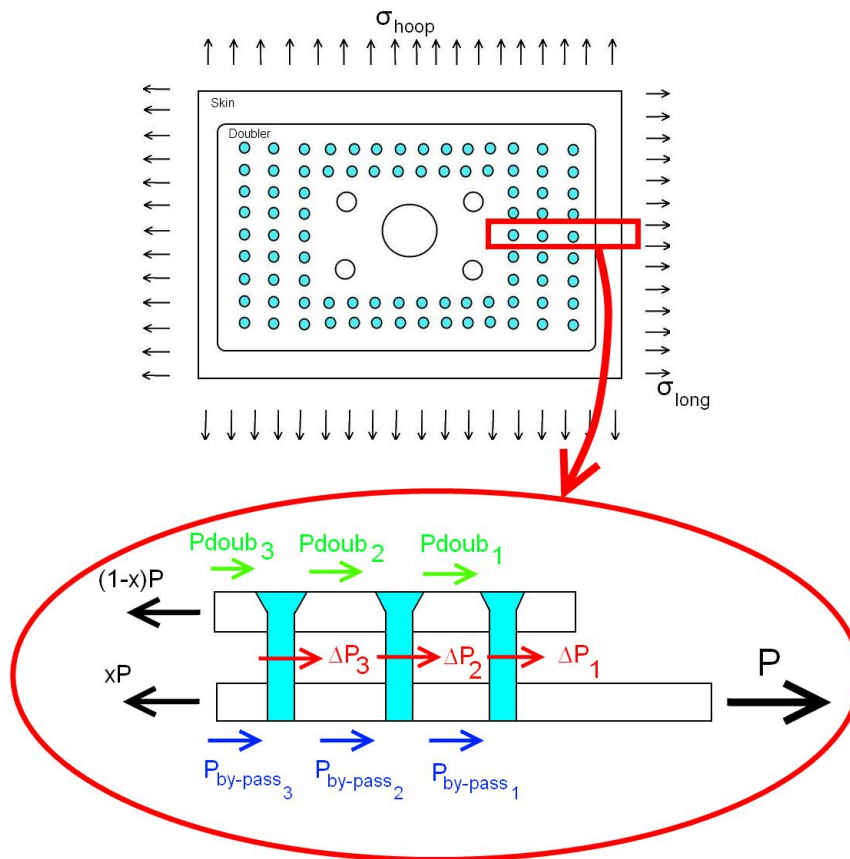


Figure 4.8- One doubler up view with a strip selected and represented

4.3.2.1 Fastener flexibility constant study

It is difficult to model the behavior of a fastener in a joint, how it receives and transfers the load. The deflection of the fastener due to shear and bending must be analyzed and correlated

with test data. The deflection of both the fastener and the plate due to bearing must be considered as well. The following formulas are for single shear.

4.3.2.1.1 Tom Swift formulation

The reference [16] has an expression for obtaining the value of the fastener constant (C). Tom Swift developed it, the equation (4.19). It is commonly used in the aeronautical industry. The variable (t_{doubler}) is the doubler thickness, and (E) is the modulus of elasticity of the plates. The variables (A) and (B) are constants dependent with the rivet material.

$$C = \frac{1}{E \cdot D} \cdot \left[A + B \cdot \left(\frac{D}{t_{\text{doubler}}} + \frac{D}{t_{\text{skin}}} \right) \right] \quad (4.19)$$

In spite of using that formula the big manufacturers have developed their own formulas to estimate that value. This is due to the following reasons: There are some materials which are not covered by Tom Swift's formula; and the big manufacturers may have their own data, based on experimental tests that may suggest little variations to the way of obtaining the fasteners constant. In the Attachment F a resume of other alternatively used formulas can be observed.

4.3.2.1.2 Constants comparison

For assessing the behavior of the different possible fastener constants (collected in the Attachment F), an example has been studied. The different fastener constants have been plotted gradually increasing the plates' thicknesses, and the results are shown in the Figure 4.9. It is observed that between the 0.05" (1.27mm) and the 0.15" (3.8mm) all the formulas converge. Generally the aircrafts' skin thickness is around these values.

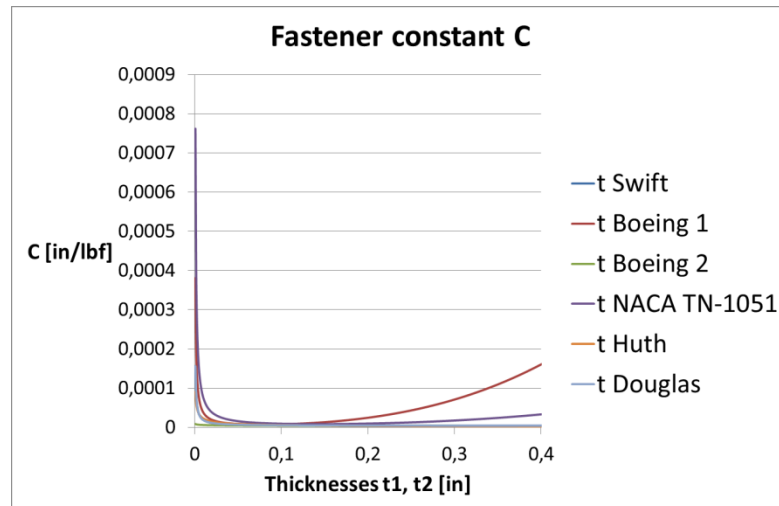


Figure 4.9- Fastener spring constant against plates' thicknesses

4.3.2.2 Comparison of different transfer load assessing models

One of the main difficulties associated with the study of the fatigue performance of a structure is that the load distribution among the different fastener lines is not equal. That fact makes necessary to precisely assess the bearing and bypass loads distribution through the fastener lines. There are two differentiated ways to get it: analytically, or through developing a FEM model.

4.3.2.2.1 Analytic model through spring constants

The analytic solution consists basically of modeling the joint as a series of springs, and then constructing a simple system of equations that can be solved in different ways.

-Plates modeling:

In a simple reinforcement consisted of a skin plate and a doubler plate, the different elastic constants (C_{plate}) of both metallic plates can be obtained mathematically with the equation (4.20), where (L_{fast}) is the distance between fasteners, and (A_{plate}) is the cross sectional area between fasteners. The equation (4.21) calculates the deflection, in function of the plate constant, and a generic applied load (P).

$$C_{plate} = \frac{L_{fast}}{A_{plate} \cdot E} \quad (4.20)$$

$$deflection = C_{plate} \cdot P \quad (4.21)$$

-Fasteners modeling:

It is not trivial to model a joint at the fastener location. There are several factor that must be taken into account. The expression which estimates well enough the spring constant of a fastener has been developed by different ways, and usually each manufacturer has its own one. In that analysis, the expression has been the one developed by Tom Swift, which can be found in the reference [16], and has the expression of the equation (4.19). A sketch of the doubler modeling can be observed in the Figure 4.10 and Figure 4.11.

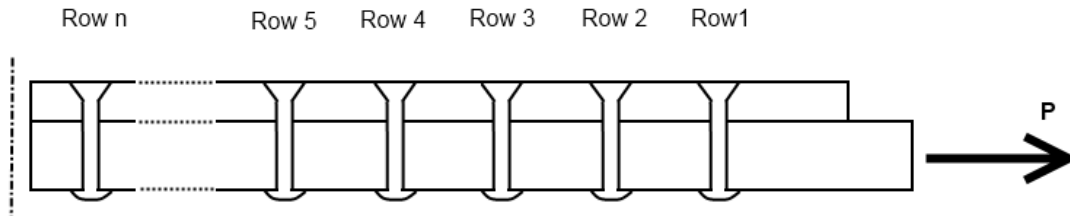


Figure 4.10- Doubler of n rivet row profile view

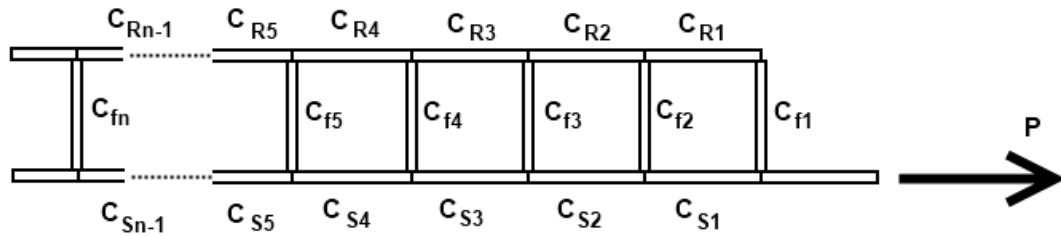


Figure 4.11- Doubler of n rivet row profile with constants schematic view

The objective is to form a system of 'n' equations and 'n' unknowns, where the result that is aimed is to obtain the transfer load distribution amongst the different row lines. The mathematical equations can be obtained using the equivalence between displacements in each rivet line. The variables (d_i) represent deflections, (C_i) represent elastic constants, and (P_i)

represent transmitted force. The sub index (i) identifies the fastener element 'n' (fn), the doubler element 'n' (Rn), or the skin element 'n' (Sn).

$$d_{f1} + d_{R1} = d_{f2} + d_{S1} \quad (4.22)$$

$$C_{f1} \cdot P_{f1} + C_{R1} \cdot P_{R1} = C_{f2} \cdot P_{f2} + C_{S1} \cdot P_{S1} \quad (4.23)$$

$$C_{f1} \cdot P_{f1} + C_{R1} \cdot P_{f1} = C_{f2} \cdot P_{f2} + C_{S1} \cdot (1 - P_{f1}) \quad (4.24)$$

$$P_{f1} (C_{f1} + C_{R1} + C_{S1}) - P_{f2} \cdot C_{f2} = C_{S1} \quad (4.25)$$

The easiest way to solve it is using matrixes. The next system of equations is obtained.

$$[Mat] \cdot \{P_f\} = \{C_s\} \cdot P \quad (4.26)$$

$$[Mat] = \begin{bmatrix} (C_{f1} + C_{R1} + C_{S1}) & -C_{f2} & 0 & \dots & 0 \\ C_{R2} + C_{S2} & (C_{f1} + C_{R1} + C_{S1}) & -C_{f3} & \dots & 0 \\ C_{R3} + C_{S3} & C_{R3} + C_{S3} & (C_{f1} + C_{R1} + C_{S1}) & \dots & 0 \\ \vdots & \vdots & \vdots & \ddots & -C_{Sn} \\ C_{Rn} + C_{Sn} & C_{Rn} + C_{Sn} & C_{Rn} + C_{Sn} & C_{Rn} + C_{Sn} & (C_{fn} + C_{Rn} + C_{Sn}) \end{bmatrix} \quad (4.27)$$

$$\{P_f\} = \begin{bmatrix} P_{f1} \\ P_{f2} \\ P_{f3} \\ \vdots \\ P_{fn} \end{bmatrix} \quad (4.28) \quad \{C_s\} \cdot P = \begin{bmatrix} C_{S1} \\ C_{S2} \\ C_{S3} \\ \vdots \\ C_{Sn} \end{bmatrix} \cdot P \quad (4.29)$$

Therefore the bearing or transfer loads can be easily found from that point.

$$\{P_f\} = [Mat]^{-1} \cdot \{C_s\} \cdot P \quad (4.30)$$

The previous matrix calculus have been implemented in a Microsoft excel file for a range from 2 to 7 rivet rows. A print screen of the developed workbook is shown in Figure 4.12

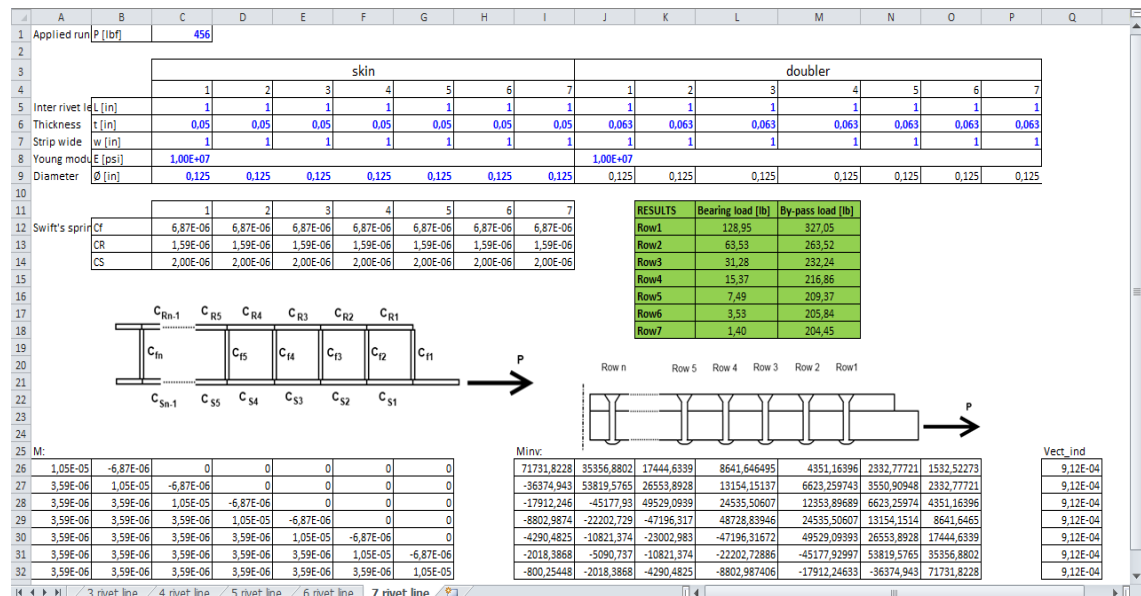


Figure 4.12- Print screen of the load transference calculus workbook

4.3.2.2.2 FEM modeling analysis methods

Three different ways of modeling a doubler reinforcement have been studied:

- One dimension model, one strip with “beam” elements
- Two dimension model, one strip with “shell” and “bush” elements
- Two dimension model, entire doubler with “shell” and “bush” elements.

All the following structural analysis has been carried by the software MSC Patran/Nastran. For analyzing the different cases, an example of an Aluminum 2024 T3 single doubler with 5 rivet line has been studied. The specific characteristics of that case are shown in the Table F.2 (Attachment F).

4.3.2.2.2.1 One dimension model, one strip with “beam” FEM elements

In this case, all the elements of the doubler are modeled as beam elements [1]. To make it able to be assessed just in one dimension, the following conservative simplification is made: just one strip of the doubler is studied, and must be the one with less rivet rows for each direction. It can be observed in the Figure 4.13, for both longitudinal and hoop direction.

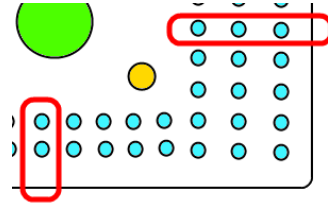


Figure 4.13- Doubler with the critical rivet strips selected

The rivets are modeled as beams fixed by both extremities, what is shown in the Figure 4.14, and with circular section. The following expressions are used. The variable (E_{fast}) is the fastener elasticity modulus, (I) is the inertia of the section, (P_f) is the fastener transfer load, (Δ) is the horizontal displacement.

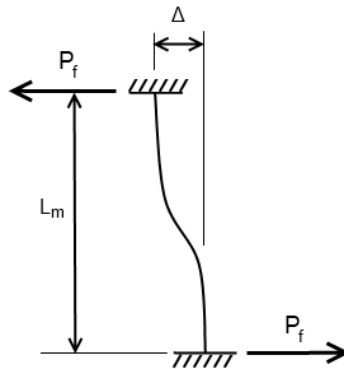


Figure 4.14- Two extremes fixed beam

$$P_f = \frac{12 \cdot E_{fast} \cdot I}{L_m^3} \Delta \quad (4.31)$$

$$\frac{\Delta}{P_f} = \frac{L_m^3}{12 \cdot E_{fast} \cdot I} = C \quad (4.32)$$

$$D_{model} = \sqrt[4]{\frac{L_m^3 \cdot 64}{12 \cdot E_{fast} \cdot C \cdot \pi}} \quad (4.33)$$

The methodology for using that model consists in the next steps:

1. Fix the distance (L_m) with the any desired value. For simplifying the calculus it can always be taken as $L_m=1$.
2. In parallel to previous step, calculate the spring constant of each rivet through the T. Swift's formula (4.19)
3. Calculate the equivalent diameter (D_{model}) that each fastener will have in the FEM model with the formula (4.33).
4. Both doubler and skin strip have a rectangular section, with its real thickness length in the vertical direction, and the width length of the studied strip in the horizontal direction.
5. Mesh the model. There must be just one beam element between rivets, and each rivet is an element by itself. It is important to remark that with that kind of mesh, the von Mises diagram will not produce trustable results, because that method is designed to obtain the fastener transfer load values, there are not enough elements like to reach trustable stress values in the skin and doubler. However, the only relevant values are the bearing or transfer load resulted from the analysis, which is realistic enough.
6. Apply the correct restrictions in displacements to the problem, apply the calculated in service load, and run the analysis. In Figure 4.15 there is an example of the mesh and load distribution analysis through that method. The restrictions chosen are the two nodes at the left totally embedded, and just allowing the 'x' translation to the rest of nodes. The FEM data can be observed at the Attachment E.

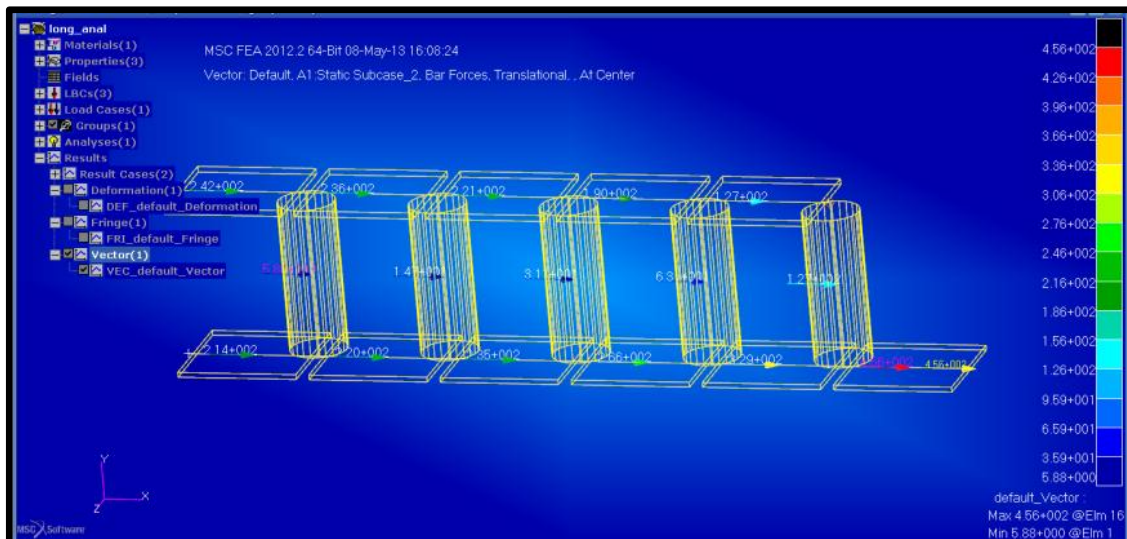


Figure 4.15- FEM 1 strip beam element transfer forces

4.3.2.2.2 Two dimension model, one strip with “shell” and “bush” FEM elements:

In that second FEM model, the philosophy consists in modeling the two plates as 2-D shell elements, and each fastener is modeled just as a bush element, with its proper constant. It can be observed in Figure 4.16.

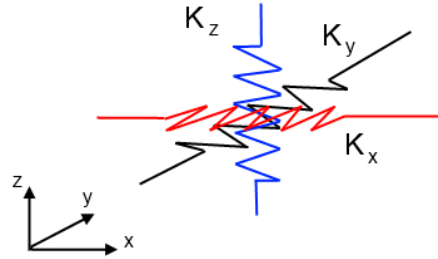


Figure 4.16- FEM bush element constant representation

The constants in the 'x' (K_x) and 'y' (K_y) direction are the same value, and are calculated through the inverse of the fastener flexibility constant. The constant in the 'z' (K_z) direction represents the axial behavior of the rivet. The variable (A_{cross}) is the cross section area of the fastener, and (L_{fast_length}) is the fastener length.

$$K_x = K_y = \frac{1}{\frac{1}{E \cdot D} \cdot \left[A + B \cdot \left(\frac{D}{t_{doubler}} + \frac{D}{t_{skin}} \right) \right]} \quad (4.34)$$

$$K_z = \frac{A_{cross} \cdot E_{fast}}{L_{fast_length}} \quad (4.35)$$

Each rivet is modeled just with one bush element. However that case is 2D, therefore the shells can be meshed with more elements. The only outputs required of that analysis are the bush element forces. With that kind of analysis, the stress values obtained through von Mises, are not realistic, and cannot be used. That's due to the hypothesis of considering the fasteners just as bush elements that join the two plates. The most important point when meshing the plates is to make the position of the fasteners coincide with the position of the plate mesh's nodes, in order to reach more reliable values. In the next picture there are the plates and the rivets meshed. The bush element forces are plotted in vector form. They correspond to the bearing or transfer loads, which will be used to calculate the stress concentration factor, and thus the fatigue and damage tolerance behavior of the reinforcement. This is shown in Figure 4.17. The restrictions chosen are the two edges at the left totally embedded, and just allowing the 'x' translation to the rest of nodes. The FEM data can be observed at the Attachment E.

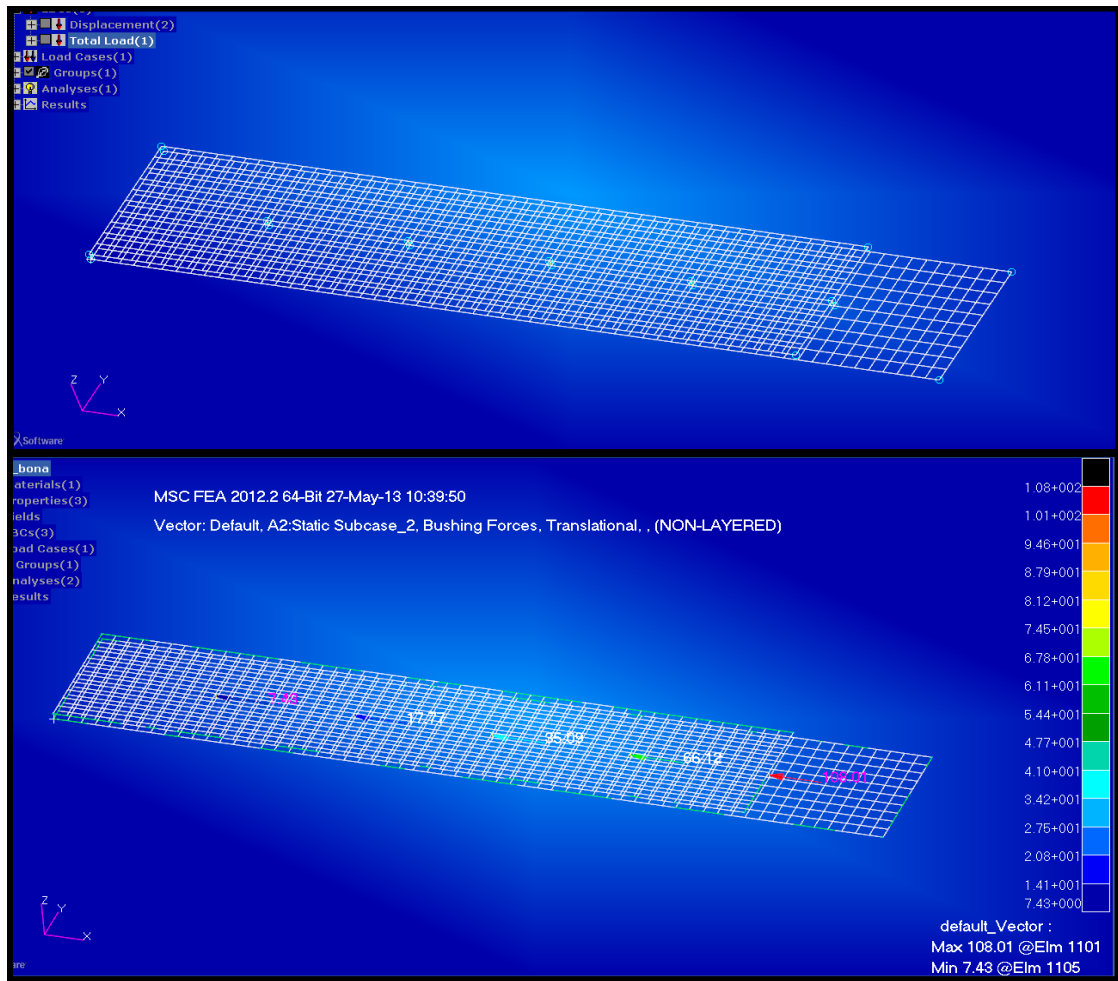


Figure 4.17- FEM 1 strip shell element mesh and transfer forces

4.3.2.2.2.3 Two dimension model, entire doubler with “shell” and “bush” FEM elements:

For analyzing the load transmission through the fasteners in a more realistic way, another studied option is to simulate the entire doubler, not just one strip. Due to the symmetry of the problem, just analyzing half a doubler, and imposing the proper restrictions is enough.

In terms of mesh requirements, that case is more complicated due to the hole of the antenna. It makes difficult to use quadrangular elements imposing the coincidence of the nodes with the fasteners. Therefore the most efficient option is to use triangular elements.

The method used to mesh it with the Patran/Nastran software after the geometry is ready is the following:

1. Meshing the plates with triangular elements. The density of the mesh can be chosen by the user, but it is not necessary a lot of meshing elements.
2. Re-mesh the previous mesh with the option “mesh on mesh”. It will give the user the option of imposing “hard points” by where the new mesh nodes will pass through.
3. After that, the software requires to redefine the properties of the new shells.

Here there is a picture example of the definitive mesh distribution, with its elements, nodes, and also the final bearing loads, Figure 4.18. The restrictions chosen are the two edges at the

left totally embedded, and just allowing the 'x' translation to the rest of nodes. The FEM data can be observed at the Attachment E.

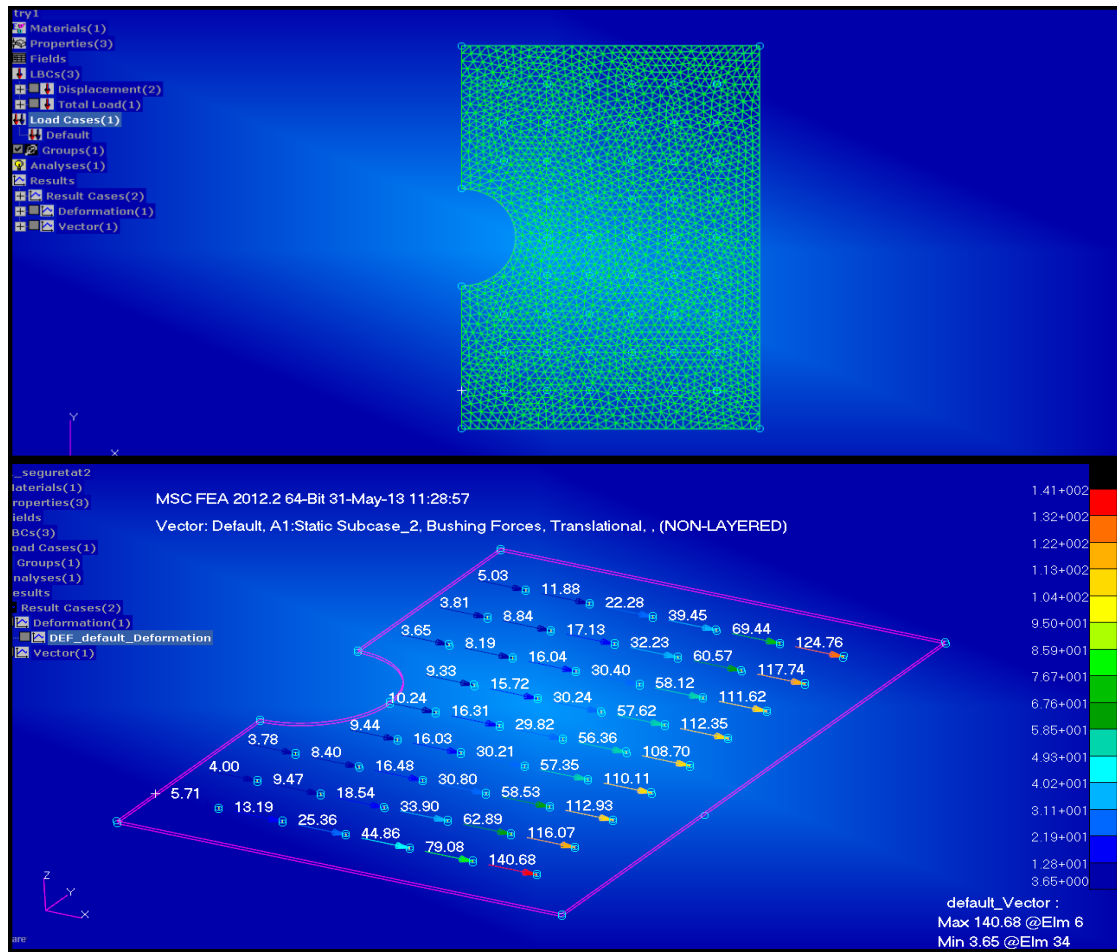


Figure 4.18- FEM entire doubler shell elements mesh and transfer forces

4.3.2.3 Study of the joint analysis optimal method

4.3.2.3.1 Comparison of different methods against experimental results

There are different method of analyzing a joint, and how the applied load is transmitted from one part of the joint to the other through the fasteners. Therefore some methods have been analyzed and in order to define an order of preferences or ranking with different criteria for when that kind of analysis is required.

The followed procedure has been to find some experimental test data for a concrete case, which has been taken as the real values. That data has been found at the reference [12], and simulates a simple case of a splice pushed from the two tips. The main types of structures analyzed in this thesis are the doublers, but a splice is useful for that purpose as well. In Figure 4.19 the example can be observed. The experimental values of the bearing or transfer load are plotted in the Figure 4.20. The variable (K) is the elastic constant of each plate.

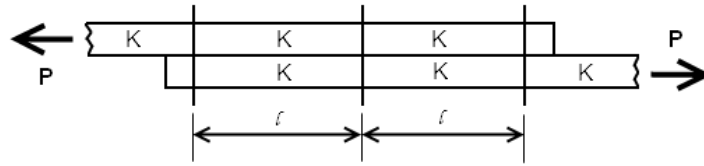


Figure 4.19- Splice profile schematic view

$$K = \frac{A_{plate} E}{L_{fast}} \quad (4.36)$$

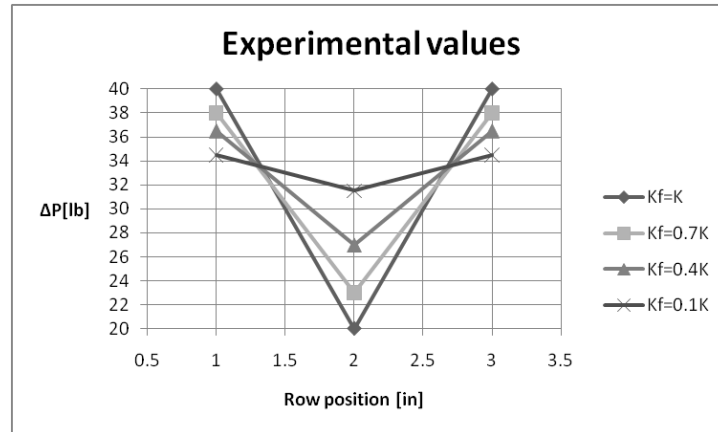


Figure 4.20- Experimental values for bearing load [2]

Three different methods have been used to simulate the case:

- Analytic method
- FEM beams method
- FEM shells method

All the working principles of these methods are explained at the section 4.3.2 of the thesis. So the next step is to analyze the variations through the different methods, and with that purpose, the following graphics are constructed, one for each value of the fastener's spring constant (K_f); $K_f=K$: Graphic in Figure 4.21; $K_f=0.7K$: Graphic in Figure 4.22; $K_f=0.4K$: Graphic in Figure 4.23; $K_f=0.1K$: Graphic in Figure 4.24. The analysis data is shown in the Attachment G.

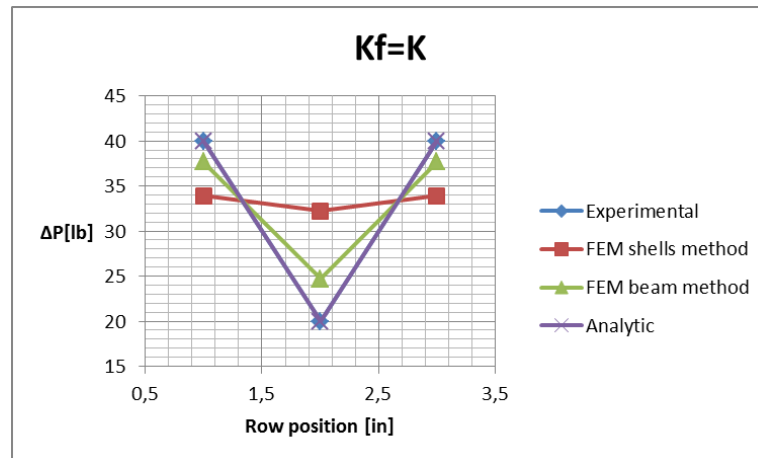


Figure 4.21- Bearing load results in function of the analysis method for $K_f=K$

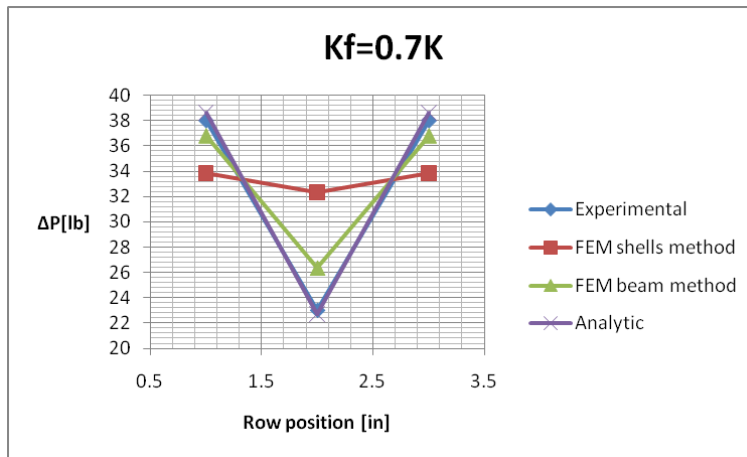


Figure 4.22- Bearing load results in function of the analysis method for Kf=0.7K

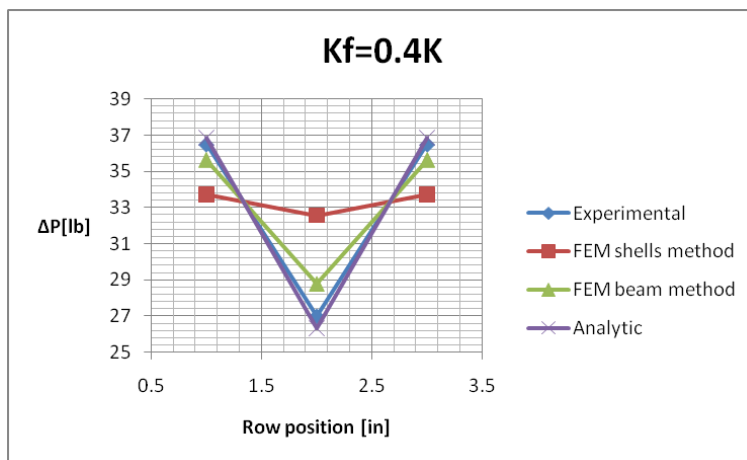


Figure 4.23- Bearing load results in function of the analysis method for Kf=0.4K

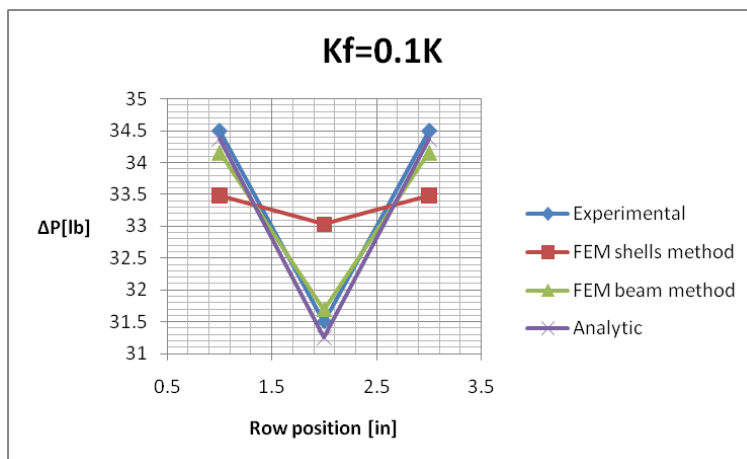


Figure 4.24- Bearing load results in function of the analysis method for Kf=0.1K

The analytic method is the more precise one, in all the different cases. It was predicable because it is always more accurate to use analytic method to any Finite Element Method if possible. The point is that in many practical engineering applications, it is not possible to

approximate the real cases to cases with an analytic solution, therefore FEM methods are required.

Another observation is that, as the difference between (K) and (K_f) increases, all the methods tend to converge to the experimental results. Thus the exactitude increases as the difference between constants increases. That effect is shown in the Figure 4.25 below for the central rivet row.

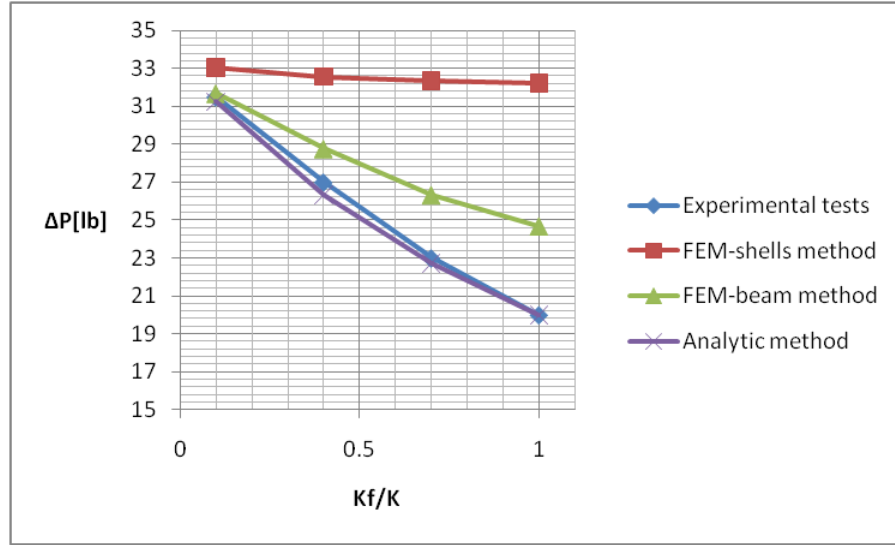


Figure 4.25- Bearing load results in function of ratio K_f/K for each analysis method

So a study of the typical values these constants may have in the pertinent application must be done before choosing the most preferable method.

In typical applications the value for the ratio K_f/K has a little value. Here a typical example of reinforcement to the aircraft model Lockheed C-130 skin is taken to demonstrate it. The values for the example are based in the Table F.2 (Attachment F).

The plate constants would be,

$$K = \frac{0.063 \cdot 1}{5 \cdot 0.125} = 1.04 \cdot 10^6 \frac{\text{lb}}{\text{in}} \quad (18548 \frac{\text{kg}}{\text{mm}}) \quad (4.37)$$

The fastener transversal constant calculated through T. Swift formula would be,

$$K_f = \left[\frac{1}{E \cdot D} \cdot \left[A + B \cdot \left(\frac{D}{t_{\text{doubler}}} + \frac{D}{t_{\text{skin}}} \right) \right] \right]^{-1} = 1.46 \cdot 10^5 \frac{\text{lb}}{\text{in}} \quad (2603 \frac{\text{kg}}{\text{mm}}) \quad (4.38)$$

And so the ratio results,

$$\frac{K}{K_f} = 0.14 \ll 1 \quad (4.39)$$

Therefore the example shows that in a common case in the aeronautical industry, the ratio of constants would be lower than 1. Thus the different methods have better approximations to the reality.

4.3.2.3.2 Ranking method definition

In terms of time, the method which requires less time is the analytic one. Despite of that fact, it must be taken into account that the analytic development is not always possible to be

carried depending on the particular case complexity. Between the two FEM methods, the fastest one of developing is the FEM-shells elements. However the implementation time difference with the FEM-beam is not so important, and the calculus time for the software is the higher in this case due to the bigger mesh.

Eventually, the ranking of usage recommended for analysis the bearing load distribution through the fastener rows in a joint in function of the carried analysis is the following list.

1. Analytic method, if possible
2. FEM-beam method
3. FEM-shell method

It must be taken into account that those methods are simplifications of the reality, and are applicable to a simple rectangular-geometry doubler. For a more complex configuration, the most accurate analysis is always the entire doubler FEM simulation, explained at the section 4.3.2.2.2.3, although it is the most complex and time-expensive method.

4.3.2.4 Analysis for multiple doublers design

4.3.2.4.1 Comparison of different methods

For static purposes, just with one doubler or reinforcement layer of constant thickness is always enough to warrant the safety of the structure. The point is that when talking about fatigue and damage-tolerance terms, if the reinforcing plate is too thick, the first rivet line will carry too much load, and thus the SCF will be too high, deteriorating the fatigue life of the structure. The solution to that problem is making a doubler with variable thickness, decreasing from the center till the boundaries of the plate. It makes the load to be more softly transmitted through the fastener rows, and so the first rivet line gets relieved in fatigue terms. But in engineering reparation terms, it uses to be too expensive to machine the doubler tapering the ends, and so the most common option is to directly replace the initial thick doubler for two or three doublers of different thickness, and so making the effective reinforcement thickness smaller at the tips.

In general, there are two philosophies for simulating the pertinent cases. In both of them just one strip of the reinforcement is analyzed. All methods are schematized in the Figure 4.26.

- Simplifying the different doublers as a single doubler of variable thickness. That philosophy will only allow calculating the load transference between the skin and the doublers “pack”. Two methods of that type have been analyzed:
 - Analytic, with the results shown in the Attachment H.
 - FEM-1D beams, with one floor, with the results in the Attachment H.
- Treating each doubler as an individual plate. That philosophy will allow assessing the way the load gets delivered among the different doubler lines. Two methods of that type have been analyzed.
 - FEM-1D beams, with various floors, with results in the Attachment H.
 - FEM-2D shells, with various floors, with results in the Attachment H.

The next step is to calculate the respective stress concentration factors for each case of study. Values of SCF can be calculated for each hole and for each material layer. So for the two first presented methods less values of SCF will be obtained, since the different doublers reinforcement layers are treated as just one. The obtained SCF values for each method are shown in Figure 4.27, and they have been calculated through the formula (1.9). The FEM mesh data for each for each case is cited in the Attachment H.

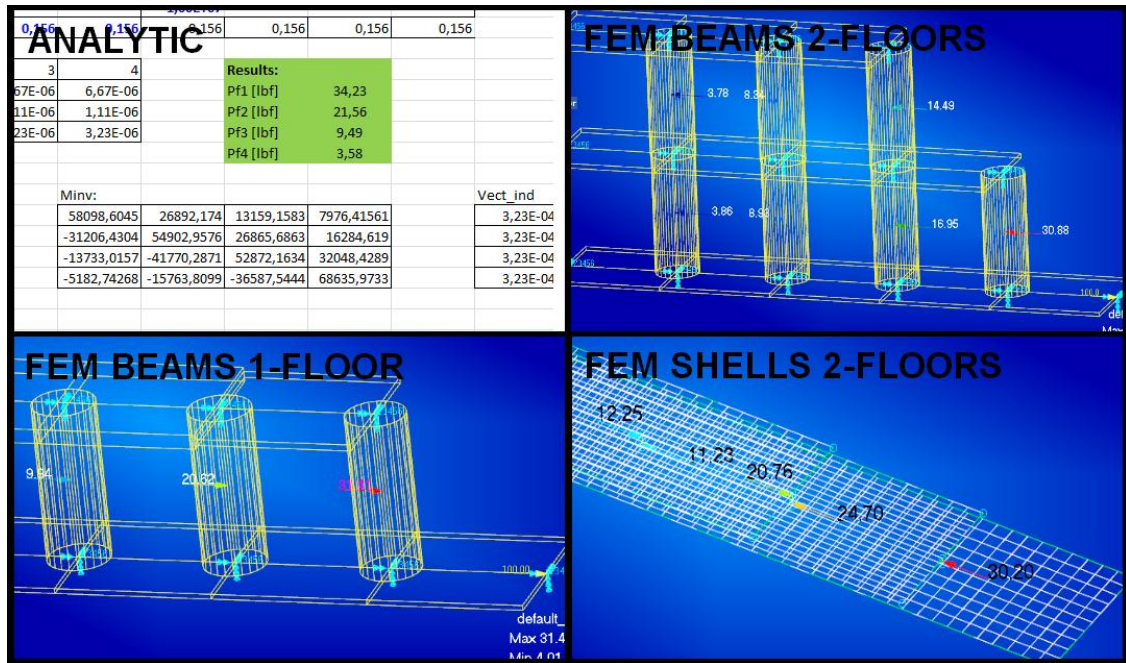


Figure 4.26- Schematic view for the 4 different analyzed methods

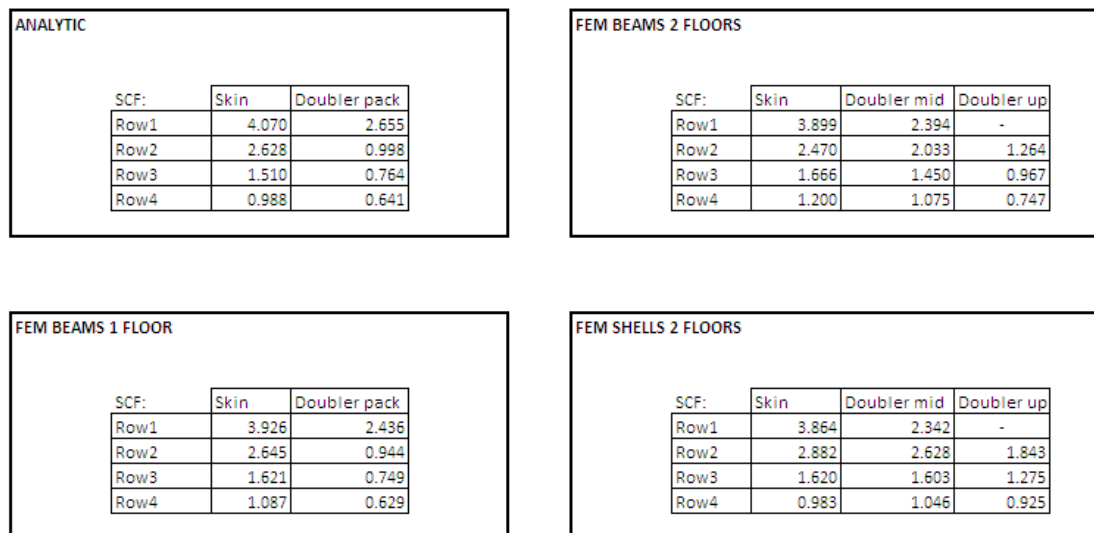


Figure 4.27- Stress concentration factor results for the 4 different analyzed methods

4.3.2.4.2 Ranking method definition

One common point the previous results is that the most critical SCF value is always placed in the skin, concretely at the first rivet row. It can be observed in Figure 4.27. In general, the difference between the different analyzing methods is not important. Also, the fact that the skin

is in all cases the worst plate in terms of stress concentration, justifies the use of the first two methods instead of the last two. Therefore the ranking of the most accurate method for studying multiple-doublers configurations:

1. Analytic
2. FEM beams 1 floor
3. FEM beams 2 floors
4. FEM shells 2 floors

As explained before in the section 4.3.2.3.2, it must be taken into account that those methods are simplifications of the reality, and are applicable to a simple rectangular-geometry doubler. For a more complex doubler configuration, the most accurate analysis is always the entire doubler FEM simulation, explained at the section 4.3.2.2.3, although it is the most complex and time expensive method.

4.3.2.5 Study of the inter-rivet distance influence in fatigue

The inter-rivet separation has an important influence over the structure in fatigue terms so the purpose of this section is studying it. A FEM case has been modeled in order to study that influence. It consists of a simple case of a doubler strip of two rivet rows like is illustrated in the Figure 4.28. The study consisted in carrying 5 different analysis of that structure, just increasing the inter-rivet separation in each configuration from 4-D to 8-D. In the Attachment I the specific data of the carried analysis for each distance between the first and the second row (D_r) value is shown.

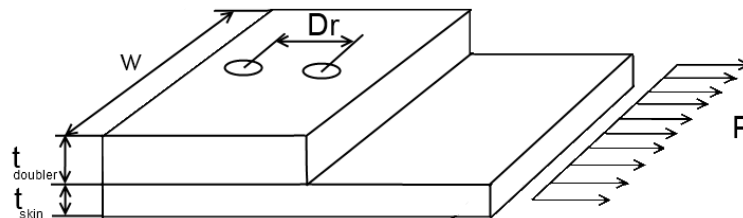


Figure 4.28- Schematic view of a two row doubler strip

Each case is simulated with a FEM model through the method of one dimension beam elements explained in the section 4.3.2.2.1. The results of the different FEM analysis for the bearing and the by-pass loads are resumed in the Table 4.5 for each case.

	P, By-pass load [lbs]		ΔP , Bearing load [lbs]	
	Row1	Row2	Row1	Row2
Case 1	365 (1624N)	325 (1445N)	91,4 (406N)	39,4 (175N)
Case 2	353 (1570N)	310 (1379N)	103 (458N)	43 (191N)
Case 3	343 (1526N)	297 (1324N)	113 (503N)	45,6 (203N)
Case 4	334 (1486N)	287 (1277N)	122 (543N)	47,4 (211N)
Case 5	327 (1455N)	278 (1237N)	129 (574N)	48,7 (216N)

Table 4.5- Results of load distribution after FEM analysis

All these values have been divided by the applied (P), in order to make non-dimensional the load results, and after they are plotted in Figure 4.29 and Figure 4.30. After that, the SCF is calculated through the formula (1.9). Their representation is shown in Figure 4.31.

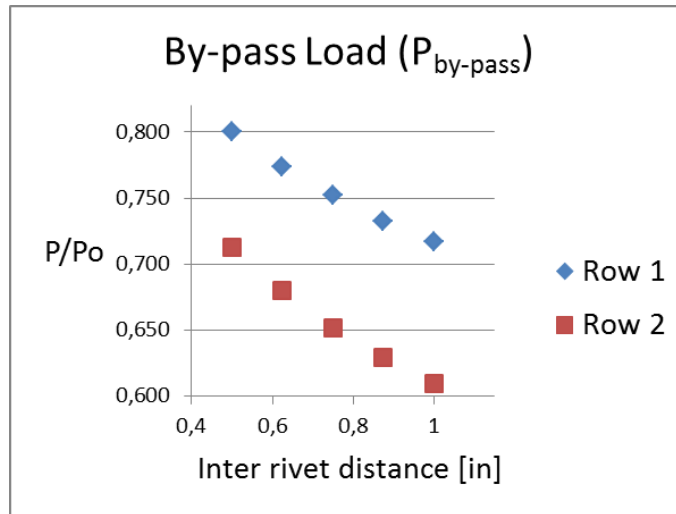


Figure 4.29- Non-dimensional by-pass load against inter-rivet distance

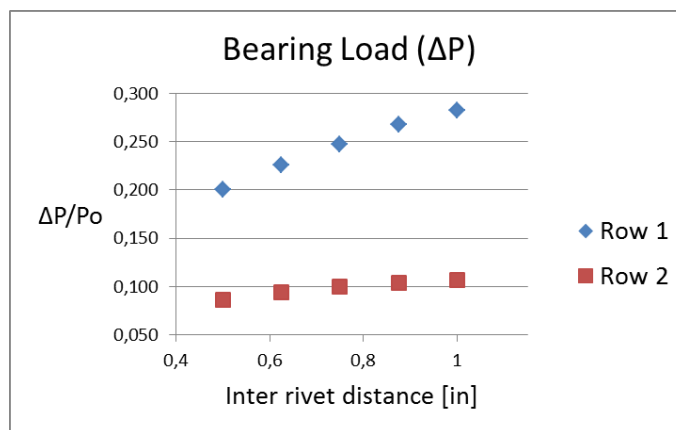


Figure 4.30- Non-dimensional bearing load against inter-rivet distance

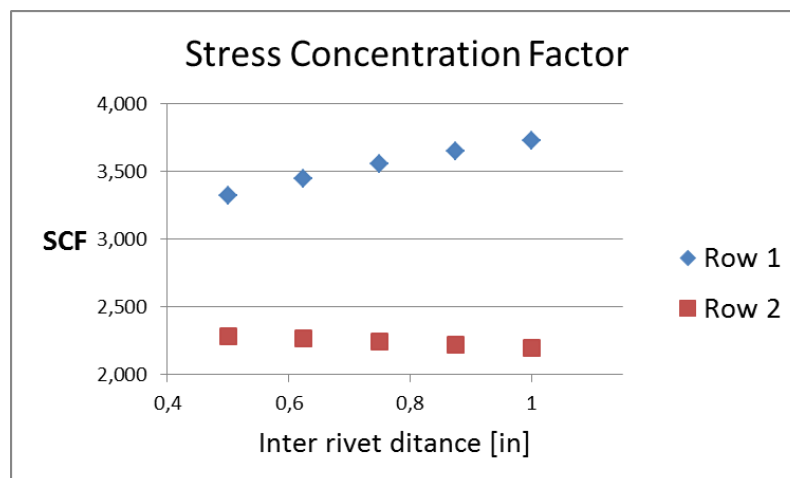


Figure 4.31- Stress concentration factor against inter rivet distance results

The stress concentration factor is more critical in the first rivet row like can be observed in the Figure 4.31, and it grows with the inter-rivet distance. It is due to the increase of the transfer or bearing load. The second row is not relevant for the fatigue analysis due to its low SCF values. When the inter-rivet separation is increased, the SCF increases as well in the first rivet row, so the fatigue behavior of the first rivet line gets worse. It may suggest so that the inter-rivet distance must be as little as possible, however it is important not to forget the center hole of the antenna that is placed at the center of the doubler. If the inter-rivet distance increases, the transfer (or bearing) loads at the rivets increases and the effective area of the doubler increases as well, and so does the load absorbed by the doubler. Then if the doubler absorbs more load, less load will arrive at the skin center hole, the bypass load at the central section will be lower, the SCF will decrease, and so the fatigue behavior improves at the center hole. Increasing the inter-rivet distance aggravates the rivet holes fatigue behavior, and improves the center antenna hole fatigue behavior. Decreasing the inter-rivet distance improves the rivet holes fatigue behavior, and aggravate the center antenna hole fatigue behavior. So it is important to look for a compromise in terms of performance when choosing the inter rivet distance. The main objective of a doubler is to absorb load, and make the load that reaches the antenna center hole smaller than it would be without it. But in the case of a splice, the objective is just to transfer the load, not to absorb. So in a splice case the inter-rivet distance must be chosen as the minimum allowable, which is $4D$.

4.4 Fatigue life determination

Once the load distribution across the doubler has been found, the next step is to find the fatigue life in number of cycles for which the aircraft modification will be designed for. For the fuselage, one cycle is taken as the GAG (Ground Air Ground) process, so it corresponds to one flight. For reaching a fatigue life number of cycles, the S-N curves must be analyzed.

4.4.1 Curves S-N

The S-N curves are built through experimental tests for each material. In the aeronautic industry the biggest manufacturers have their own ones. In this project, the used curves are the ones which correspond to the reference [3]. For a concrete material the curves give, in function of the maximum, minimum, and mean stress from the load spectrum, a number of fatigue life cycles. In Figure 4.32 it can be observed for Aluminum 2024 T3 material, and a 1.6 stress concentration factor value. Values of 30ksi of maximum stress and -0.37 of stress ratio R are taken for the example.

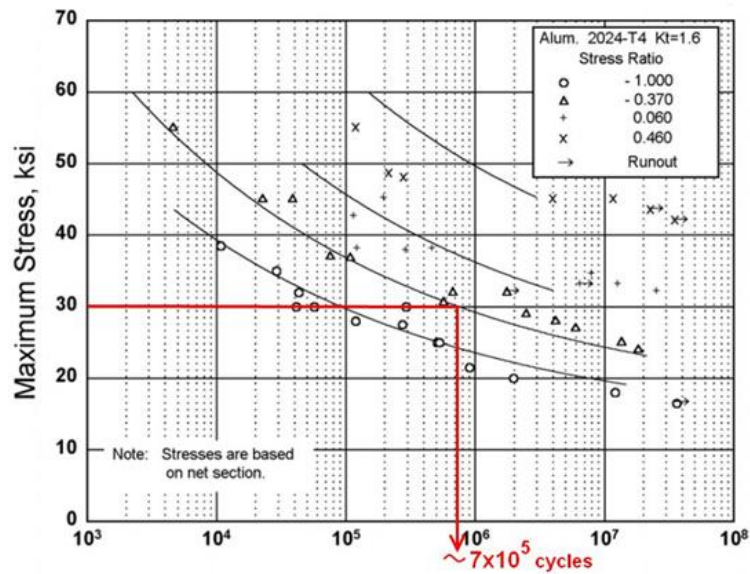


Figure 4.32- Fatigue life cycles determination [3]

The same reference [3] also provides of the logarithmic formulas extracted from the graphics, what allows carrying a more accurate calculus. The values from the previous example are used in the proper formula. The variable (S_{eq}) is the equivalent stress, (S_{max}) is the maximum stress, (R) is the stress ratio (minimum stress divided by maximum stress), and (N_f) is the fatigue cycles number.

$$S_{eq} = S_{max}(1-R)^{0.57} = 35.90 \text{ ksi} \quad (247.51 \text{ MPa}) \quad (4.40)$$

$$\text{Log} N_f = 12.25 - 5.16 \log(S_{eq} - 18.7) \rightarrow N_f = 7.5 \cdot 10^5 \text{ cycles} \quad (4.41)$$

The result is relatively near to the one directly extracted from the graphic. The only possible problem is that these tables are not constructed for every SCF. Therefore in a case in which the calculated SCF value is not corresponding to one table, a possible solution is to take the table for the next SCF allowable, adopting so a conservative behavior.

4.4.2 Scatter factor

The scatter factor is a value which is applied to the life number of cycles dividing it, so it significantly reduces the projected fatigue life of the structure. There are many different philosophies for defining it, and usually each manufacturer, civil, or military regulations, have its own one specification for it. The FAR adheres to use a scatter factor of 3 in stress strength for fatigue life analysis of safe-life structures. This factor is intended for account for fretting, clamped assembly stresses, size and surface effects, cumulative damage inaccuracies and other factors that affect fatigue life that are not included in the S-N tables [3] [4].

4.5 Developed software

In Figure 4.33 there is an image taken from the developed excel file, which implements all the previously calculus related with the fatigue analysis for one configuration.

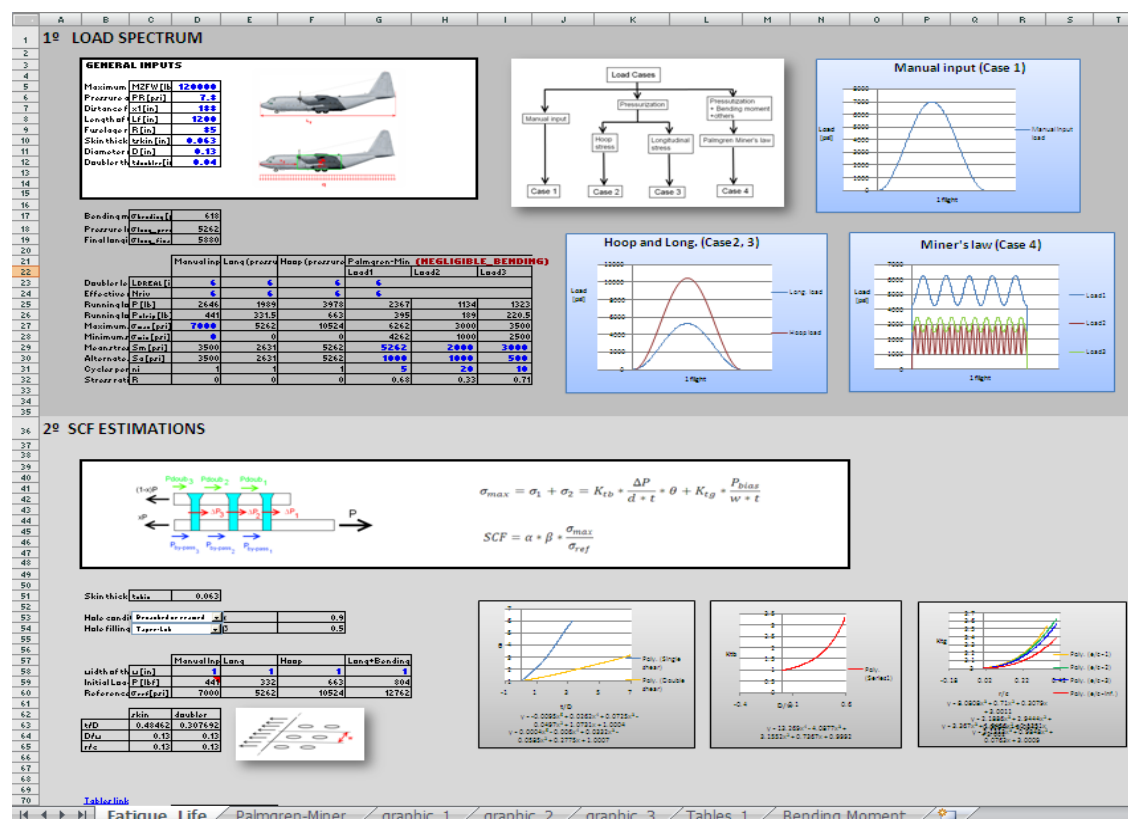


Figure 4.33- Fatigue excel print screen

5 Damage tolerance analysis

5.1 Damage tolerance analysis flowchart

The flowchart of the damage tolerance analysis procedure is shown in Figure 5.1. All the steps are better explained within the following sections.

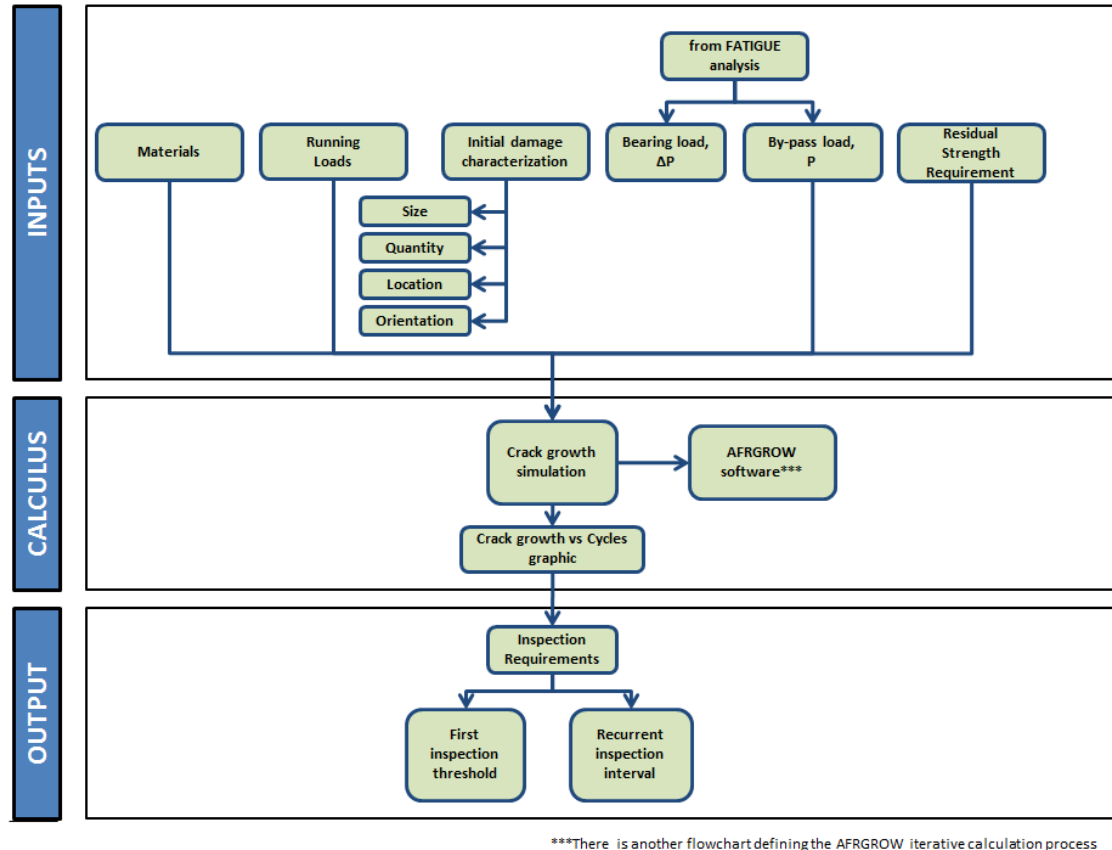


Figure 5.1- Damage tolerance analysis flowchart

5.2 Crack growth analysis

5.2.1 Initial damage characterization

The specification for the mean initial size is based on a study for the USA Air Force by McDonnell-Douglas in the 1970's. Experimental tests were made, and the final result for the quality flaws was that the 99% of the initial crack sizes were below or 0.005" (0.127mm). Therefore, a study for the rogue flaws was made and it was conservatively determined that the rogue crack initial flaw usually was around 0.05" (1.27mm). [23]

5.2.1.1 Initial damage size

The initial damage size assumption is defined in the reference [17]. The values are shown in Table 5.1, in function of some parameters defined in Figure 5.2. The variable (a_c) is the half crack length value, (b_c) is the crack length without hole, and (c_c) is the crack depth without hole.

Initial damage		
Picture ref.	Slow crack growth	Fail safe
a_c	0.05 in (1.27mm)	0.020 (0.5mm)
b_c	0.250 (6.35mm)	0.100 (2.54mm)
c_c	0.125 (3.17mm)	0.050 (1.27mm)

Table 5.1- Primary damage clasification

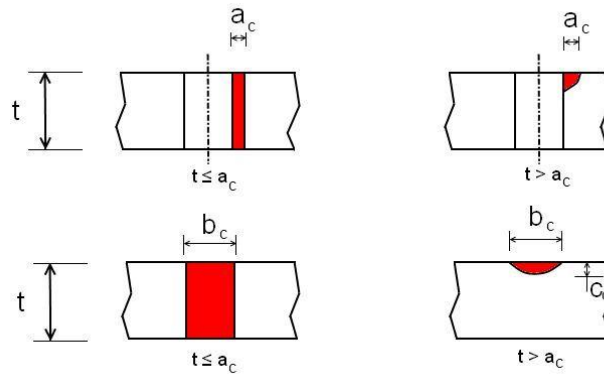


Figure 5.2- Damage characterization's lengths

5.2.1.2 Initial damage location and orientation

The damage location in the damage tolerance study of a joint is carried at the worst place, and with the worst possible crack leading edge orientation. In a doubler antenna reinforcement plate design, the most critical sections are the first rivet row, and the cutout's hole. The first rivet row is critical because the transmitted load is always maximum on the first line, what implicates an increase of the stress concentration. The cutout antenna center hole is critical due to the big diameter it has in comparison with any other hole on the skin. A possible generic disposition can be observed in Figure 5.3 for longitudinal and hoop. The critical orientation of the crack is when the crack edge is in 90 degrees phase compared with the applied stress direction.

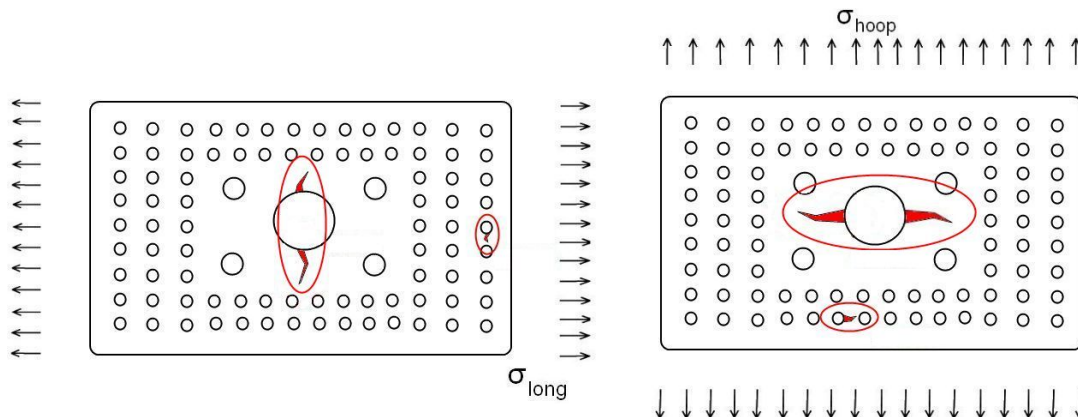


Figure 5.3- Initial crack damages for hoop and longitudinal stress states

5.2.2 Load spectrum

It is already defined in fatigue analysis, in the section 1.4.2.2.

5.2.3 Stress intensity factor

The stress intensity factor (K_I) can be analyzed in two different ways: either with a general, the equation (5.1); or regarding a cyclic loading, the equation (5.2) [2].

$$K_I = \beta_{IC} \Delta\sigma (\pi a_c)^{1/2} \quad (5.1)$$

$$K_I = \sigma_{\max} (1-R)^m (\pi a_c)^{1/2} \quad (5.2)$$

In Figure 5.4 there is a combination of various load cycles, the total stress intensity factor can be determined through the next formula, taken from the reference [2]. The variable (K_{In}) is the (K_I) for a determined load cycle, (β_{IC}) is a correction factor, and (m) is a constant which depend on the material.

$$K_I = \sum_{i=1}^n K_{In} \quad (5.3)$$

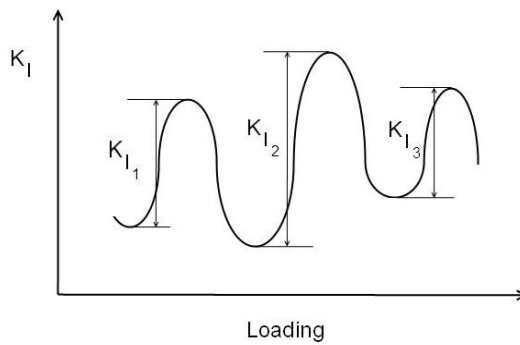


Figure 5.4- Combination of different magnitude K_I [2]

5.2.4 Crack growth rate study

The crack growth rate (da/dN) is a parameter which requires to be defined before simulating any crack growth. There are several expressions defined which are commonly used in DT simulations: Paris' equation, Forman's equation, NASGRO equation, Walker's equation, etc. The Attachment J contains a summary of the possible formulation.

5.2.4.1 Crack growth simulation steps procedure

In Figure 5.5 there is the iterative algorithm that the existing damage tolerance software uses in order to simulate the crack growth. The steps are explained here:

1. There are some initial conditions which must be adopted. After that point, the initial correction factor and the applied stress are computed.
2. After that the stress intensity factor (ΔK_n) is calculated with the pertinent formula.
3. The following step is to extract the crack growth rate (da/dN) from one of the possible formulas studied in the section 5.2.4.

4. Calculate the medium value between the present and the previous iteration.
5. Determine the cycle's increment (ΔN) corresponding to the iteration crack growth increment.
6. Analyze whether the critical conditions are reached or not. There are two possible critical conditions:
 - a. Critical crack length (a_c), that exactly means to reach the critical stress intensity factor (ΔK_n).
 - b. Critical value of residual strength, that exactly means reaching the residual strength requirement (σ_{res}).
7. The following step has two options: finishing the analysis if critical conditions are reached, or return into the iterative process simulating the next cycle.

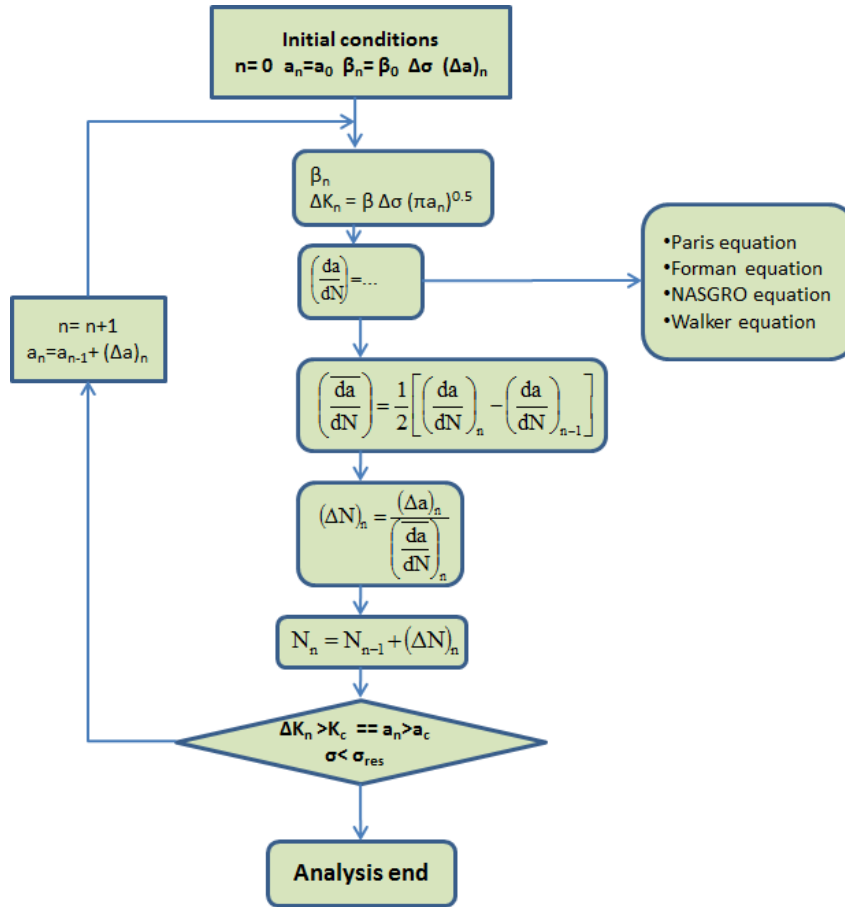


Figure 5.5- Crack growth simulation iterative procedure

The previous explanation is useful for when there is just one fracture growing. When there are several cracks growing at the same time, MSD should be considered.

5.3 Inspection requirements

5.3.1 Non-destructive inspection methods

The six most common NDT methods are explained, with the minimum detectable flaw sizes and geometries, in the Attachment K, with the references [18], [19], [7].

5.3.2 Inspection determination intervals

There are two necessary outputs from the DT analysis of a component illustrated in Figure 5.6:

- Threshold or initial inspection requirement
- Recurrent inspection requirement

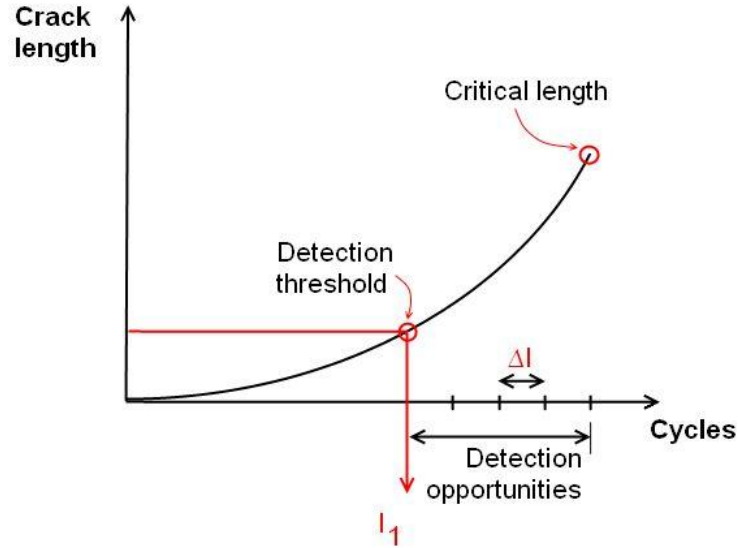


Figure 5.6- Crack growth inspection plan method

5.3.2.1 Threshold inspection

It is the number of cycles for the first inspection. The first inspection threshold (I_1) can be defined in two ways:

- The half the total number of cycles the structure can withstand ($\frac{N_{fail}}{2}$) [17].
- The minimum detectable length. That minimum detectable length obviously depends on the inspection method to be carried (Attachment K). It will give the cycles value (N_{det}).

The following expression represents that calculus.

$$I_1 = \min \left\{ \frac{N_{fail}}{2} ; N_{det} \right\} \quad (5.4)$$

5.3.2.2 Recurrent inspection

As from the first inspection, the possibility that the structure may have a detectable crack is assumed. So a frequency of inspections (ΔI) must be defined to ensure that if it exists, it will be found before it reaches critical dimensions. It is the inspection period to be adopted after the first inspection. So it is the time between the structure failure and the first inspection, divided by a scatter factor ($K_{scatter}$) which adds safety. A value of 3 or 4 usually is a good option, because it ensures the possibility of detecting at least 3 or 4 times the crack before the component fail or collapse. It finally depends on each manufacturer or maintenance company own experience and criteria; however, it is analyzed in the following part. [4]

$$\Delta I = \frac{(N_{fail} - N_{det})}{K_{scatter}} \quad (5.5)$$

5.3.2.3 Scatter factor definition

In damage tolerance terms, the scatter factor defines the minimum of real opportunities of crack detection once an inspection method has been defined. The entity that carries the analysis must define it having into account various factors, like the age of the aircraft, the aircraft defect inspection program, the philosophy used the initial design, etc. That factor is very influent in the inspection program, therefore has to be properly justified and approved by the correspondent aeronautical entity.

5.4 AFGROW method

5.4.1 Inputs per growth analysis

The AFGROW software inputs are represented in Figure 5.7.

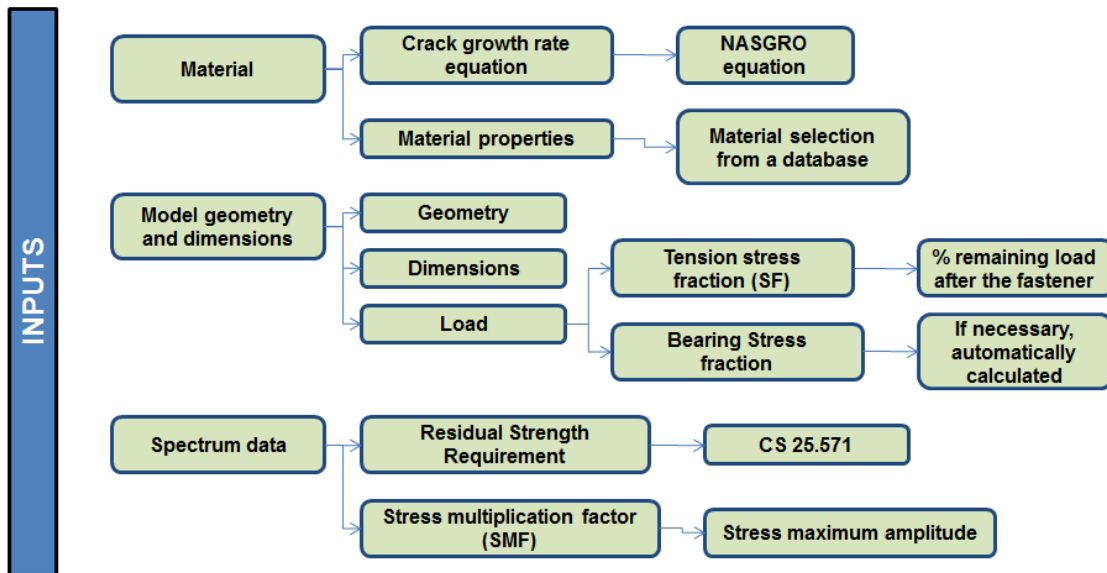


Figure 5.7- AFGROW inputs flowchart

5.4.2 Analysis methodology

5.4.2.1 Studied cases

The most critical sections in damage tolerance terms are the first rivet line, and the cut-out hole. So two cases are considered for the longitudinal and hoop direction. The “Case 1”, is divided in three phases of study. The “Case 2” is just divided in two phases of study. These cases can be seen in Figure 5.8.

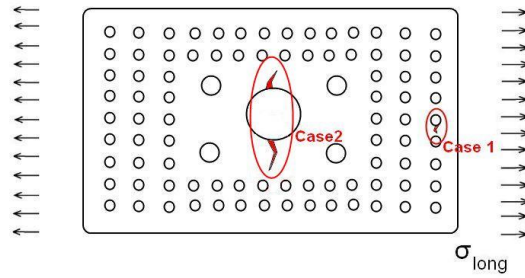


Figure 5.8- One-doubler with the two critical sections selected

5.4.2.2 Methodology

To begin the analysis, an initial crack is assumed. Then the crack growth is simulated until it fails (reaches the critical flaw size or the residual strength requirement), and so reaches the next rivet holes, which temporally stop the crack growth. However, once the nearest holes have been reached they are assumed to have an initial flaw as well, which will initiate the growth again. For the Case1 is assumed that when the crack grows through more than four rivet lines, the doubler structure fails, and is represented in Figure 5.9. However, for the Case2 that failure is assumed when the flaw grows further than the first rivet line, since the initial antenna cutout hole is much bigger than a rivet hole, and it is represented in Figure 5.10.

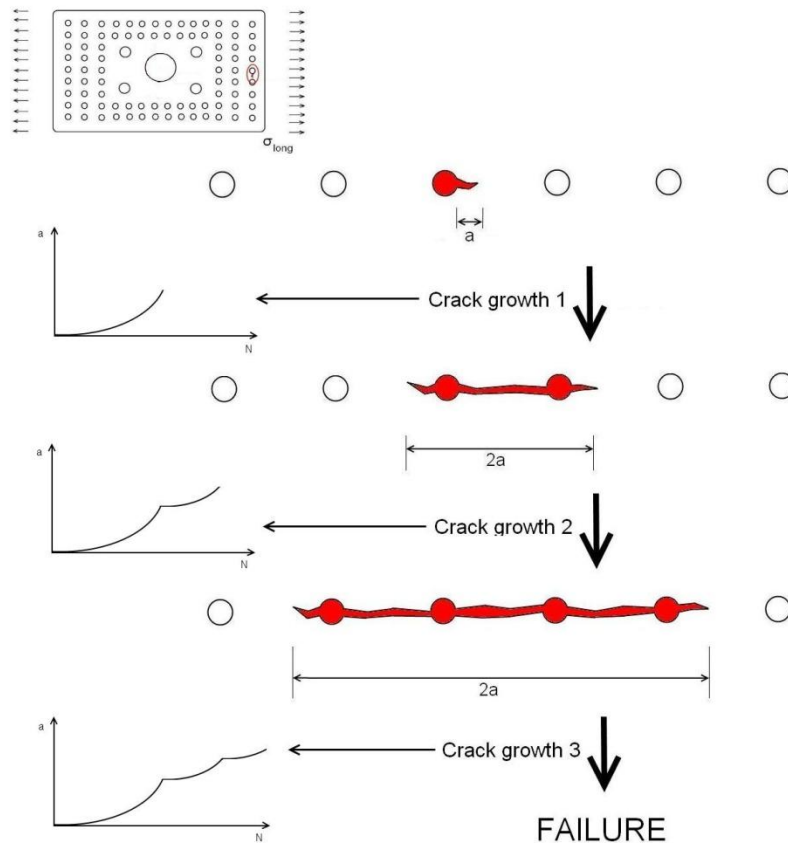


Figure 5.9- Representation of the analyzing method for the first row, Case1

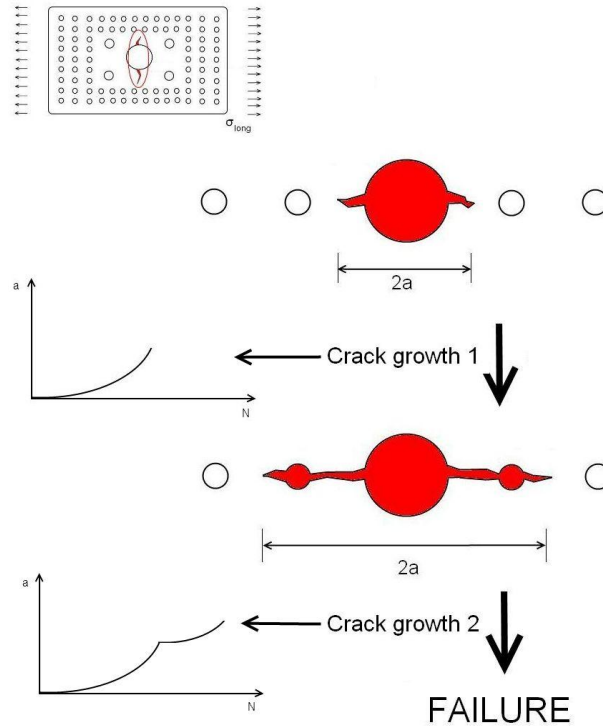


Figure 5.10- Representation of the analyzing method for antenna center hole, Case2

5.4.2.3 Results interpretation

For each one of the previously explained cases, an example graphic of crack length versus cycles is obtained for each phase in a excel file through the AFGROW software. The different files must be fitted together constructing so the final graphic for the crack length. In Figure 5.11 an example of that graphic can be observed. The inputs and the outputs are indicated, and it corresponds to a three phase's case.

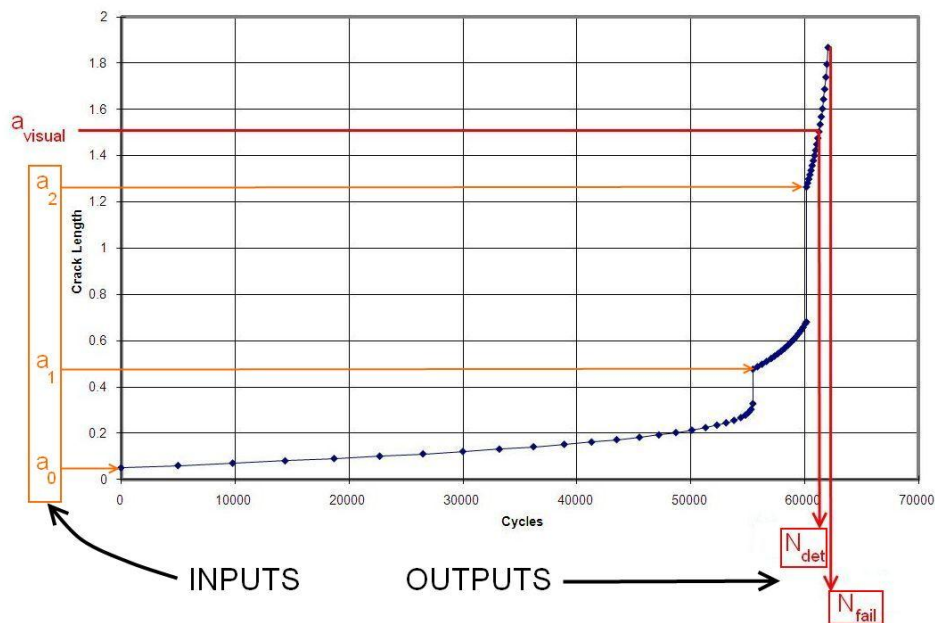


Figure 5.11- Crack growth graphic with inputs and outputs

Eventually, the procedure to be applied to get the inspection plan is explained in the section 5.3.2.

5.5 Fatigue influence of modifying multiple-doublers configuration position

The objective of this section is to study the effect of the doublers configuration, in function of whether the reinforcing plates are superposed one upon each other in the same side of the aircraft skin (doubler and tripler), or if they are placed respectively in the inside and the outside of the aircraft (stacked doublers), where the rivets work in double-shear mode.

The stacked doublers are used in the following situations:

- When the ultimate rivet strength is not enough for the application.
- For avoiding the eccentricity, when thick plates are involved. If the plates were thick enough and just one doubler was implemented, it could not be treated as a plane stress. This is because the distance between the symmetry edge of the different plates would be big enough like to create a significant bending moment which could create a problematic eccentricity on the zone.
- For carrying a fail-safe design, where alternative load paths are required.

5.5.1 Configuration example case study

The followed analyzing method consists in the definition of a 2 doublers configuration design example, and the subsequent study of its behavior in 2 different configurations, represented in Figure 5.12. The objective is the comparison between the results for the Case 1 and Case 2.

- Case1: Doubler and tripler: two internally superposed doublers.
- Case2: Stacked doublers: the smallest doubler is placed on the opposite side of the Case1, so one internal and one external doubler is the final configuration.

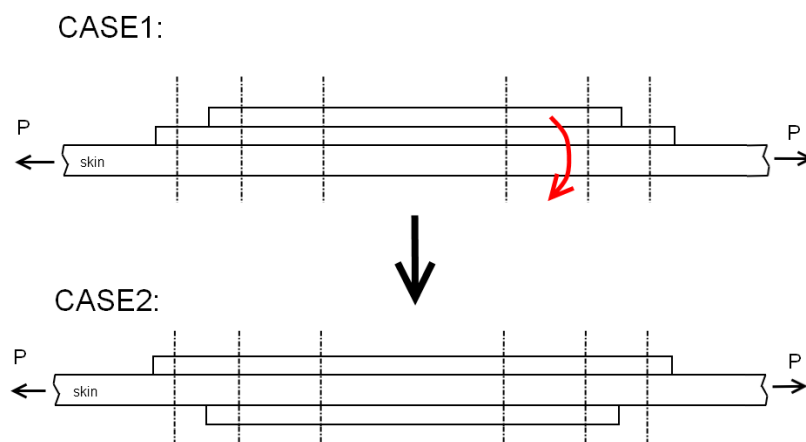


Figure 5.12- Case one versus case two

5.5.1.1 FEM model 1D beam elements simulation

In the FEM model with beam elements, the zone studied consists just in one strip of the repair, like shown in Figure 5.13. The specific data for the example is shown in the Attachment L.

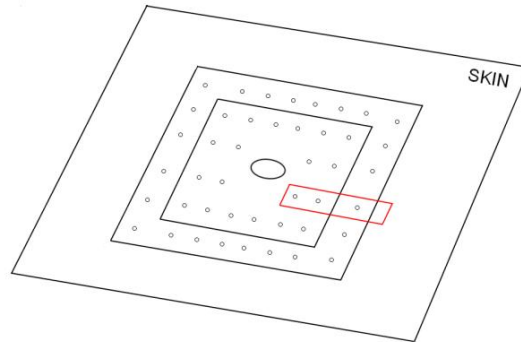


Figure 5.13- Two doublers with the selected zone of study

5.5.1.1.1 Case 1:

The MSC PATRAN/NASTRAN software is used for this simulation. In Figure 5.14 the outputs are shown. The relevant values of the analysis are the fastener transfer loads. The restrictions chosen are the three nodes at the left totally embedded, and just allowing the x translation to the rest of nodes. The FEM data can be observed at the Attachment E.

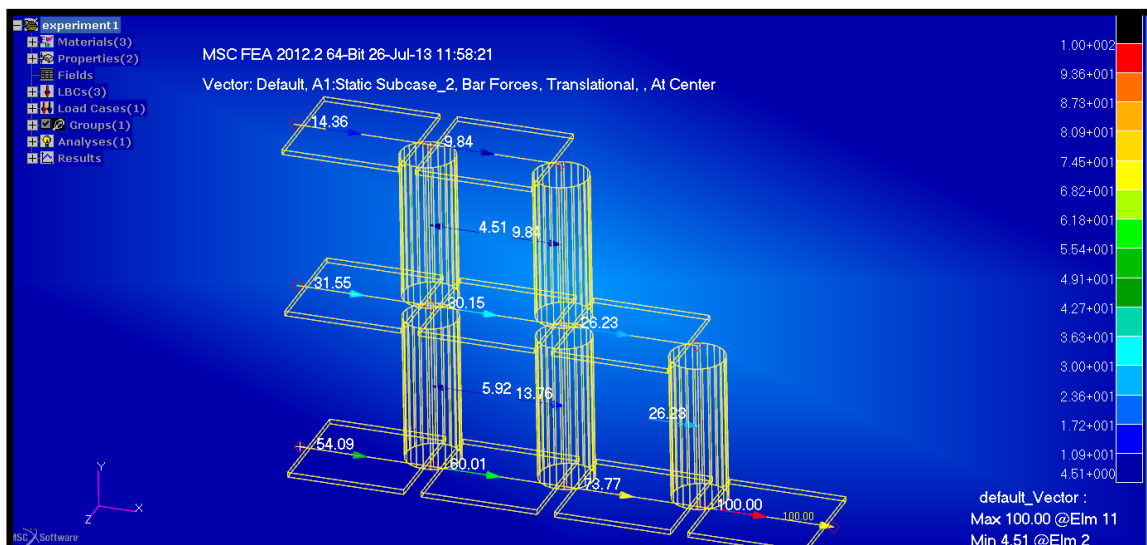


Figure 5.14- Case 1 one strip beam elements transfer loads result

5.5.1.1.2 Case 2:

The MSC PATRAN/NASTRAN software is again used for this simulation. In Figure 5.15 the outputs are shown. The restrictions chosen are the three nodes at the left totally embedded, and just allowing the 'x' translation to the rest of nodes. The FEM data can be observed at the Attachment E.

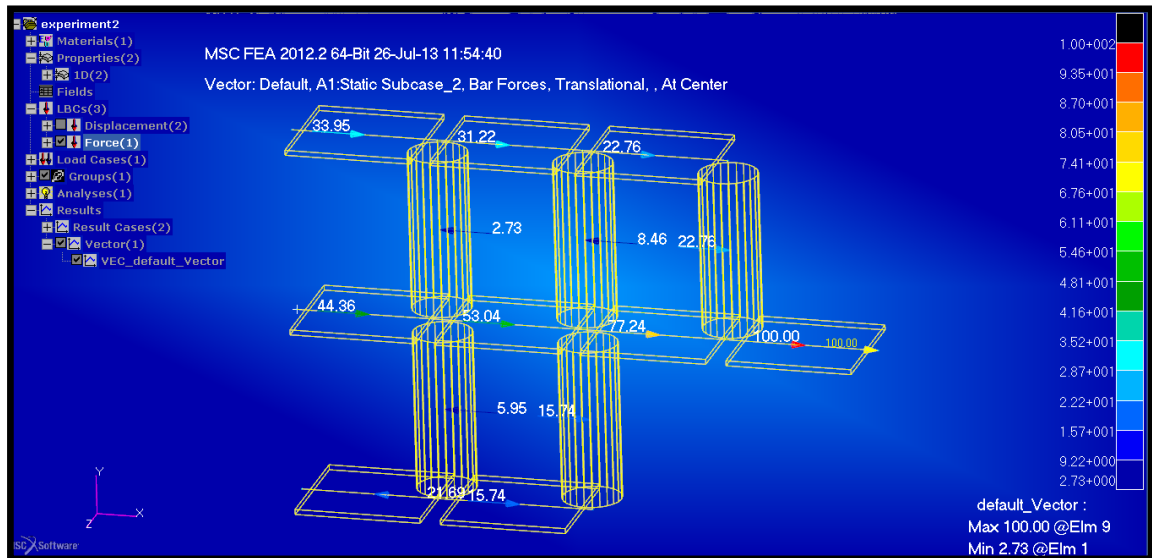


Figure 5.15- Case 2 one strip beam elements transfer loads result

To verify the reality of the previously used methods, an entire doubler simulation with FEM “shell” elements for the same 2 cases is done. It is shown in the Attachment L.

5.5.1.2 Critical fatigue zone and initial crack definition

The rows where the rivet load is higher are those in which the fatigue behavior gets critical. It is shown in Figure 5.16 for both cases.

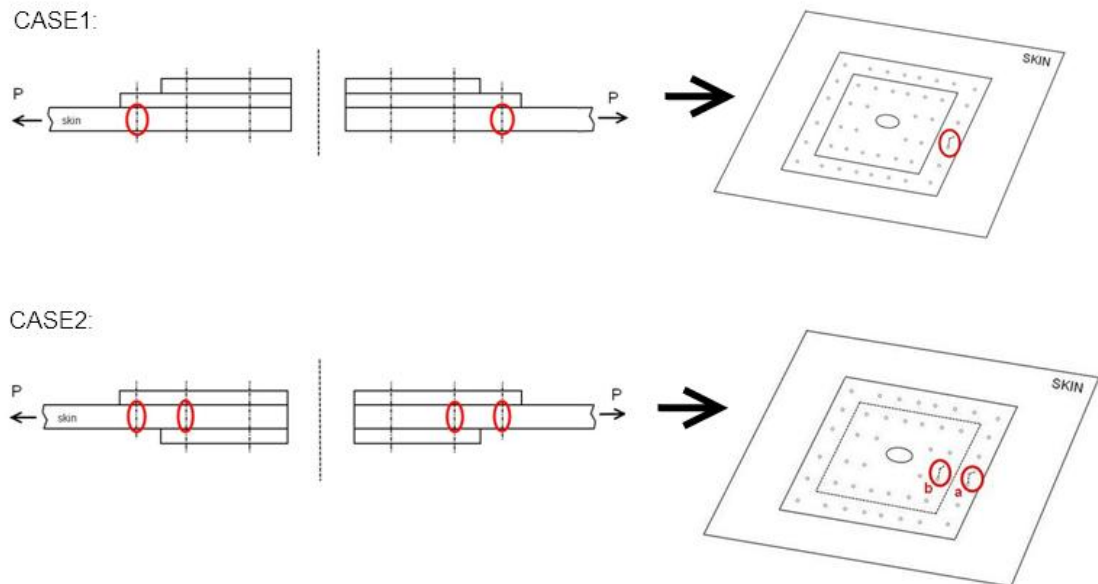


Figure 5.16- Critical zone and initial crack definition

5.5.1.2.1 Case 1

A single through crack at the hole of 0.05” (1.27mm) at the first rivet row is considered. The crack configuration can be observed at the following picture. In terms of load spectrum, 10ksi (69MPa) with a residual strength requirement of 17ksi (117MPa) have been considered. The

material is Aluminum 2024 T3. The by-pass stress ratio input is 0.7377, like can be extracted from Figure 5.14.

5.5.1.2.2 Case 2

Two sub-cases of 0.05" single through cracks at the hole are separately considered, one at the first row (a), and the other at the second rivet row (b). In terms of load spectrum, 10ksi with a residual strength requirement of 17ksi have been considered. The material is Aluminum 2024 T3. The by-pass stress ratio input is 0.7724 for the sub-case (a), and 0.7580 for the sub-case (b), like can be extracted from Figure 5.15.

5.5.1.3 AFGROW simulation of the cases

5.5.1.3.1 Case1:

The result of the analysis is 177634 cycles, shown in the Figure 5.17.

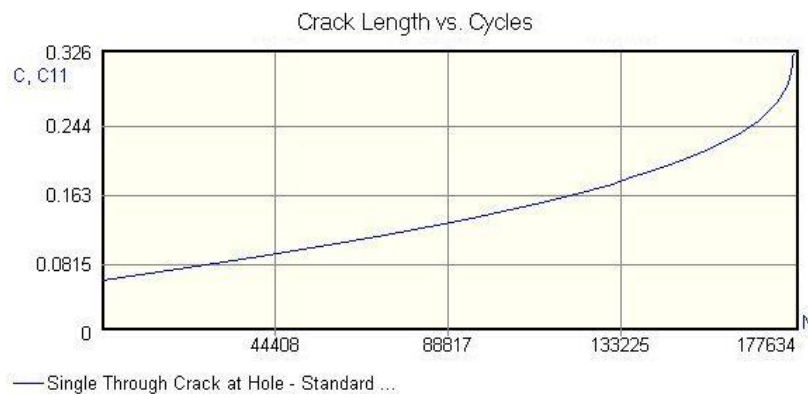


Figure 5.17- Crack growth for case1

5.5.1.3.2 Case2:

The result of the same analysis for the sub-cases (a) and (b) are 179764 and 178856 cycles respectively.

5.5.2 Analysis of the results

The target of the previous analysis was to check how the load is distributed through the rivet lines. The fact of using two different FEM methods was to check whether the behavior of each one of them is similar to the other, and it has been like that. When changing from the CASE1 to the CASE2 the load transmitted at the first rivet row decreases, and the total load absorbed by the doublers structure is higher, so they are more effective. The CASE1 has a shorter life in damage tolerance terms in front of the CASE2. So the CASE2's fatigue behavior is better than in the CASE1. In addition, the reinforcing doubler is more effective in CASE2, since the load that reaches the skin at the cut-out section is smaller. It happens because the rivets absorb more load, and the cause of that is that they are working in double-shear, so they are able to absorb higher load values. Another inconvenient of the CASE2 is that the skin cannot be examined in an inspection through a visual method. The only options are other non-destructive methods, which would considerably increase the maintenance costs.

5.5.2.1 Table of results summarized:

Table 5.2 contains a summary of the cases 1 and 2 with some conclusions of them.



Comparison table resume	CASE1	CASE2
Configuration description	Internal doubler and tripler different size	Stacked doublers different size
Configuration image		
Advantages	<ul style="list-style-type: none"> -Visual inspection possibility -Easier installation procedure -Better aerodynamic behavior -Little maintenance costs 	<ul style="list-style-type: none"> -More effective statically -Better fatigue and DT behavior -The rivets work in double-shear
Disadvantages	<ul style="list-style-type: none"> -Worse fatigue and DT behavior than Case2 -Less effective statically than Case2 	<ul style="list-style-type: none"> -Requires non-destructive methods for inspection -Installation procedure may be more complicated depending on the place -Increases maintenance costs

Table 5.2- Advantages and disadvantages of cases 1 and 2

5.6 Developed software

In Figure 5.18 there is an image taken from the developed excel file, which implements the previously calculus related with the damage tolerance analysis for one configuration.

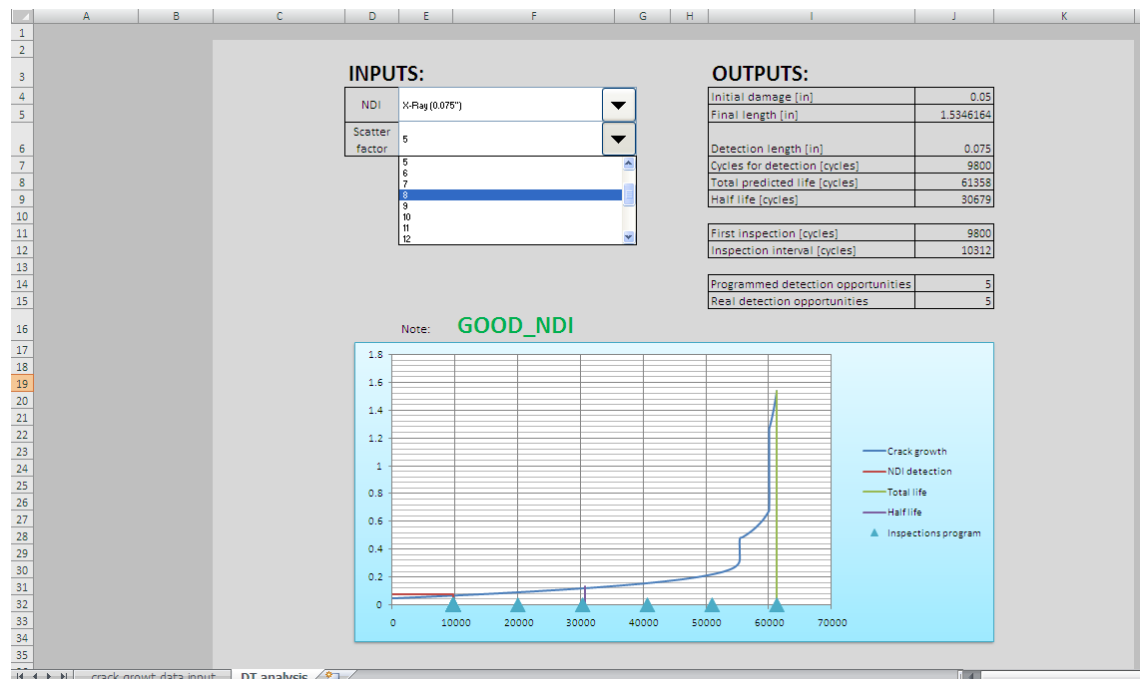


Figure 5.18- Damage tolerance excel print screen

6 Conclusions

✓ A procedure and four Microsoft excel files supporting the methodology have been developed during a six-month internship at the company OGMA, Indústria Aeronáutica de Portugal, SA. Three excel files enable determining the static, fatigue, and damage tolerance behavior of a doubler reinforcement structure. The fourth file supports the fatigue calculus with an analytic matrix calculus. The methodology principles are explained at the current report, which allows any engineer user to carry the proper structural analysis in order to certify the structural calculation in front of the pertinent aeronautical authority, in this case EASA.

✓ The initial objective of checking a design in less than two hours was achieved.

✓ An analytical and fast method of determining whether an antenna installation will require just a doublers reinforcement structure or a deeper structural modification has been defined and verified through FEM methods.

✓ In fatigue and damage tolerance terms, it is simpler and more conservative to analyze separately one direction stress than bi-axial stresses of the same magnitude.

✓ Different methods of analyzing a simplified joint riveted structure have been studied. It has resulted in an optimal ranking of methods, and their proper explanation. It optimizes the fatigue and damage tolerance analysis.

✓ Different methods of analyzing a simplified multiple-doublers reinforcement structure have been analyzed, resulting in an optimal ranking of methods, which coincide with the previous one.

✓ The stress concentration factor in the first rivet row of a doubler reinforcement structure grows with the inter-rivet distance. However, the absorbed by-pass load decreases, and so does the real effectiveness of the doubler. A compromised solution in that point must be achieved by the engineer when designing the configuration.

✓ A damage tolerance simple analysis method has been accurately defined. It has been through the AFGROW software, but can be applied with any other damage tolerance software.

✓ Given an internal multiple-doublers reinforcements configuration, it is better structurally in static, fatigue, and damage tolerance terms to change one of the internal doublers to an external position.

7 Future work

7.1 Application of riveted doublers to a composite material fuselage

The newest large aircraft models of Boeing and Airbus have a composite material fuselage. It is mainly composed of carbon fiber and epoxy materials. It causes a big issue in terms of how is the best way to carry reparations (the procedure for an antenna installation would be similar) in that kind of fuselages. There are two options: bonded composite repairs, and riveted repairs. The bonded repairs are preferable in terms of weight increase, stress concentration, aerodynamics, esthetically... However they have some important inconvenient in terms of difficulties in surface preparation, high specialized personal is required, non-destructive methods are required, they are difficult to localize...

The fastened material can be both metallic and composite as well. Metallic Titanium material is optimal to avoid corrosion with the carbon fiber.

So the work carried in the current thesis can be completed with a study of the statics, fatigue, and damage tolerance of the structural modification that an antenna installation implies to composite material fuselage.

8 Bibliography

- [1] **Alteon, a Boeing Company.** *Aircraft Structural Repair for Engineers.*
- [2] **Niu, Michael C.Y.** *Airframe Stress Analysis and Sizing.* s.l. : Hong Kong Conmilit Press, 1997.
- [3] **FAA.** *Metallic Material Properties Development and Standarization 01.* s.l. : FAA, 2003. MMPDS-01.
- [4] **Niu, Michael C.Y.** *Airframe Structural Design.* s.l. : Hong Kong Conmilit Press, 1988.
- [5] **EASA.** *CS-25 Certification Specifications for Large Aeroplanes.* s.l. : EASA, 2013. CS-25.
- [6] **Schijve, J.** *Fatigue of Structures and Materials.* s.l. : Kluwer Academic Publishers, 2004.
- [7] **FAA.** *Airworthiness Directive A277 100.* s.l. : FAA, 1994. FAA/AD-A277 100.
- [8] **Wanhill, R.J.H.** *Fatigue and Corrosion in Aircraft Cabin Pressure Lap Splices.* s.l. : National Lucht-en Ruimtevaartlaboratorium (NLR), 2000.
- [9] **eFunda.** Stresses and Displacements near Crack Tips. [Online] 05 de August de 2013.
http://www.efunda.com/formulae/solid_mechanics/fracture_mechanics/fm_lefm_stress.cfm.
- [10] **Afgrow.** DTD Handbook. [Online] Afgrow, 5 August 2013.
http://www.afgrow.net/applications/DTDHandbook/sections/page2_2_4.aspx.
- [11] **FAA.** *Advisory Circular 43.13-2B.* s.l. : FAA, 2008. FAA/AC43.13-2B.
- [12] **Young, Warren C. e Budynas, Richard G.** *Roark's Formulas for Stress and Strain.* s.l. : Mc Graw Hill, 2002.
- [13] **EOL.** C-130 Basic Specifications. *C-130 Investigators Handbook.*
- [14] **Pilkey, Walter D.** *Stress Concentration Factors.* s.l. : John Wiley & Sons, Inc, 1997.
- [15] **NASA.** Fastener Design Manual. 1990.
- [16] **Swift, T.** *Repairs to Damage Tolerant Aircrafts.* 1990. FAA-AIR-90-01.
- [17] **USAF.** *Damage Tolerance Design Handbook: Guidelines for the Analysis and Design of Damage Tolerant Aircraft.* 1978.
- [18] **FAA.** *Advisory Circular 43-204.* s.l. : FAA, 1997. FAA/AC43-204.
- [19] **testing, NDT Non-Destructive.** Overview of Non-Destructive testing. [Online] NDT-Resoure center, 10 August de 2013. <http://www.ndt-ed.org/>.
- [20] **FAA.** *Airworthiness Directive A274 777.* s.l. : FAA, 1993. FAA/AD-A274 777.
- [21] —. *Fatigue Crack Growth Database for Damage Tolerance Analysis AR-05/15.* s.l. : FAA, 2005. FAA/AR-05/15.

- [22] **NASA.** Non-Destructive Evaluation Requirements for Fracture-Critical Metallic Componentets. *Technical Standard*. 2008.
- [23] **FAA.** *Damage Tolerance Assessment Handbook, Vol. 2: Airframe Damage Tolerance Evaluation*. 1994.
- [24] **Broek, D.** *The Practical Use of Fracture Mechanics*. s.l. : Kluwer Academic Publishers, 1988.
- [25] **Justino, L.M.** *Systematic Procedure for Design and Certification of Structural Repairs*. 2008.
- [26] **Lourenço, B.V.** *Damage Tolerance Design*. 2010.

Attachment A. Flat plate stress calculation coefficients

(At center) $\sigma_{\max} = \sigma_b = \frac{\beta W}{t^2}$ where $W = qa_1b_1$

a_1/b b_1/b	$a = b$						$a = 1.4b$						$a = 2b$					
	0	0.2	0.4	0.6	0.8	1.0	0	0.2	0.4	0.8	1.2	1.4	0	0.4	0.8	1.2	1.6	2.0
0		1.82	1.38	1.12	0.93	0.76		2.0	1.55	1.12	0.84	0.75		1.64	1.20	0.97	0.78	0.64
0.2	1.82	1.28	1.08	0.90	0.76	0.63	1.78	1.43	1.23	0.95	0.74	0.64	1.73	1.31	1.03	0.84	0.68	0.57
0.4	1.39	1.07	0.84	0.72	0.62	0.52	1.39	1.13	1.00	0.80	0.62	0.55	1.32	1.08	0.88	0.74	0.60	0.50
0.6	1.12	0.90	0.72	0.60	0.52	0.43	1.10	0.91	0.82	0.68	0.53	0.47	1.04	0.90	0.76	0.64	0.54	0.44
0.8	0.92	0.76	0.62	0.51	0.42	0.36	0.90	0.76	0.68	0.57	0.45	0.40	0.87	0.76	0.63	0.54	0.44	0.38
1.0	0.76	0.63	0.52	0.42	0.35	0.30	0.75	0.62	0.57	0.47	0.38	0.33	0.71	0.61	0.53	0.45	0.38	0.30

Attachment B. MMPDS relevant tables

Attachment B.1. Shear strength correction factor

Table 8.1.2.1(b). Shear Strength Correction Factors for Solid Protruding Head Rivets*

Rivet Diameter, in.	1/16	3/32	1/8	5/32	3/16	1/4	5/16	3/8
Single-Shear Rivet Strength Factors								
Sheet thickness, in.:								
0.016	0.964
0.018	0.981	0.912
0.020	0.995	0.933
0.025	1.000	0.970	0.920
0.032	...	1.000	0.964	0.925
0.036	0.981	0.946	0.912
0.040	0.995	0.964	0.933
0.045	1.000	0.981	0.953
0.050	0.995	0.970	0.920
0.063	1.000	1.000	0.961	0.922	...
0.071	0.979	0.944	0.909
0.080	0.995	0.964	0.933
0.090	1.000	0.981	0.953
0.100	0.995	0.972
0.125	1.000	1.000
Double-Shear Rivet Strength Factors								
Sheet thickness, in.:								
0.016	0.687
0.018	0.744	0.518
0.020	0.789	0.585
0.025	0.870	0.708	0.545
0.032	0.941	0.814	0.687	0.560
0.036	0.969	0.857	0.744	0.630	0.518
0.040	0.992	0.891	0.789	0.687	0.585
0.045	1.000	0.924	0.834	0.744	0.653
0.050	...	0.951	0.870	0.789	0.708	0.545
0.063	...	1.000	0.937	0.872	0.808	0.679	0.550	...
0.071	0.966	0.909	0.852	0.737	0.622	0.508
0.080	0.992	0.941	0.891	0.789	0.687	0.585
0.090	1.000	0.969	0.924	0.834	0.744	0.653
0.100	0.992	0.951	0.870	0.789	0.708
0.125	1.000	1.000	0.935	0.870	0.805
0.160	0.992	0.941	0.891
0.190	1.000	0.981	0.939
0.250	1.000	1.000

* Sheet thickness is that of the thinnest sheet in single-shear joints and the middle sheet in double-shear joints. Values based on tests of aluminum rivets, Reference 8.1.

Attachment B.2. Single shear strength of solid rivets

Table 8.1.2(b). Single Shear Strength of Solid Rivets^a

Table 0712(b): Single Shear Strength of Solid Rivets													
Undriven			Driven		Rivet Designation	Rivet Size							
Rivet Material	F _u (ksi)		Rivet Material	F _u ^b (ksi)		1/16	3/32	1/8	5/32	3/16	1/4	5/16	3/8
	Min	Max				Driven Single Shear Strength, lbs ^c							
5056-H32	24	n/a	5056-H321 ^d	28*	B ^f	99	203	363	556	802	1450	2290	3275
2117-T4	26	n/a	2117-T3	30*	AD	106	217	389	596	860	1555	2455	3510
2017-T4	35	42	2017-T3	38*	D	134	275	493	755	1085	1970	3115	4445
2024-T4	37	n/a	2024-T31	41*	DD	145	297	532	814	1175	2125	3360	4795
7050-T73	41	46	7050-T731 ^d	43*	E ^h	152	311	558	854	1230	2230	3520	5030
Monel	49	59	Monel	52*	M	183	376	674	1030	1490	2695	4260	6085
Ti-45Cb	50	59	Ti-45Cb	53*	T	187	384	687	1050	1515	2745	4340	6200
A-286	85	95	A-286	90*	-	317	651	1165	1785	2575	4665	7375	10500

- a All rivets must be sufficiently driven to fill the rivet hole at the shear plane. Driving changes the rivet strength from the undriven to the driven condition and thus provides the above driven shear strengths.
b Shear stresses are for the as driven condition on B-basis probability.
c Based on nominal hole diameter specified in Table 8.1.2(a).
d The temper designations last digit (1), indicates recognition of strengthening derived from driving.
e The bucktail's minimum diameter is 1.5 times the nominal hole diameter in Table 8.1.2(a).
f Should not be exposed to temperatures over 150°F.
g Driven in the W (fresh or ice box) condition to minimum 1.4D bucktail diameter.
h E (or KE, as per NAS documents).

Attachment B.3. Static joint strength

Table 8.1.2.2(f). Static Joint Strength of 100° Flush Head Aluminum Alloy Solid Rivets in Machine-Countersunk Aluminum Alloy Sheet

Rivet Type		MS20426AD (2117-T3) ($F_u = 30$ ksi)			MS20426D (2017-T3) ($F_u = 38$ ksi)			MS20426DD (2024-T31) ($F_u = 41$ ksi)			
Sheet Material		Clad 2024-T42									
Rivet Diameter, in. (Nominal Hole Diameter, in.)		3/32 (0.096)	1/8 (0.1285)	5/32 (0.159)	3/16 (0.191)	5/32 (0.159)	3/16 (0.191)	1/4 (0.257)	3/16 (0.191)	1/4 (0.257)	
Sheet thickness, in.:		Ultimate Strength ^a , lbs									
		178 ^b
			193	309 ^b
		206		340	479 ^b	...	580 ^{b,c}
			216	363	523	705 ^b	657 ^c	859 ^{b,c}	...	886 ^b	...
		...		373	542	739	690	917 ^c	...	942	...
		560	769	720	969 ^c	...	992
		575	795	746	1015	1552 ^{b,c}	1035	1647 ^{b,c}	...
		818	...	1054	1640 ^c	1073	1738 ^c	...
		853	...	1090	1773	1131	1877	...
		1891	...	2000	...
		1970	...	2084	...
		Rivet shear strength ^d	217	388	596	862	755	1090	1970	1175	2125
		Sheet thickness, in.:		Yield Strength ^{a,e} , lbs							
132
	153			231
188				261	321	...	345
	213			321	402	471	401	515	...	614	...
...				348	453	538	481	557	...	669	...
...	...			498	616	562	623	...	761
...	...			537	685	633	746	861	842	1053	...
...	745	...	854	1017	913	1115	...
...	836	...	1018	1313	1021	1357	...
...	1574	...	1694	...
...	1753	...	1925	...
Head height (ref.), in.	0.036			0.042	0.055	0.070	0.055	0.070	0.095	0.070	0.095

Attachment B.4. Ultimate single-shear strength

Table 8.1.5(a). Ultimate Single Shear Strength of Threaded Fasteners

Shear Stress of Fastener, ksi			35	38	75	90	95	108	125	132	145	156
Fastener Diameter		Basic Shank Area	Ultimate Single Shear Strength, lbs.									
in.	Size ^a											
0.112	#4	0.0098520	345	374	739	887	936	1060	1230	1300	1425	1535
0.125	1/8	0.012272	430	466	920	1105	1165	1325	1530	1620	1775	1910
0.138	#6	0.014957	523	568	1120	1345	1420	1615	1870	1970	2165	2330
0.156	5/32	0.019175	671	729	1435	1725	1820	2070	2395	2530	2780	2990
0.164	#8	0.021124	739	803	1580	1900	2005	2280	2640	2785	3060	3295
0.188	3/16	0.027612	966	1045	2070	2485	2620	2980	3450	3645	4005	4310
0.190	#10	0.028353	992	1075	2125	2550	2690	3060	3540	3740	4110	4420
0.216	#12	0.036644	1280	1390	2745	3295	3480	3955	4580	4840	5315	5720
0.219	7/32	0.037582	1315	1425	2815	3380	3570	4060	4700	4960	5445	5860
0.250	1/4	0.049087	1715	1865	3680	4420	4660	5300	6140	6480	7115	7660
0.312	5/16	0.076699	2680	2915	5750	6900	7290	8280	9590	10100	11100	11950
0.375	3/8	0.11045	3865	4200	8280	9935	10450	11900	13800	14550	16000	17200
0.438	7/16	0.15033	5260	5710	11250	13500	14250	16200	18750	19800	21750	23450
0.500	1/2	0.19635	6870	7460	14700	17650	18650	21200	24500	25900	28450	30600
0.562	9/16	0.24850	8700	9440	18600	22350	23600	26800	31050	32800	36000	38750
0.625	5/8	0.30680	10700	11650	23000	27600	29150	33100	38350	40500	44500	47900
0.750	3/4	0.44179	15450	16750	33100	39750	42000	47700	55200	58300	64000	68900
0.875	7/8	0.60132	21050	22850	45100	54100	57100	64900	75200	79400	87200	93800
1.000	1	0.78540	27450	29850	58900	70700	74600	84800	98200	103500	113500	122500
1.125	1-1/8	0.99402	34750	37750	74600	89500	94400	107000	124000	131000	144000	155000
1.250	1-1/4	1.2272	43000	46600	92000	110000	116500	132500	153000	162000	177500	191000
1.375	1-3/8	1.4849	52000	56400	111000	133500	141000	160000	185500	196000	215000	231500
1.500	1-1/2	1.7671	61800	67100	132500	159000	167500	190500	220500	233000	256000	275500

a Fractional equivalent or screw number.

Table 8.1.5(b). Ultimate Tensile Strength of Threaded Fasteners

Tensile Stress of Fastener, ksi			55	62	62.5	125	140	160	180
Fastener Diameter		Nominal Minor Area ^b	MIL-S-7742 Ultimate Tensile Strength, lbs. ^{c,d}						
in.	Size ^a								
0.112	4-40	0.0050896	280	316	318	636	713	814	916
0.138	6-32	0.0076821	423	476	480	960	1075	1225	1380
0.164	8-32	0.012233	673	758	765	1525	1710	1955	2200
0.190	10-32	0.018074	994	1120	1130	2255	2530	2890	3250
0.250	1/4-28	0.033394	1835	2070	2085	4170	4680	5340	6010
0.312	5/16-24	0.053666	2950	3325	3350	6710	7510	8590	9660
0.375	3/8-24	0.082397	4530	5110	5150	10300	11500	13150	14800
0.438	7/16-20	0.11115	6110	6890	6950	13850	15550	17750	20000
0.500	1/2-20	0.15116	8310	9370	9450	18900	21150	24150	27200
0.562	9/16-18	0.19190	10550	11900	11950	23950	26850	30700	34500
0.625	5/8-18	0.24349	13350	15100	15200	30400	34050	38950	43800
0.750	3/4-16	0.35605	19550	22050	22250	44500	49800	57000	64100
0.875	7/8-14	0.48695	26750	30150	30400	60900	68200	77900	87700
1.000	1-12	0.63307	34800	39250	39550	79100	88600	101000	114000
1.125	1-1/8-12	0.82162	45200	50900	51400	102500	115000	131500	147500
1.250	1-1/4-12	1.0347	56900	64200	64700	129000	144500	165500	186000
1.375	1-3/8-12	1.2724	70000	78900	79500	159000	178000	203500	229000
1.500	1-1/2-12	1.5345	84400	95100	95900	191500	214500	245500	276000

a Fractional equivalent or number and threads per inch.

b The tension fastener allowables above are based on the nominal minor diameter thread area for MIL-S-7742 threads from Table 2.2.1 of Handbook H-28.

c Values shown above heavy line are for 2A threads, all other values are for 3A threads.

d Nuts and fastener heads designed to develop the ultimate tensile strength of the fastener are required to develop the tabulated tension loads.

Table 8.1.5(b₂). Ultimate Tensile Strength of Threaded Fasteners (Continued)

Tensile Stress of Fastener, ksi			160	180	220	260
Fastener Diameter		Maximum Minor Area ^b	MIL-S-8879			
in.	Size ^a		Ultimate Tensile Strength, lbs. ^{c,d}			
0.112	4-40	0.0054367	869	979	1195	1410
0.138	6-32	0.0081553	1305	1465	1790	2120
0.164	8-32	0.012848	2055	2310	2825	3340
0.190	10-32	0.018602	2975	3345	4090	4840
0.250	1/4-28	0.034241	5480	6160	7530	8900
0.312	5/16-24	0.054905	8780	9880	12050	14250
0.375	3/8-24	0.083879	13400	15100	18450	21800
0.438	7/16-20	0.11323	18100	20350	24900	29400
0.500	1/2-20	0.15358	24550	27600	33750	39900
0.562	9/16-18	0.19502	31200	35100	42900	50700
0.625	5/8-18	0.24700	39500	44500	54300	64200
0.750	3/4-16	0.36082	57700	64900	79400	93800
0.875	7/8-14	0.49327	78900	88800	108500	128000
1.000	1-12	0.64156	102500	115500	141000	166500
1.125	1-1/8-12	0.83129	133000	149500	182500	216000
1.250	1-1/4-12	1.0456	167000	188000	230000	271500
1.375	1-3/8-12	1.2844	205500	231000	282500	333500
1.500	1-1/2-12	1.5477	247500	278500	340500	402000

a Fractional equivalent or number and threads per inch.

b The tension fastener allowables above are based on the maximum minor diameter thread area for MIL-S-8879 threads from Tables II and III of MIL-S-8879.

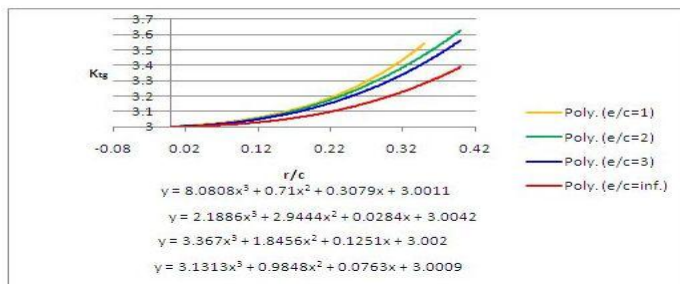
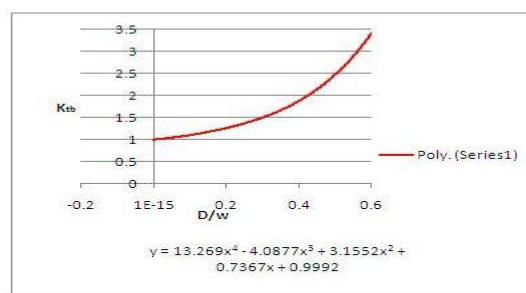
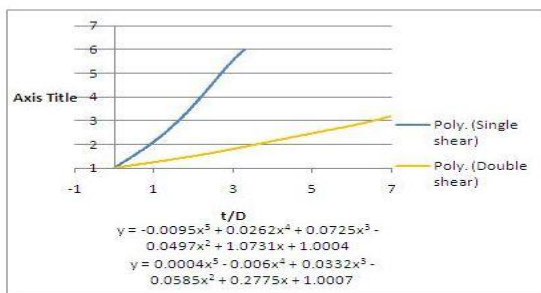
c Values are for 3A threads.

d Nuts and fastener heads designed to develop the ultimate tensile strength of the fastener are required to develop the tabulated tension loads.

Attachment C. SCF calculus constants

α	
Standard drill	1
Broached or	0.9
Cold worked	0.7

β	
Open hole	1
Steel lock bolt	0.75
Rivets	0.75
Threaded bolt	0.75
Hi-lock	0.75
Taper-Lok	0.5

**Figure C.1- SCF constants plot**

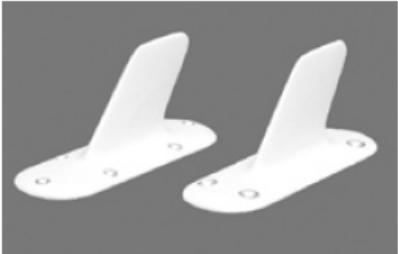
Attachment D. Antenna example data sheet

L-Band Antennas

L-Band S65-5366-7L

S65-5366-7L: Rugged, high-efficiency, all metal aluminum casting, DC grounded. Hermetically sealed. For use with transponder, DME, ATC, IFF, and Mode-S application. For commercial, military and general aviation aircraft.

NSN: 5985-01-072-8282



Specifications

L-Band S65-5366-7L

Electrical

Frequency	960 to 1220 MHz
VSWR	1.4:1 (1000-1100); 1.7:1 (960-1220)
Pattern	Omni/Az; Cos/EI
Polarization	Vertical
Impedance	50 OHMS
Power	4000 w/pk; 250 w/cont
Lightning Protection	DC grounded

Mechanical

Weight	4 oz.
Height	2.2"
Material	A356-T61 aluminum casting
Finish	Skydrol resistant enamel
Connector	C
Drag	1 oz. Mach .85 @ 35,000'

Environmental

Temperature	-65°F to +185°F
Vibration	10 G's
Altitude	70,000'

Federal & Military Specs

FAA TSO C68b	C74c & C112
	MIL-STD-883C, MIL-E-5400, MIL-A-25708, MIL-A-25730, MIL-A-9094, MIL-B-5087, MIL-A-7772

Figure D.1- Antenna manufacturer's data sheet

Attachment E. FEM data resume

Figures 2.6 and 2.8				
Structural element	Material	Thickness [in]	FEM (element)	Number of el.
Plate	Aluminum '2024 T3	0,063	SHELL (TRIA)	5430
Figure 2.7				
Structural element	Material	Thickness [in]	FEM (element)	Number of el.
Plate	Aluminum '2024 T3	0,063	SHELL (QUAD)	5000
Figure 3.6 and 3.7				
Structural element	Material	Thickness [in]	FEM (element)	Number of el.
Plate	Aluminum '2024 T3	0,063	SHELL (QUAD)	800
Figure 4.10				
Structural element	Material	Thickness [in]	FEM (element)	Number of el.
Skin	Aluminum '2024 T3	0.032 (0.813mm)	CBAR	6
Doubler	Aluminum '2024 T3	0.04 (1.016mm)	CBAR	5
Rivet 0.125" (3.962mm)	Aluminum '2024 T4	-	CBAR	5
Figure 4.12				
Structural element	Material	Thickness [in]	FEM (element)	Number of el.
Skin	Aluminum '2024 T3	0.032 (0.813mm)	Shell (QUAD)	600
Doubler	Aluminum '2024 T3	0.04 (1.016mm)	Shell (QUAD)	500
Rivet 0.125" (3.962mm)	Aluminum '2024 T4	-	CBUSH	5
Figure 4.13				
Structural element	Material	Thickness [in]	FEM (element)	Number of el.
Skin	Aluminum '2024 T3	0.032 (0.813mm)	Shell (TRIA)	4018
Doubler	Aluminum '2024 T3	0.04 (1.016mm)	Shell (TRIA)	4018
Rivet 0.125" (3.962mm)	Aluminum '2024 T4	-	CBUSH	51
Figure G.2				
Structural element	Material	Thickness [in]	FEM (element)	Number of el.
Upper splice	Aluminum '2024 T3	0.1 (2.54mm)	Shell (QUAD)	600
Lower splice	Aluminum '2024 T3	0.1 (2.54mm)	Shell (QUAD)	500
Rivet 0.125" (3.962mm)	Aluminum '2024 T4	-	CBUSH	5
Figure G.4				
Structural element	Material	Thickness [in]	FEM (element)	Number of el.
Upper splice	Aluminum '2024 T3	0.1 (2.54mm)	CBAR	3
Lower splice	Aluminum '2024 T3	0.1 (2.54mm)	CBAR	3
Rivet 0.125" (3.962mm)	Aluminum '2024 T4	-	CBAR	3
FEM-1D beams, one floor (from Attachment H)				
Structural element	Material	Thickness [in]	FEM (element)	Number of el.
Thicker doubler	Aluminum '2024 T3	0.09 (2.286mm)	CBAR	3
Thinner doubler	Aluminum '2024 T3	0.039 (0.991mm)	CBAR	1
Skin	Aluminum '2024 T3	0.031 (0.787mm)	CBAR	5
Rivet thin zone 0.156" (3.962mm)	Aluminum '2024 T4	-	CBAR	1
Rivet thick zone 0.156" (3.962mm)	Aluminum '2024 T4	-	CBAR	3
FEM-beam two floors (from Attachment H)				
Structural element	Material	Thickness [in]	FEM (element)	Number of el.
Upper doubler	Aluminum '2024 T3	0.051 (1.295mm)	CBAR	3
Lower doubler	Aluminum '2024 T3	0.039 (0.991mm)	CBAR	4
Skin	Aluminum '2024 T3	0.031 (0.787mm)	CBAR	5
Rivet up 0.156" (3.962mm)	Aluminum '2024 T4	-	CBAR	3
Rivet down 0.156" (3.962mm)	Aluminum '2024 T4	-	CBAR	4
FEM-shells two floors (from Attachment H)				
Structural element	Material	Thickness [in]	FEM (element)	Number of el.
Upper doubler	Aluminum '2024 T3	0.051 (1.295mm)	Shell (QUAD)	300
Lower doubler	Aluminum '2024 T3	0.09 (2.286mm)	Shell (QUAD)	400
Skin	Aluminum '2024 T3	0.031 (0.787mm)	Shell (QUAD)	500
Rivet 0.156" (3.962mm)	Aluminum '2024 T4	-	CBUSH	7
Figures L.2 and L.3				
Structural element	Material	Thickness [in]	FEM (element)	Number of el.
Upper doubler	Aluminum '2024 T3	0.032 (0.813mm)	Shell (TRIA)	81
Lower doubler	Aluminum '2024 T3	0.032 (0.813mm)	Shell (TRIA)	170
Skin	Aluminum '2024 T3	0.032 (0.813mm)	Shell (TRIA)	270
Rivet 0.125" (3.175mm)	Aluminum '2024 T4	-	CBUSH	16
Figure 5.14				
Structural element	Material	Thickness [in]	FEM (element)	Number of el.
Upper doubler	Aluminum '2024 T3	0.032 (0.813mm)	CBAR	2
Lower doubler	Aluminum '2024 T3	0.032 (0.813mm)	CBAR	3
Skin	Aluminum '2024 T3	0.032 (0.813mm)	CBAR	4
Rivet up 0.125" (3.175mm)	Aluminum '2024 T4	-	CBAR	2
Rivet down 0.125" (3.175mm)	Aluminum '2024 T4	-	CBAR	3
Figure 5.15				
Structural element	Material	Thickness [in]	FEM (element)	Number of el.
Upper doubler	Aluminum '2024 T3	0.032 (0.813mm)	CBAR	3
Lower doubler	Aluminum '2024 T3	0.032 (0.813mm)	CBAR	3
Skin	Aluminum '2024 T3	0.032 (0.813mm)	CBAR	4
Rivet up 0.125" (3.175mm)	Aluminum '2024 T4	-	CBAR	3
Rivet down 0.125" (3.175mm)	Aluminum '2024 T4	-	CBAR	3

Figure E.1- FEM analysis data

Attachment F. Fastener spring constants

In the Table F.1 there is a resume of the most common formulas for estimating the rivets constants. All the parameters are defined in the section Nomenclature.

Swift	$C = \frac{1}{E \cdot D} \cdot \left[A + B \cdot \left(\frac{D}{t_{\text{doubler}}} + \frac{D}{t_{\text{skin}}} \right) \right] ; A=5; B=0.8 \text{ for Al rivets}$
Boeing1	$C = \frac{4 \cdot (t_i + t_j)}{9 \cdot G_{\text{fast}} \cdot A_{\text{shear}}} + \frac{t_i^3 + 5 \cdot t_i^2 \cdot t_j + 5 \cdot t_j^2 \cdot t_i + t_j^3}{40 \cdot E_{\text{fast}} \cdot l_{\text{fast}}} + \frac{1}{t_i} \cdot \left(\frac{1}{E_{\text{fast}}} + \frac{1}{E_i} \right) + \frac{1}{t_j} \cdot \left(\frac{1}{E_{\text{fast}}} + \frac{1}{E_j} \right)$
Boeing2	$C = \frac{2 \left(\frac{t_i}{D} \right)^{0.85}}{t_i} \left(\frac{1}{E_i} + \frac{3}{8E_{\text{fast}}} \right) + \frac{2 \left(\frac{t_j}{D} \right)^{0.85}}{t_j} \left(\frac{1}{E_j} + \frac{3}{8E_{\text{fast}}} \right)$
NACA TN-1051	$C = \frac{8}{t_{\text{av}} \cdot E_{\text{fast}}} \cdot \left(0,13 \cdot \left(\frac{t_{\text{av}}}{D} \right)^2 \cdot \left[2,12 + \left(\frac{t_{\text{av}}}{D} \right)^2 \right] + 1 \right) ; t_{\text{av}} = \frac{t_{\text{doubler}} + t_{\text{skin}}}{2}$
Grumman	$C = \frac{(t_i + t_j)^2}{E_{\text{fast}} D^3} + 3,72 \left(\frac{1}{t_i E_i} + \frac{1}{t_j E_j} \right)$
Huth	$C = \left(\frac{t_i + t_j}{2D} \right)^{aa} \frac{bb}{n} \left(\frac{1}{t_i E_i} + \frac{1}{n t_j E_j} + \frac{1}{2 t_i E_f} + \frac{1}{2 n t_j E_{\text{fast}}} \right) ; aa=2/5; bb=2.2 \text{ for metallic joints}$
Douglas	$C = \frac{1}{D E_j} \left(A + B \cdot D \left(\frac{1}{t_i} + \frac{E_j}{t_j E_i} \right) \right) ; A=5 ; B=0.8 \text{ for Al rivets}$

Table F.1 – Fastener spring constant formulas resume

In the following Table F.2 there is typical data of a structural antenna installation, for two plates of Aluminum 2024 T3 skin material.

Plate i material modulus of elasticity [psi]	E_i	10500000 (72395MPa)
Plate j material modulus of elasticity [psi]	E_j	10500000 (72395MPa)
Fastener material modulus of elasticity [psi]	E_{fast}	10500000 (72395MPa)
Fastener shear modulus [psi]	G	4000000 (27579MPa)
Skin thickness [in]	t_{skin}	0,05 (1.27mm)
Doubler thickness [in]	t_{doubler}	0,063 (1.60mm)
Diameter of the fastener [in]	D	0,125 (3.175mm)

Table F.2- Example data

In the following Table F.3 there is the comparison of the values of the fastener constant calculated with the different formulation.

Swift [in/lb]	6.54E-06 (3.66E-04mm/kg)
Boeing 1 [in/lb]	9.13E-06 (5.11E-04mm/kg)
Boeing 2 [in/lb]	6.66E-06 (3.73E-04 mm/kg)
NACA TMN-1051 [in/lb]	1.43E-05 (8.01E-04 mm/kg)
Grumman [in/lb]	1.33E-05 (7.45E-04 mm/kg)
Huth [in/lb]	1.27E-05 (7.11E-04 mm/kg)
Douglas [in/lb]	4.24E-06 (2.37E-04 mm/kg)

Table F.3- Fastener constant results compilation

Attachment G. Comparison of different methods analysis data

The specific data for the analysis is shown in the following table:

Modulus of elasticity	E [psi]	10000000 (68947MPa)
Distance between the plates in the FEM beams model	L _m [in]	1 (25.4mm)
Plates' thicknesses	t [in]	0.1 (2.54mm)
Strip width	w [in]	1 (25.4mm)
Applied force	P [lbs]	100 (45.36kg)
Fastener diameter	D [in]	0.125 (0.056kg)

Table G.1- Example data

The analysis of the splice through the different methods is shown below. The green values in the pictures are the bearing or transfer load results.

Analytic method:

The results of the calculus are properly shown in Figure H.1, for the 3 pertinent cases. It has been calculated through a developed Microsoft Office Excel file.

Loads:	Kf1	Kf2	Kf3	Kf4
Row1	40.00	38.64	36.84	34.38
Row2	20.00	22.73	26.32	31.25
Row3	40.00	38.64	36.84	34.38

*unities [lb]

Figure G.1- Constants results for analytic matrixes analysis

FEM-shells method:

The simulated FEM-shell geometry and load fastener transmission vector is shown in figures G.2 and G.3. The restrictions chosen are the edge at the left totally embedded, and just allowing the 'x' translation to the rest of nodes. The FEM data can be observed at the Attachment E.

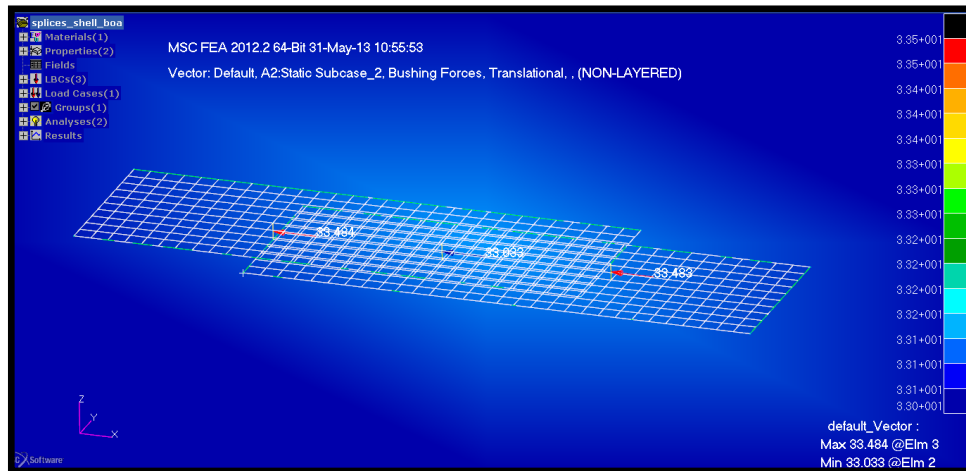


Figure G.2- FEM 1 strip splice shell element transfer forces

FEM-SHELLS METHOD				
Bush Constants				
	Kf1	Kf2	Kf3	Kf4
Kx=Ky	1.00E+06	7.00E+05	4.00E+05	1.00E+05
Kz1,2,3,4=	1227185	1227185	1227185	1227185
*unities [lb/in]				
Loads:	Kf1	Kf2	Kf3	Kf4
Row1	33.89	33.83	33.72	33.48
Row2	32.21	32.34	32.56	33.03
Row3	33.89	33.83	33.72	33.48
*unities [lb]				

Figure G.3- Constants results for FEM with shell elements analysis

FEM beams method:

The simulated FEM-beam geometry and load fastener transmission vector is shown in figures G.4 and G.5. The restrictions chosen are the node at the left totally embedded, and just allowing the 'x' translation to the rest of nodes. The FEM data can be observed at the Attachment E.

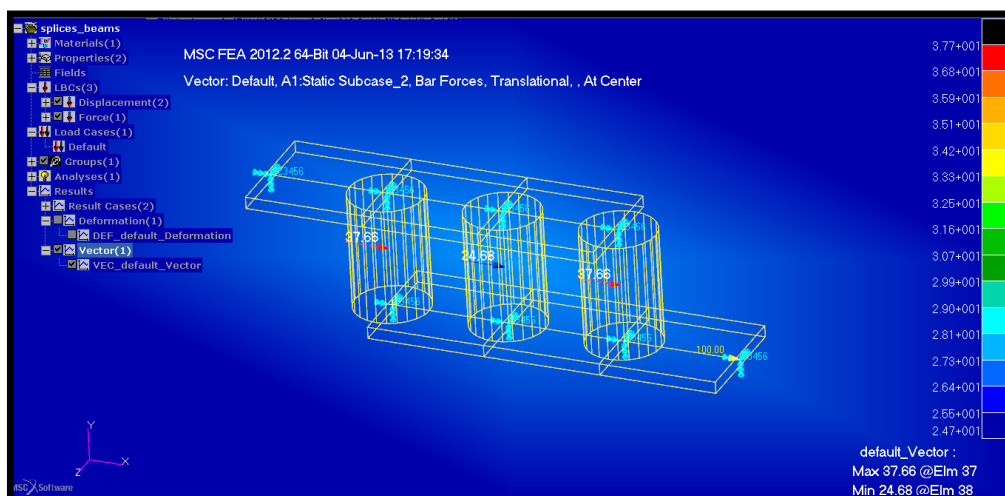


Figure G.4- FEM 1 strip splice beam element transfer forces

FEM-BEAMS METHOD					
Fastener's Constants			Equivalent diameters		
C1	1.00E-06		D1	0.642	
C2	1.43E-06		D2	0.587	
C3	2.50E-06		D3	0.510	
C4	1.00E-05		D4	0.361	
*unities [in/lb]			*unities [in]		
Loads:	Kf1	Kf2	Kf3	Kf4	
Row1	37.66	36.83	35.62	34.16	
Row2	24.68	26.33	28.77	31.69	
Row3	37.66	36.83	35.62	34.16	
*unities [lb]					

Figure G.5- Constants results for FEM with beam elements analysis

Attachment H. Comparison of multiple doublers' methods

Analytic case:

ANALYTIC			
	Bearing loads	By-pass load skin	By-pass load doubler pack
Pf1 [lb]	34.23	65.77	34.23
Pf2 [lb]	21.56	44.20	55.80
Pf3 [lb]	9.49	34.71	65.29
Pf4 [lb]	3.58	31.13	68.87
*all results in [lb]			

Figure H.1- Load distribution results using the analytic method

FEM-1D beams, one floor:

The restrictions chosen are the two nodes at the left totally embedded, and just allowing the 'x' translation to the rest of nodes. The FEM data can be observed at the Attachment E.

FEM BEAMS 1 FLOOR			
	Bearing loads	By-pass load skin	By-pass load doubler
Pf1 [lb]	31.41	68.59	31.41
Pf2 [lb]	20.62	47.97	52.03
Pf3 [lb]	9.94	38.03	61.97
Pf4 [lb]	4.01	34.02	65.98
*all results in [lb]			

Figure H.2- Load distribution results using the FEM method with variable thickness

FEM-beam two floors:

The restrictions chosen are the three nodes at the left totally embedded, and just allowing the 'x' translation to the rest of nodes. The FEM data can be observed at the Attachment E.

FEM BEAMS 2 FLOORS					
	Floor1		Floor2		
	Bearing loads	By-pass loads skin	Bearing loads	By-pass loads mid doubler	By-pass loads upper doubler
Row1	30.88	69.12	-	-	-
Row2	16.95	52.17	14.49	33.34	14.49
Row3	8.93	43.24	8.34	33.93	22.83
Row4	3.86	39.38	3.78	34.01	26.61

*all results in [lb]

Figure H.3- Load distribution results using the FEM 1 strip 2 doublers method

FEM-shells two floors:

The restrictions chosen are the three edges at the left totally embedded, and just allowing the 'x' translation to the rest of nodes. The FEM data can be observed at the Attachment E.

FEM SHELLS 2 FLOORS					
Results	Floor1		Floor2		
	Bearing loads	By-pass loads skin	Bearing loads	By-pass loads mid doubler	By-pass loads upper doubler
Row1	30.2	69.8	-	-	-
Row2	24.7	45.1	20.76	34.14	20.76
Row3	11.23	33.87	12.25	33.12	33.01
Row4	3.86	30.01	4.24	32.74	37.25

*all results in [lb]

Figure H.7- Load distribution results using the FEM 1 strip 2 doublers method

Attachment I. Inter-rivet distance study data

The data for the example case of study is shown in the following Table I.1.

w	0.787in (20mm)
t _{doubler}	0.04in (1.02mm)
t _{skin}	0.032in (0.81mm)
Dr	Variable
P ₀	456lbs (207kg)

Table I.1- Example data

	Rivet diameter [in]	Applied factor	Inter rivet distance Dr [in]
Case 1	0.125 (3.17mm)	4·D	0.5 (12.70mm)
Case 2	0.125 (3.17mm)	5·D	0.625 (15.87mm)
Case 3	0.125 (3.17mm)	6·D	0.75 (19.05mm)
Case 4	0.125 (3.17mm)	7·D	0.875 (22.22mm)
Case 5	0.125 (3.17mm)	8·D	1 (25.40mm)

Table I.2- Inter-rivet distance tabulation cases

The geometric parameters are shown in the Table I.3, obtained through the specific tables from the reference [2]. The calculated values for the stress concentration factor in each row for each configuration are resumed in the Table I.4.

Hole condition	α	1
Hole filling condition	β	0,75
Stress concentration factor, bearing stress	K_{tb}	1,19
Stress concentration factor, bypass	K_{tg}	3,09
Bearing distribution factor	θ	1,3

Table I.3- Selected stress concentration factor parameters from

	Stress Concentration Factor				
	Case 1	Case 2	Case 3	Case 4	Case 5
Row 1	3,319	3,444	3,553	3,652	3,728
Row 2	2,283	2,264	2,240	2,218	2,193

Table I.4- Stress concentration factor results

Attachment J. Crack growth rate formulas summary

The ΔK was taken instead of SCF to symbolize the range of the fatigue loading cycle. The following expressions at the Table J.1 have been taken from the references [20], [21]. All the parameters are defined in the section Nomenclature.

Paris	$\frac{da}{dN} = C_p (\Delta K)^m$
Walker 1	$\frac{da}{dN} = \frac{C_p (\Delta K)^m}{(1-R)}$
Walker 2	$\frac{da}{dN} = \frac{C_p (\Delta K)^m}{(1-R)^p}$, for wide oscillations of R
Forman 1	$\frac{da}{dN} = \frac{C_p (\Delta K)^m}{(1-R)K_c - \Delta K}$, for R=0
Forman 2	$\frac{da}{dN} = \frac{C_p [(1-R)^{n-1} \Delta K]^m}{[(1-R)^n K_c - (1-R)^{n-1} \Delta K]^L}$
Forman 3	$\frac{da}{dN} = C_p (1-R)^{(n-1)(m-L)} \frac{(\Delta K)^m}{[(1-R)K_c - \Delta K]^L}$
NASGRO	$\frac{da}{dN} = C_p \left(\frac{(1-f)}{(1-R)} \Delta K \right)^n \frac{\left(1 - \frac{\Delta K_{th}}{\Delta K} \right)^{pp}}{\left(1 - \frac{K_{max}}{K_c} \right)^{qq}}$

Table J.1- Stress concentration factor results

Attachment K. Non-Destructive Testing

- **Visual inspection:**

Application: Detection of surface defects in all materials.

Advantages: It is simple to use in areas where other methods are impractical. Optical aids further enhance this method.

Disadvantages: Reliability depends upon the ability and experience of the user. Accessibility required for direct visibility.

- **Eddie current:**

Application: Detection of surface cracks in metallic surfaces. Cracks, pits, inter-granular corrosion and heat treat condition.

Advantages: Useful for checking attachment holes for not detectable cracks by visual or penetrant methods. Fast, sensitive and portable.

Disadvantages: Trained operator required. It has sensitive variations depending on the material. Special probes are required for each application. Reference standards are required.

- **Liquid penetrant inspection:**

Application: Detection of surface cracks in all metals, castings, forgings, machined parts, and welded areas.

Advantages: It is simple to use, accurate, fast and easy to interpret.

Disadvantages: Defect must be open to surface and accessible to operator. Defect must be covered by smeared metal. The part must be cleaned before and after the check.

- **Magnetic particle:**

Application: Detection of surface or near surface defects in ferromagnetic materials of any shape or heat treat condition.

Advantages: It is simple in principle, easy, portable, and fast.

Disadvantages: Trained operator required. Parts must be cleaned before and demagnetized after check. The magnetic flux must be normal to plane of defect to yield indications.

- **Radiography X-Ray:**

Application: Detection of internal flaws and defects such as cracks, corrosion, inclusions, and thickness variations.

Advantages: It eliminates many disassembly requirements. It has high sensitivity, and provides a permanent record on film.

Disadvantages: The radiation is hazard. Trained operators and film processing equipment is required. The crack plane must be nearly parallel to the x-Ray beam. Especial equipment is required to position the x-Ray tube and film.

- **Ultrasonic:**

Application: It allows the detection of surface and subsurface defects and cracks in the most of metals.

Advantages: It is fast, dependable, easy to operate, and the results are immediately known. It is accurate, with high sensitivity, and portable.

Disadvantages: Trained operator is required. Electrical source is required. The crack plane orientation must be known to choose the wave mode to be used. Test standards are required to establish the instrument sensitivity.

The Table K.1 contains the minimum detectable crack lengths for each NDT method.

NDI method	Crack location	Part thickness [mm]	Crack type	Crack dimension, a [mm]	Crack dimension, c[mm]
General visual	-	-	-	76 (3in)	-
Detailed visual	-	-	-	38 (1.5in)	-
Eddy current	Open surface	$t \leq 1.27$ $t \leq 1.27$	Through Partly through	t 0.51 1.27	1.27 2.54 1.27
	Edge or hole	$t \leq 1.91$ $t \leq 1.91$	Through Corner	t 1.91	2.54 1.91
Liquid Penetrant	Open surface	$t \leq 1.27$ $1.27 \leq t \leq 1.91$ $t \leq 1.91$	Through Through Partly through	t t 0.64 1.91	2.5 3.81-t 3.18 1.91
	Edge or hole	$t \leq 2.54$ $t \leq 2.54$	Through corner	t 2.54	3.81 3.81
Magnetic Particle	Open surface	$t \leq 1.91$ $t \leq 1.91$	Through Partly through	t 0.97 1.91	3.18 4.78 3.18
	Edge or hole	$t \leq 1.91$ $t \leq 1.91$	Through corner	t 1.91	6.35 6.35
Radiography	Open surface	$t \leq 2.72$ $t \leq 2.72$	Partly through Partly through Embedded	0.7t 0.7t 0.35t	1.91 0.7t 0.7t
Ultrasonic	Open surface	$t \leq 2.54$	Partly through	0.76 1.65	3.81 1.65
			Embedded	0.43	2.21
				0.33	0.99

Table K.1- Minimum detectable crack sizes based on standard NDE methods [22]

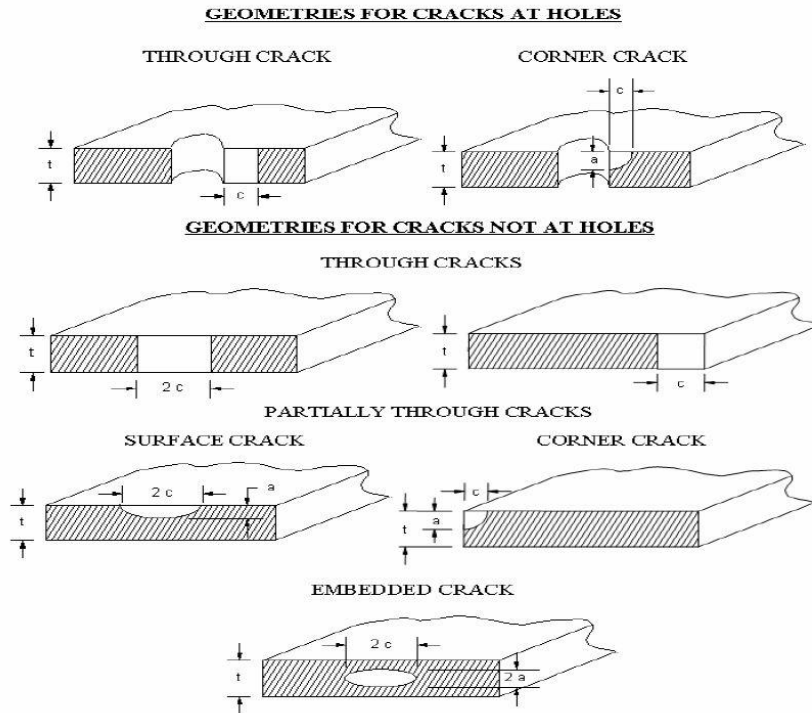


Figure K.1- Assumed flaw geometries [22]

Attachment L. Multiple-doublers configuration examples data

The specific data used for the example is shown in the Table L.1.

Material	Aluminum 2024 T3
Rivets diameter [in]	0.125 (3.17mm)
Plates thicknesses [in]	0.032 (0.81mm)
Inter-rivet distance [in]	0.787 (19.99mm)
Applied force [lbs]	100 (45.36kg)

Table L.1- Example data

FEM model entire doublers simulation:

For simulating an entire symmetrical doubler, just with studying a quart part of it is enough, like can be observed in Figure L.1. Loads in the longitudinal and in the hoop direction are applied to the model.

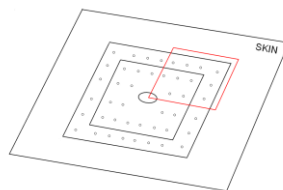


Figure L.1- Two doublers with the selected zone of study

Case1:

The case configuration used, triangular mesh, and the transfer bush forces for the Case1 can be seen in Figure L.2. The restrictions chosen are the six edges which reach the center hole totally embedded, and just allowing the x and y translation to the rest of nodes. The FEM data can be observed at the Attachment E.

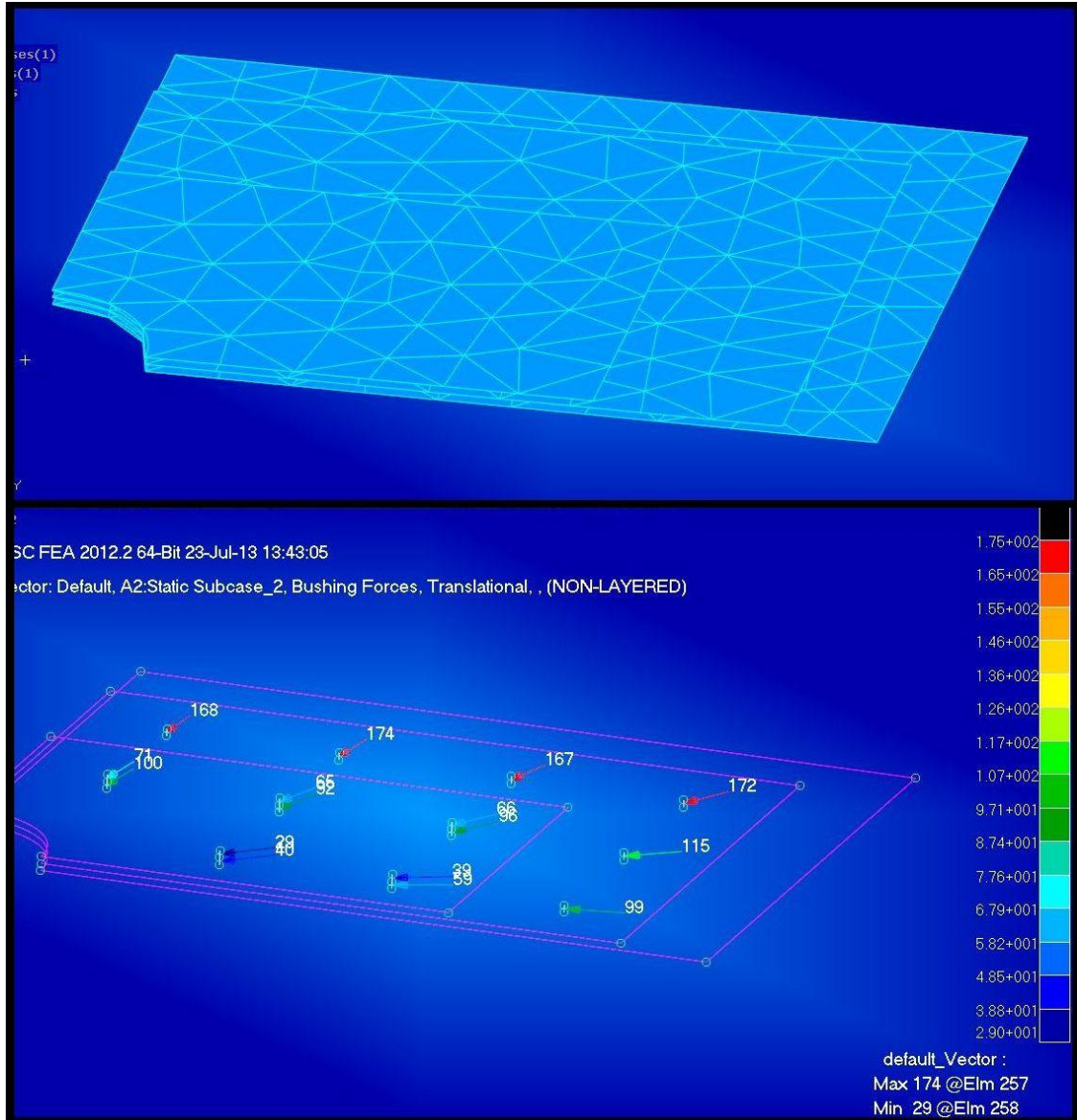


Figure L.2- Case 1 entire doubler with shell elements

Case2:

The case configuration used, triangular mesh, and the transfer bush forces for the Case2 can be observed in Figure L.3. The restrictions chosen are the six edges which reach the center hole totally embedded, and just allowing the x and y translation to the rest of nodes. The FEM data can be observed at the Attachment E.

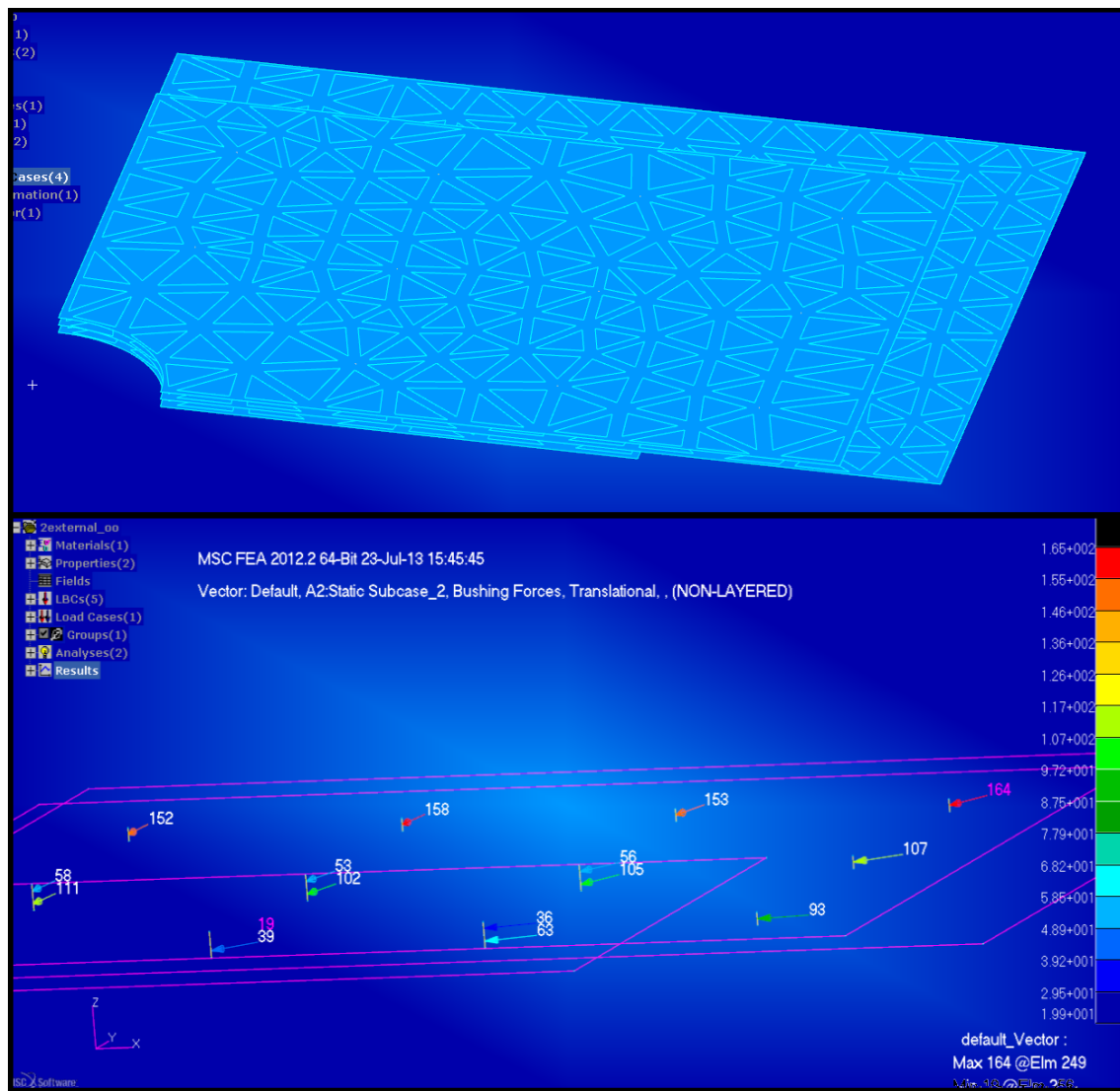


Figure L.3- Case 2 entire doubler with shell elements transfer forces